Using Petrographic and Geochemical Analyses to Elucidate the Genesis of Au-Ag Epithermal Deposits on Florida Mountain, Silver City District, Idaho

By

Lucas Hunter Monroe

A Thesis Defense Submitted to the Faculty of the Department of Geosciences in Partial Fulfillment of the Requirements for a Master of Science Degree in Geology

Auburn, Alabama

May 1, 2021

Approved by

Laura D. Bilenker, Chair, Assistant Professor of Geosciences

Willis E. Hames, Professor of Geosciences

Haibo Zou, Professor of Geosciences

Abstract

Florida Mountain (FM) is classified as a low-sulfidation epithermal deposit and has a rich history of Au-Ag economic mining. It is one of a trio of similar deposits in southwestern Idaho within the Northern Great Basin and along the Yellowstone hotspot track. This study used petrography and geochemistry to elucidate the genesis of Florida Mountain, a deposit that has not been the subject of extensive study. Previous research focused on high-grade veins and information from historical mining to provide a geologic framework for the district. During summer 2019, 60 samples from seven lithologic units were collected from drill core and retired open pits. Samples were characterized by petrographic analysis prior to geochemical analyses. Electron microprobe analysis was used to measure trace element concentrations in sulfide minerals associated with high metal grades, and to better evaluate mineralogical textures and relationships. Important mineral phases identified include electrum, silver selenide, and pyrite, which were analyzed for their Au, Ag, Ti, Cu, S, Fe, As, and Se content. Elevated Au and Ag concentrations were measured in pyrite grains and varied across individual crystals. Laser ablation inductively coupled plasma mass spectrometry was also used to quantify lower amounts of the trace elements and confirmed variations in the concentrations of Au, Ag within individual pyrite grains (e.g., rim vs. core) correlating with different mineralogical textures and associations. Preliminary Ar-Ar geochronology on adularia crystals from FM samples determined an age range consistent with the Yellowstone hotspot (15.352-15.95 Ma). These new data and observations provide insight into the source of fluids and metals as well as the sequence of events that resulted in the formation of the FM Au-Ag epithermal deposit.

Acknowledgments

I would like to thank my advisor Dr. Laura Bilenker for her support and guidance. The completion of this thesis would not have happened as smoothly and timely without the help from her. I want to also thank my committee members, Dr. Bill Hames and Dr. Haibo Zou. Their suggestions and corrections were valuable during the evolution of this thesis. I am also grateful to Integra Resources Corp. and all those at the mine site that help with the collection of samples and better understanding the site. Those individuals include VP of Exploration Max Baker and the contract geologists Mitch Collins, Sebastien Bricka, and Alex Deathrage. I also want to thank Raeann Garcia, my office mate, for her help during field work at the mine site and with encouraging me. I would like the thank Dr. Zeki Billor for his help during the LA-ICP-MS work. Thank you to all the faculty and graduate students who always asked how my progress was going and making sure I could always answer questions about my thesis. Finally, I would like to thank my family for the never-ending encouragement and uplifting gestures to make sure I knew what I am doing is a great accomplishment.

Format Style or journal: Economic Geology

Computer Software used: Microsoft Word, Microsoft Excel, Adobe Illustrator, Adobe Photoshop, Iolite v.4.

Table of Contents

List of Tables

List of Figures

Introduction

Florida Mountain is one of a trio of low-sulfidation epithermal deposits located in southwestern Idaho within the Silver City district. Low-sulfidation epithermal deposits are a major target of modern exploration and produce large quantities of gold and silver; global production is 6% Au (gold) and 16% Ag (silver) (Simmons et al., 2005). Florida Mountain itself has produced a large amount of Au (257,500 oz.) and Ag (18 million oz.) throughout its 51-year production history. Even though Florida Mountain has been the subject of extensive production, current exploration shows there is still a high potential for profitable mining. The neighboring epithermal ore deposits, DeLamar Mountain and War Eagle Mountain (Fig. 1), have also been historically productive and have similar potential (Integra Resources, 2019).

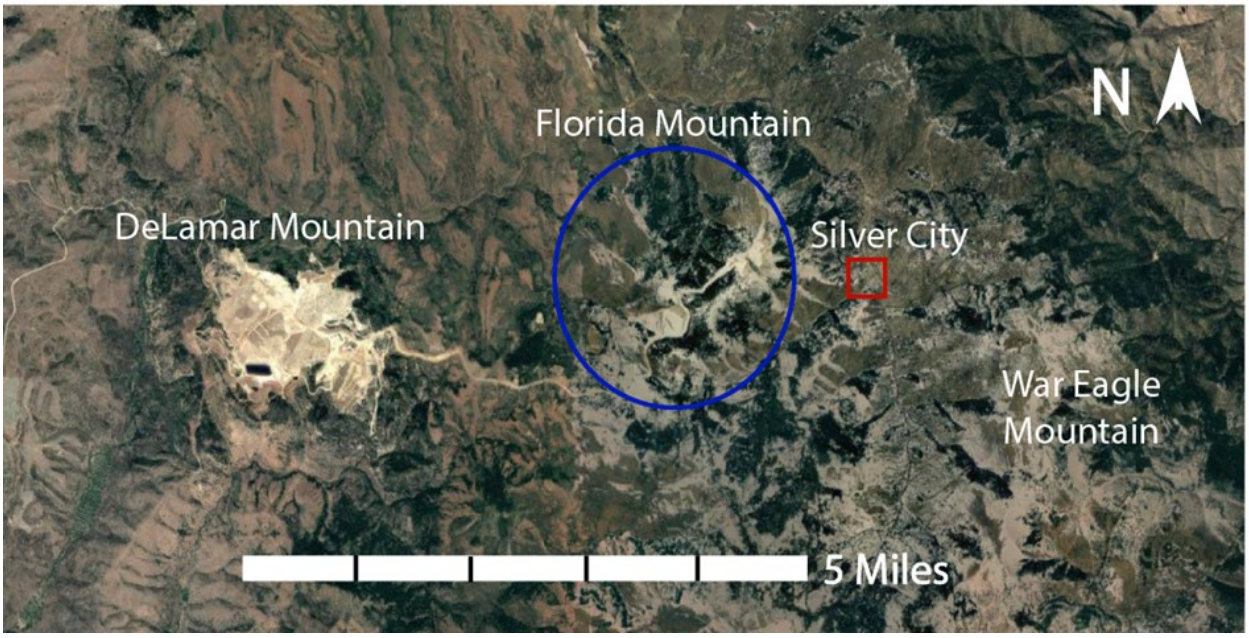

Figure 1. Google Earth image of the trio of low-sulfidation epithermal deposits and Silver City. Five-mile scale bar is broken into one-mile increments. Blue circle indicates Florida Mountain, and the red square is Silver City. Historical mining is visible at DeLamar Mountain.

Epithermal deposits attract mining companies because they form at shallow crustal depths (<1.5 km) and can host high ore grades. These ore deposits form from hydrothermal systems driven by heat from a local magma body with fluids across a spectrum of physical and chemical properties, which has led to a three-pronged classification system developed incrementally over the years (e.g., Hedenquist and Lowenstern,1994; Sillitoe and Hedenquist, 2003; Simmons et al., 2005). The current classification system separates epithermal deposits into low-, intermediate-, and high-sulfidation. Each is based on the pH, temperature, salinity, and redox conditions of the hydrothermal fluids from which they formed, which reflect fluid source. These parameters have been constrained by mineral, rock, and fluid inclusion analyses (e.g., Hedenquist and Houghton, 1987; Hedenquist, 1992; Hedenquist and Lowenstern, 1994; Hedenquist et al., 2000) and result in the unique textures and mineral assemblages of each epithermal deposit class. In the first works on epithermal deposit classification and their genetic models, stable isotope

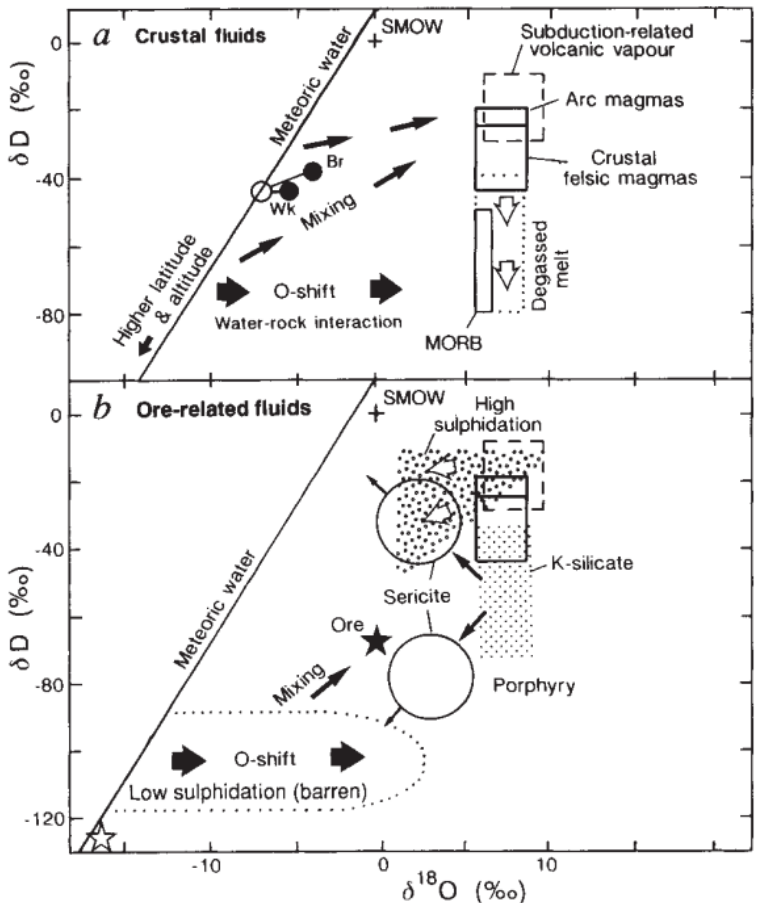

Figure 2. The O and H isotope compositions of different crustal fluids from Hedenquist and Lowenstern (1994).

ratios of oxygen (O) and hydrogen (H) provided measurable geochemical evidence of fluid source(s) (Fig. 2) (e.g., Hedenquist and Lowenstern, 1994). The fluids that form low-sulfidation mineralization are either solely, or primarily, meteoric water that significantly dilutes any rising magmatic fluids (Fig. 2 and 3). Because of this, they are near neutral pH and low in salinity, which results in a stable environment for sulfides, quartz, adularia, and calcite. On the other end of the spectrum, the hydrothermal fluids in high-sulfidation systems have a significantly higher proportion of magmatic input. These epithermal deposits occur in closer proximity to the magma chamber, which minimizes meteoric water influence (Fig. 3). This creates an acidic, hotter, more saline environment that causes high rates of wall-rock dissolution. Intermediate-sulfidation epithermal deposits form in the transitional area between high- and low-sulfidation

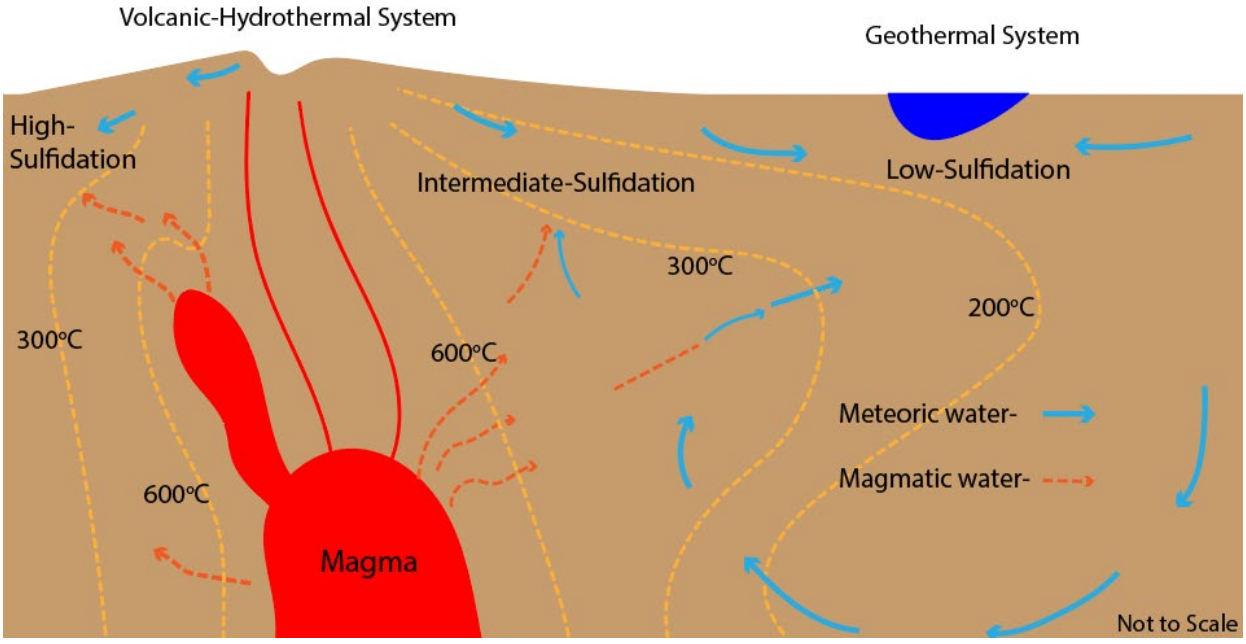

Figure 3. A schematic diagram of the fluid source(s) and pathways within an epithermal system. Note where low-, intermediate-, and high-sulfidation deposits form relative to the related magma body (redrawn from Hedenquist and Lowernstern, 1994; Sillitoe and Hedenquist, 2003).

where comparable parts of magmatic fluids and meteoric water make up the ore fluids (Simmons et al., 2005). The redox state of the fluids controls whether the system precipitates sulfides or sulfates. Low-sulfidation systems like Florida Mountain are more reducing, which results in the stability of sulfides rather than the sulfates that occur in high-sulfidation systems. Overall, the current classification scheme for epithermal deposits is based on the source of the fluids and primary mineral assemblages, which controls the depositional conditions and resulting mineralogy.

The compositions and appearances of the minerals and rocks present in these systems are records of the geologic processes that formed them. Thus, much important information can be gained by studying epithermal systems in detail, in addition to insight that can be used to better understand hydrothermal gold and silver occurrences in the shallow portions of the Earth's crust.

Previous Research: Silver City District

The Silver City district has been subject to a long history of mining but there have been only a few studies focused on the formation of Florida Mountain and many questions remain unanswered. The first studies to examine the mineral deposits in the area were carried out by Waldemar Lindgren (1900, 1933). The focus of this work was to document and compare the gold and silver veins found in Idaho, including the Silver City deposits. It was not until much later, in the 1980s and 1990s, when epithermal deposit research intensified with published descriptions of the geology of similar high-grade veins in northern Nevada (Vikre, 1985). Stable oxygen and hydrogen isotope analyses were conducted to investigate a potential connection between the hydrothermal activity of the area and the Yellowstone geothermal system. The isotope

analyses offered insight into the paleohydrology of the region and implied a direct connection between the two (Vikre, 1987). In addition to being one of three epithermal deposits located in the Silver City district, Florida Mountain is located within the Northern Great Basin (NGB) where many other high-grade Ag-Au epithermal deposits are found (Fig. 4) (John, 2001; Simmons et al., 2005; Kamenov et al., 2007; Saunders et al., 2008). Saunders (1990) studied the Sleeper epithermal deposit in the NGB in Nevada and discovered indicators of colloidal gold transportation in epithermal systems in northern Nevada and the Silver City district (Saunders, 1990, 1994; Saunders et al., 2008). By studying the electrum

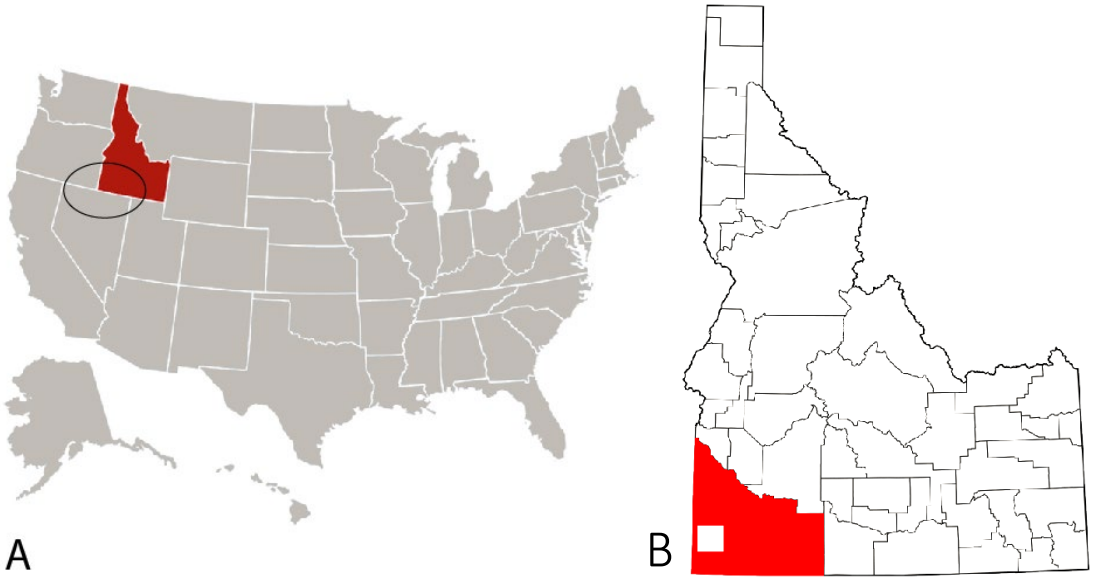

Figure 4. **A)** Idaho in red on U.S. map with a circle around the approximate location of the Northern Great Basin (Idaho, 2019). **B)** Idaho map with Owyhee County in red and Silver City in the white square (Owyhee County, Idaho, 2019).

bands and colloform banding in the Sleeper epithermal deposit, these studies reported that the textures were different from one another and interpreted this to indicate multiple fluid origins. It was also noted that the total amount of gold found at Sleeper was higher than predicted based on the calculated fluid capacity, which could be explained by the hypothesis of the gold being transported physically (i.e., as a colloid) rather than chemically (Saunders, 1990, 1994; Saunders et al., 2008).

It has also been proposed that the initiation of the Yellowstone hotspot fueled the formation of the epithermal deposits in the NGB (e.g., Saunders et al., 1996; Hames et al. 2009; Mason, 2015). All of the deposits analyzed to date in the NGB have an age of approximately 16 million years, which coincides with the start of the Yellowstone hotspot (Camp, 1995; Pierce and Morgan, 2012). In addition, similar lead isotope ratios have been measured in samples of basalt from the Silver City district and the earliest Yellowstone hotspot eruptive products and indicative of a mantle origin (Kamenov et al., 2007; Hames et al., 2009).

The most recent and detailed studies to address the formation of the Silver City district ore deposits are three master's theses completed at Auburn University under the direction of Dr. James Saunders. The first study focused on the geochemistry and geochronology of low-sulfidation epithermal deposits throughout the NGB (Unger, 2008; Hames et al., 2009). Unger (2008) considered several sites in Nevada alongside War Eagle Mountain in the Silver City district (Fig. 1). $^{40}Ar/^{39}Ar$ geochronology produced an age for the deposits of the NGB region, which suggest that hydrothermal activity began around 16.5 Ma and lasted until at least 15.6 Ma, supporting the hypothesis that the NGB is genetically related to the initiation of the Yellowstone hotspot (Unger, 2008).

Aseto (2012) described the geology, geochronology, and geochemistry of War Eagle Mountain using outcrop samples from the Orofino and Poorman veins and reported mineralization dates similar to those of Unger (2008) and Hames et al. (2009): 15.9-15.4 Ma. $^{40}Ar/^{39}Ar$ dating of the adularia from these deposits made it possible to construct these ages as well.

Most recently, Mason (2015) described the geology and geochemistry of the Au-Ag veins at Florida Mountain. Using surface samples across the deposit as well as its Black Jack-Trade Dollar vein, Mason's isotopic and geochronological analyses showed that the source of the ore was magmatic and of similar age as the Yellowstone hotspot. Petrographic observations of mineral assemblages and textures supported possible colloidal transport, cooling, and boiling (Mason, 2015; Mason et al., 2015).

The igneous rocks that host the deposits within the Silver City have been mapped by a handful of studies (e.g., Lindgren, 1900; Asher, 1968; Pansze, 1975; Halsor et al., 1988) but were most recently re-visited with a master's thesis at Kansas State University by Hasten (2012). This work focused on describing the petrogenesis of volcanic rocks in and around the Silver City district based on field observations and geochemical data. Detailed X-Ray Fluorescence (XRF) analyses provided the elemental composition of the rocks while radiogenic and stable isotopes provided insight into the genetic and chronological relationships of the units.

Source of Ore Fluid in the Silver City District

Kamenov et al. (2007) and Aseto (2012) conducted lead isotope analyses on samples from the NGB, including the Silver City district (which include veins from War

Eagle, DeLamar and Florida Mountain) which documented an isotopically primitive source of the lead alloyed within the gold and suggested that the gold could have be sourced from the mantle via the Yellowstone plume. This supported the hypothesis that the Yellowstone hotspot was the source of the Silver City district deposits and that the gold was likely transported into the system as colloids from a magmatic source (c.f., Saunders et al., 2008).

Mason (2015) also completed lead, copper, and sulfur isotope analyses on ore-stage minerals from DeLamar, War Eagle, and Florida Mountain (Trade Dollar vein) to confirm the source of the metals deposited in the Silver City district. The data were compared to other deposits in the NGB (Mason et al., 2015). Lead isotope ratios were measured in galena at Florida Mountain and the results also confirmed a genetic connection between that Silver City ores and the Yellowstone hotspot (Hanan et al., 2008). Mason (2015) used copper isotopes were used as well because they are not significantly affected by secondary biological processes (Mathur et al., 2005) and likely reflect redox changes (e.g., Markl et al., 2006). The results indicated a magmatic copper source of ore-stage naumannite, electrum, and chalcopyrite, consistent with the lead isotope data. Sulfur isotope analyses were also completed to determine the source of the sulfur and, therefore, sulfides in the high-grade veins at Florida Mountain. The sulfur isotopic composition of Florida Mountain chalcopyrite also points to a magmatic source when considering the main geologic reservoirs for which data exist (e.g., Seal, 2006).

Research Questions

This study sheds light on the genesis of metal deposits not only at Florida Mountain but throughout the Silver City district, with implications for the entire NGB.

New opportunities for drill core sampling have allowed for a more detailed perspective of this deposit. There are three main research questions: 1) When did the epithermal deposit at Florida Mountain form and can mineralization be attributed to the Yellowstone hotspot? 2) What is the source of the ore? 3) What indicators exist to assist ongoing exploration?

Geologic Setting and Field Observations

All three of the Silver City epithermal deposits were mined historically, but only Florida Mountain and DeLamar Mountain have been the source of modern production. The main mine site resides close to several open pits on DeLamar Mountain. Florida Mountain is located about 8 km to the northeast and hosts smaller open mine pits: Blackjack, Stone Cabin, and Tip Top (Figs. 1 and 5).

Figure 5. The three open pit mines of Florida Mountain (Integra Resources, 2019).

Florida Mountain and the Silver City district are located in the Owyhee volcanic field in southwestern Idaho (Fig. 4), and the basement rock is an Upper Cretaceous granodiorite with an age of approximately 65 Ma, correlative with the Idaho batholith

(Halsor et al., 1988). Above the granodiorite, Halsor et al. (1988) described a Tertiary nonconformity on top of which there is basalt of variable thickness. The basalt was observed in contact with the granodiorite in only a few of the drill cores that Halsor et al. examined. Then, there is a series of two latite layers that are followed by a rhyolite layer with banding in the upper most part of it. Occasionally, there is a thin layer of tuff breccia found between the uppermost latite and the lowest rhyolite. Mineralization, including pyrite and adularia, has been reported to be associated with rhyolite at ~16 Ma (Pansze, 1975), although Halsor et al. (1988) mentions unpublished dates up to 17.8 Ma. In summary, the unit types seen at Florida Mountain are granodiorite, lower basalt, quartz latite, porphyritic latite, tuff breccia, and a porphyritic rhyolite. Confirmation and refinement the lithological observations of Halsor et al. (1988) were completed during four weeks of onsite summer field work in June and July 2019 (Fig. 6).

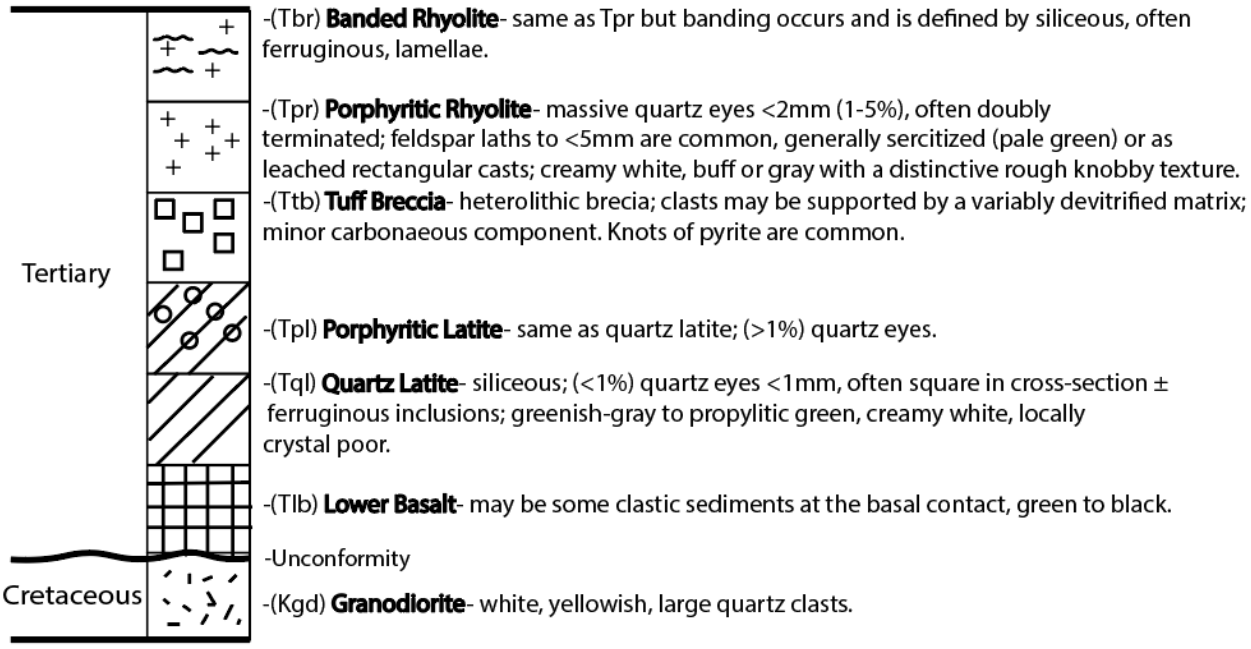

Figure 6. Updated stratigraphic column based on 2019 field work and old stratigraphic columns from Integra Resources.

Sample Selection and Field Mapping

Field work began with detailed drill core sampling and field observations. This was made possible logistically and financially by Integra Resources, the company currently exploring the Silver City district. Integra Resources provided access to extensive computer records of drill core logs. Samples were chosen based on their lithology, degree of mineralization, and textures (e.g., sulfides, adularia, veins). Representative samples were collected from each lithological unit present at Florida Mountain (Fig. 6). In total, 55 samples from seven units were collected from the Florida Mountain core. An additional five surface samples were taken from the Stone Cabin open mine pit (Fig. 7 and 8). Representative samples from the Florida Mountain drill cores can be seen in Figure 9.

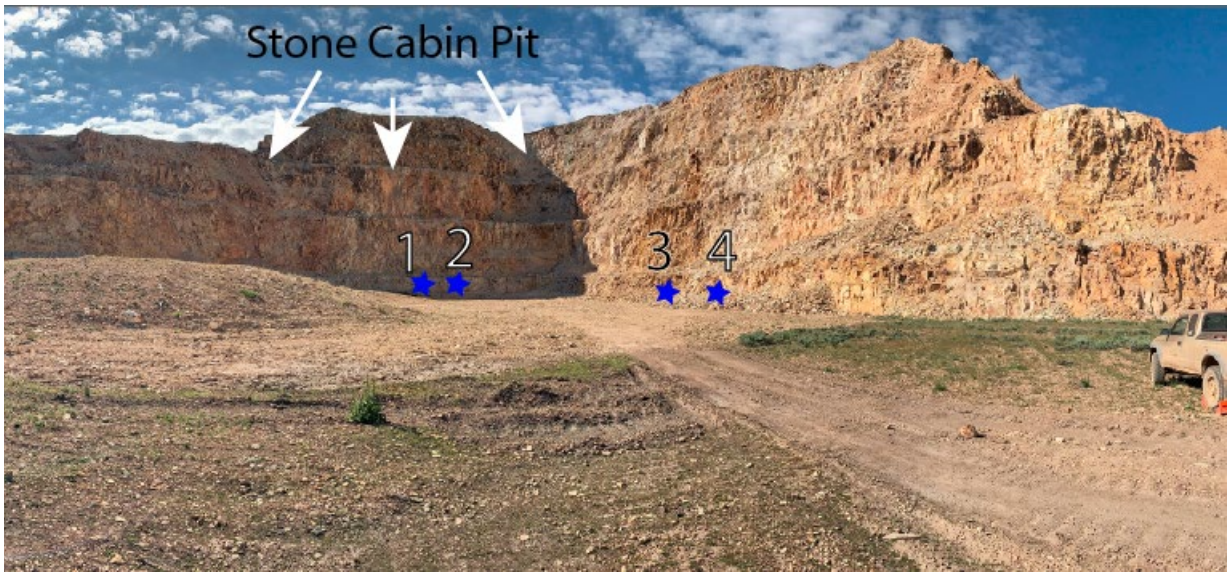

Figure 7. The Stone Cabin pit with locations of surface samples. All visible rock in the Stone Cabin pit is porphyritic rhyolite. Samples 1, 2, and 4 are labeled in white to indicate little oxidation; two samples from location 3 (labeled in black) were moderately oxidized. Blue stars are approximate location of samples. Truck for reference in lower right corner.

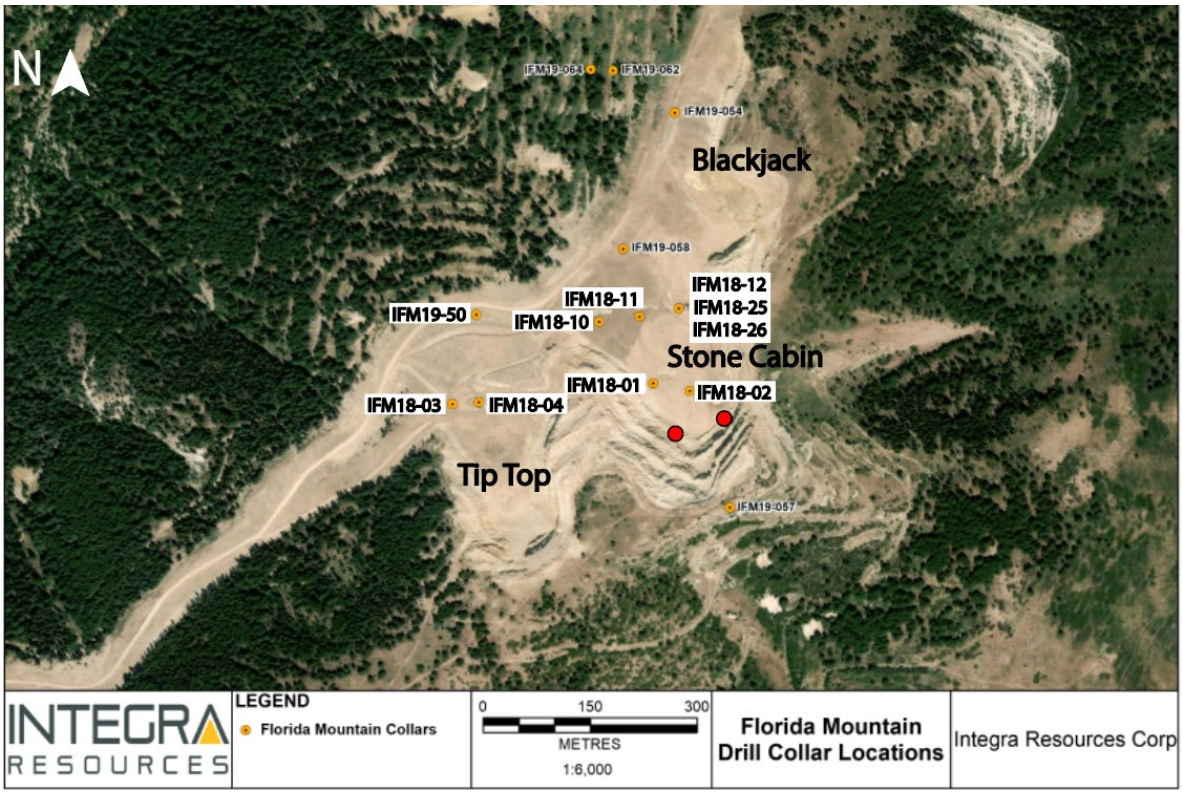

Figure 8. Map view of Figure 7; red circles denote approximate locations of surface samples in the Stone Cabin Pit. Map showing drill hole locations on Florida Mountain. The drill holes used in this study are highlighted with large white labels. Smaller labels denote unsampled drill holes. All three Florida Mountain open pits are labeled (Tip Top, Stone Cabin, and Blackjack). The labels read as I = Integra, FM = Florida Mountain, the number after FM = year drilled, and number after dash is hole ID.

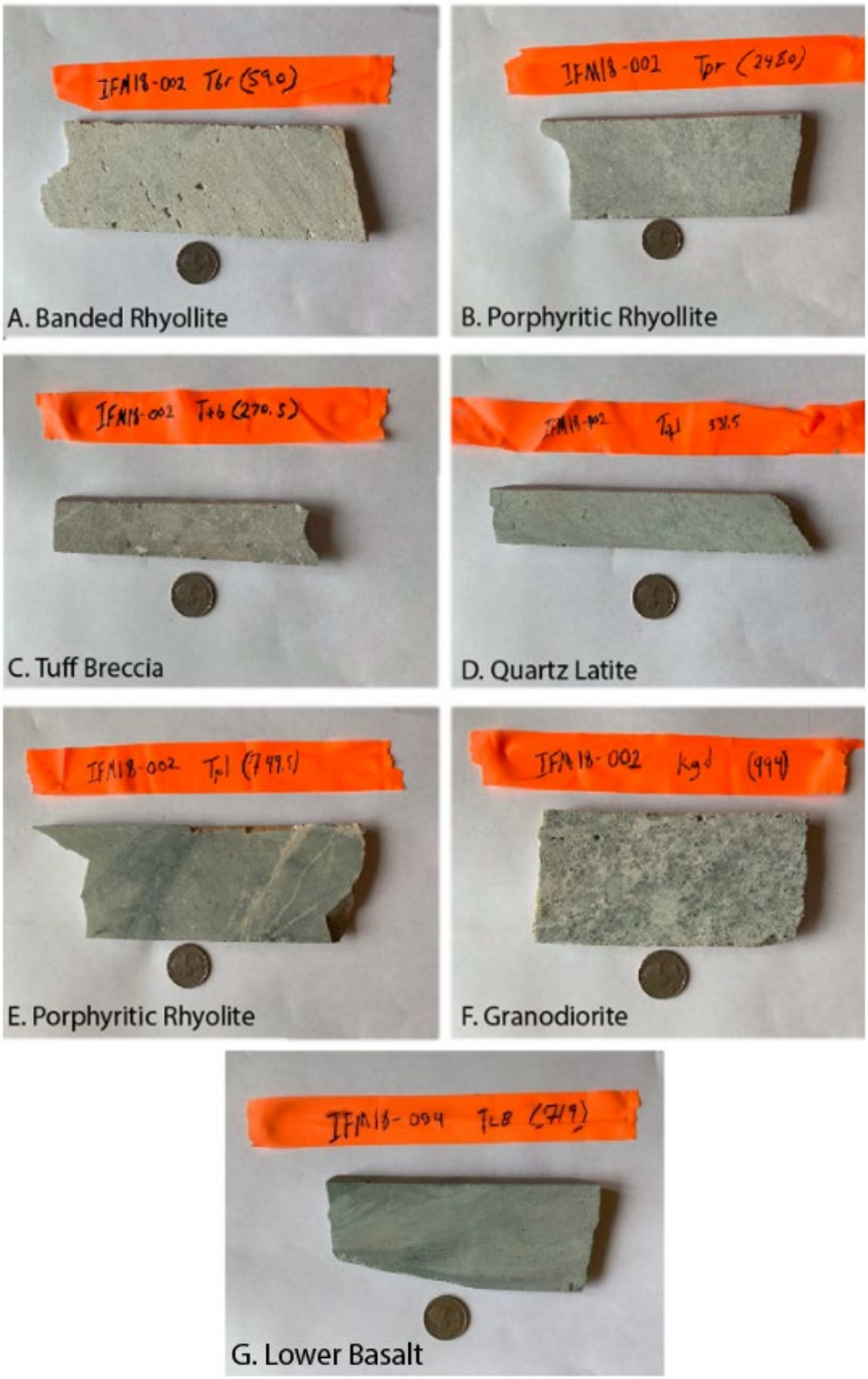

Figure 9. Representative drill core samples taken from Florida Mountain with a U.S. quarter for scale. They are labeled with the hole number, unit abbreviation, and depth in feet.

Additional field work involved detailed mapping of two sections in the DeLamar Mountain area. The resulting two geological maps (Figs. 10 and 11) will be used by Integra Resources in their ongoing exploration. Even though the areas are not a part of Florida Mountain (Fig. 12), the proximity of DeLamar Mountain and its many similarities made the mapping experience and observations beneficial for our ultimate understanding of the formation of the Silver City district, and therefore, Florida Mountain. This geologic context will also help us to disentangle the relationship between DeLamar and Florida Mountains on a local scale.

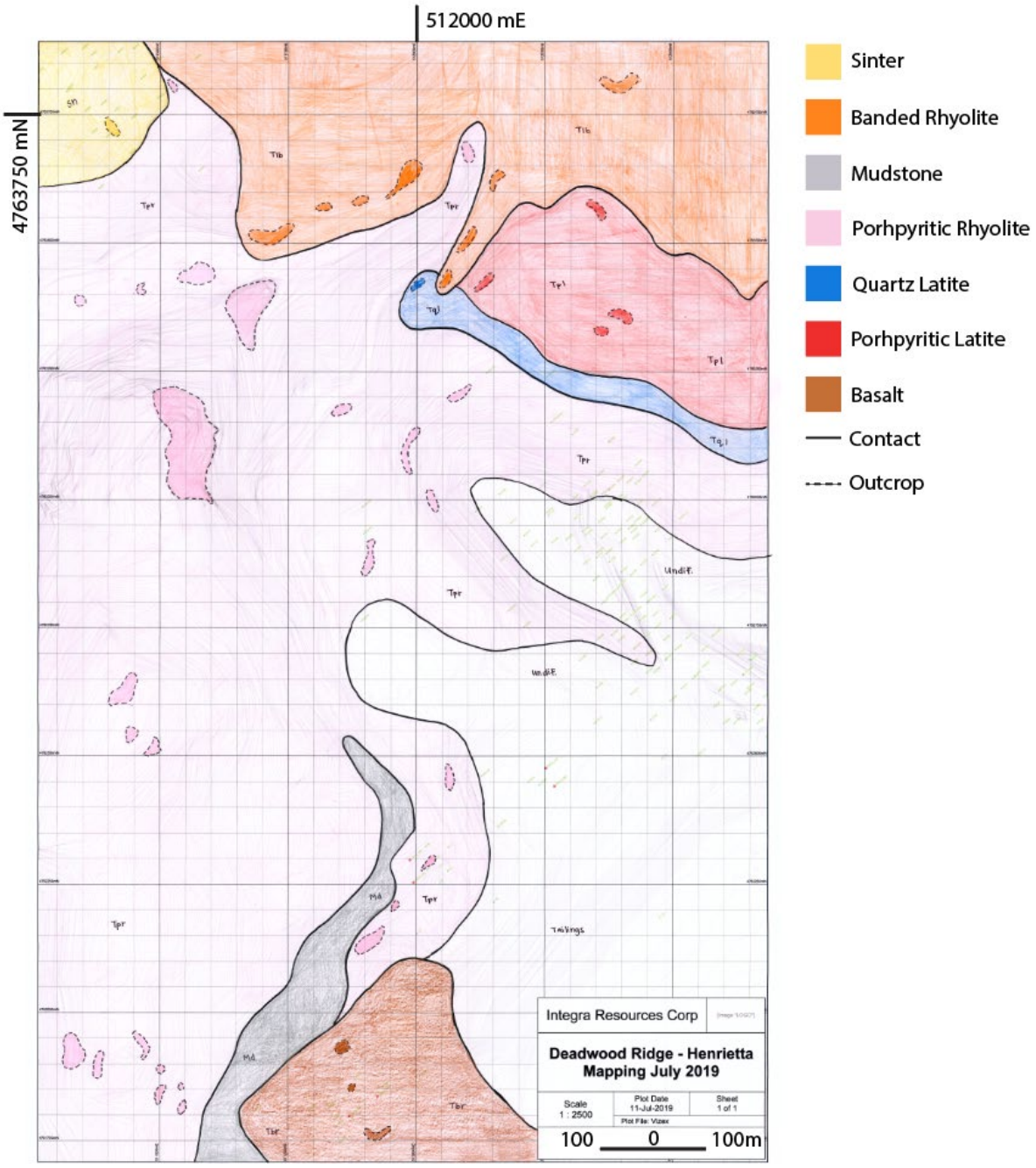

Figure 10. Scanned draft map of the area called Deadwood Ridge on DeLamar Mountain. Field mapping was completed by the present author in collaboration with Raeann Garcia. The map scale is 1:2500.

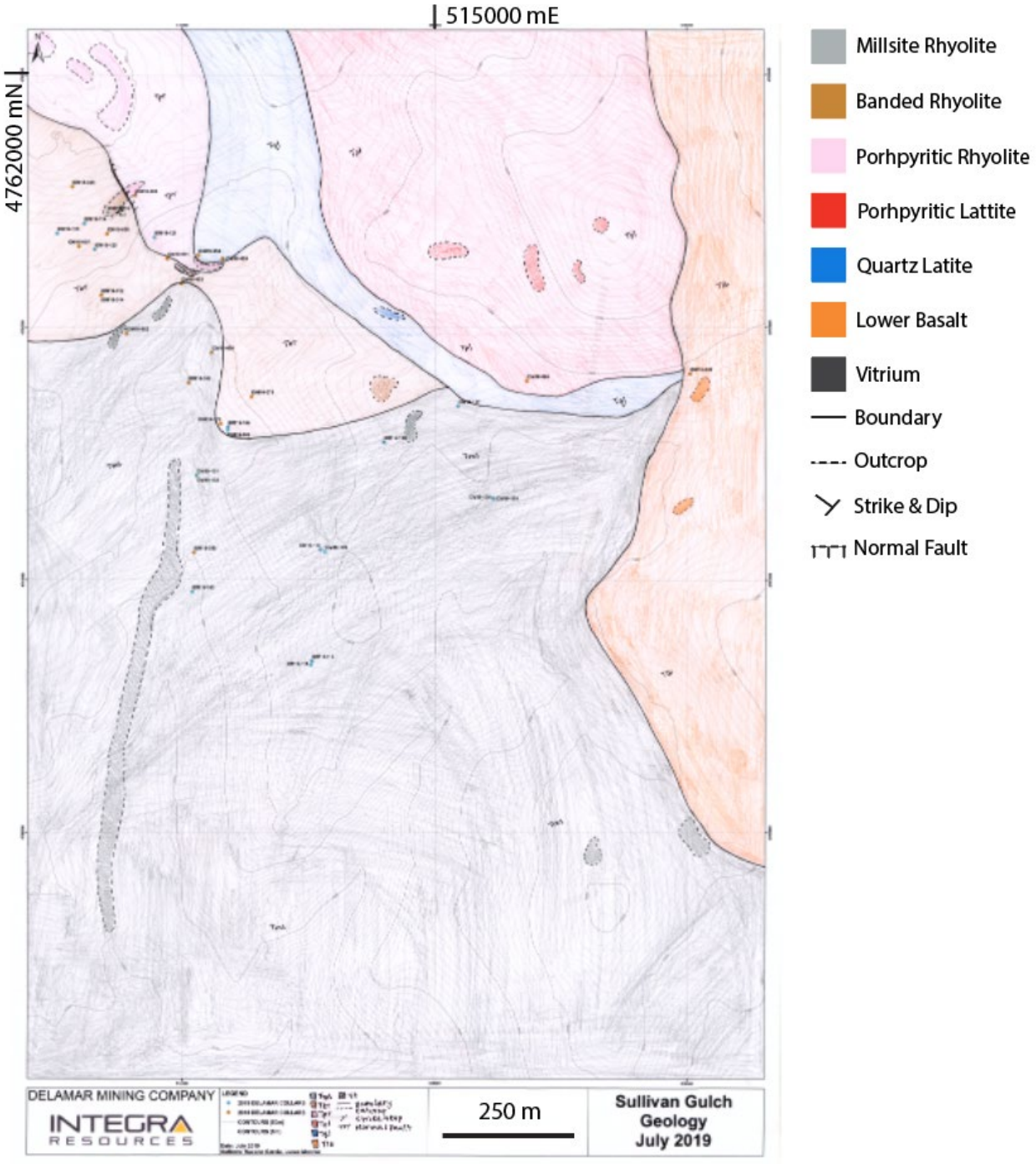

Figure 11. Scanned draft map of the area called Sullivan Gulch on DeLamar Mountain. Field mapping was completed by the present author in collaboration with Raeann Garcia. The map scale is 1:2500.

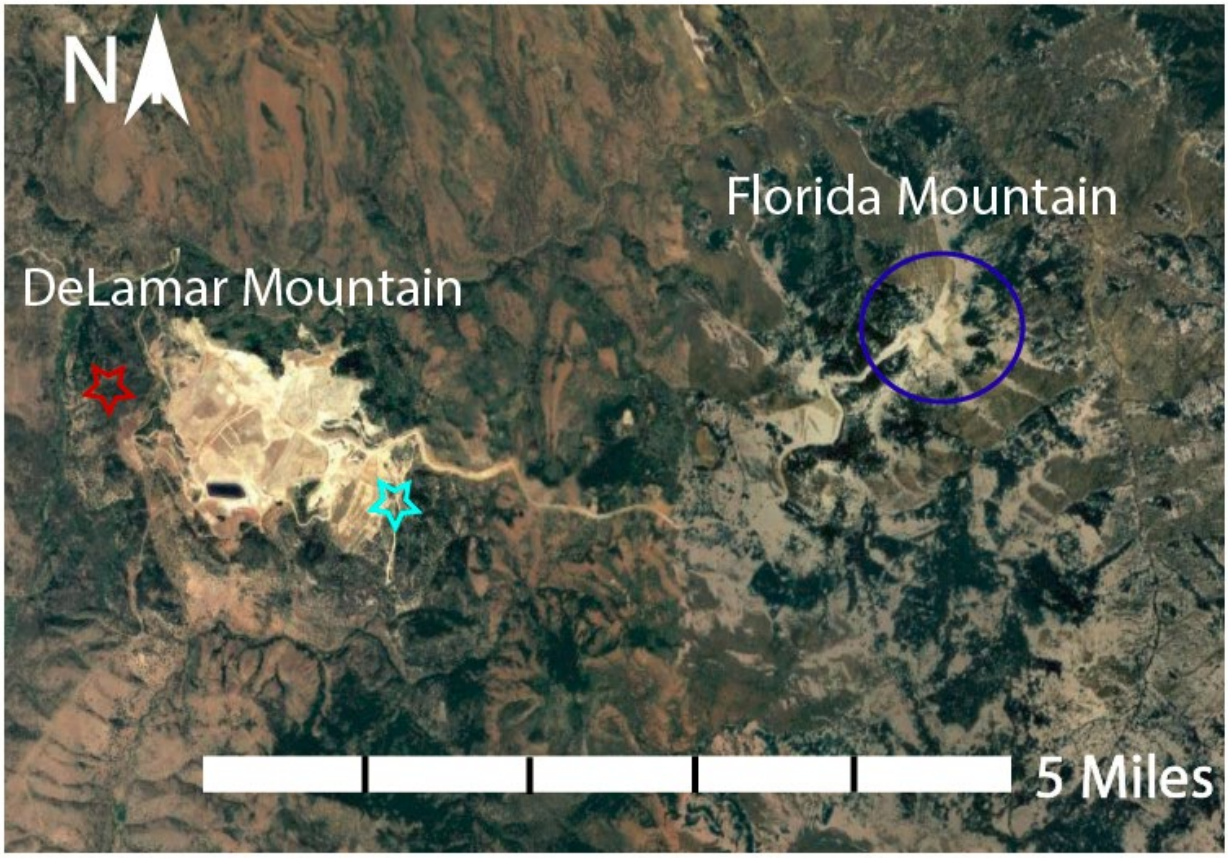

Figure 12. Google Earth image of DeLamar Mountain (left side) and Florida Mountain (right side; blue circle. Figs. 7, 8). Five-mile scale bar has one-mile increments. Red star is the approximate location of the Deadwood Ridge mapping area (Fig. 10) and light blue star is the approximate location of the Sullivan Gulch mapping area (Fig. 11).

Methodology

Sample Preparation

Once the samples were collected, they were sent back to Auburn University so that they could be prepared for future analyses. Billets were cut from the core slabs using a tile saw and sent to Spectrum Petrographics Inc. (Vancouver, WA) to be made into thin sections.

Petrographic Analyses

Petrographic analyses were done by using a Nikon Eclipse Ci-POL microscope paired with the Nikon DS-RI2 camera in the Auburn Department of Geosciences. This set up allowed for the capture of both transmitted and reflected light (RL) photomicrographs. Crossed polarized (XPL) transmitted light allowed for an initial analysis of matrix characteristics, mineralogy, mineralization, and oxidation severity. Reflected light analysis allowed for the observation of opaque phases such as sulfides. Images recorded during petrographic analysis were used to guide the subsequent geochemical analyses.

Electron Microprobe Analysis

Electron microprobe analysis (EMPA) was completed to observe textures, mineralogy, and to quantify the chemical composition of phases associated with the mineralization. Energy dispersive spectroscopy (EDS), wavelength dispersive spectrometry (WDS) and backscattered electron (BSE) imaging were performed using the JEOL JXA-8600 electron microprobe in the Auburn University Electron Microprobe Analysis Lab (AU-EMPA). The Geller automation system with dPict32 was used for mapping, dQant32 for WDS, and dSpec for spectrometer and stage controls. Typically, a ~20 nA beam current and a 15 kV accelerating voltage were used during EDS and WDS analyses but increased to ~50 nA while collecting maps of elemental concentrations. The WDS maps were imported into ImageJ, to assign false color to concentration maps for interpretation. Gold, Ag, Ti, Fe, Cu, As, Se and S were measured in the sample sulfides in addition to natural, synthetic, and elemental

standards. Quantitative analyses were performed on minerals associated with high Au and Ag grades (e.g., pyrite, electrum, chalcocite, and silver phases).

Laser Ablation Inductively Coupled Plasma Mass Spectrometry

Trace element concentrations were also measured by Laser Ablation Inductively Coupled Plasma Mass Spectrometry (LA-ICP-MS) in the Auburn Laser Lab. Areas within pyrite and associated minerals were targeted based on the EMPA results and petrographic observations. Concentrations of Ti, Fe, Cu, Se, Ni, Zn, As, Ag, Sb, Au, and Pb were measured with a NWR193 193nm laser ablation system (Elemental Scientific Lasers, Inc.) coupled to an Agilent 7900 ICP-MS. Line and spot diameters were 25 μm and the laser conditions were 35% with a rep rate of 20 Hz. Reference material NIST 612 was analyzed at the beginning, middle, and end of the session. The raw data was processed using the iolite v.4 software.

Results

Petrography

Petrographic analyses of thin sections from all seven of the lithological units observed at Florida Mountain revealed a range of textures, mineral assemblages, and extent of oxidation. Descriptions of each thin section proceed from the bottom to the top of stratigraphy (Fig. 6).

Granodiorite (Kgd)

The Cretaceous granodiorite consists of a large proportion of quartz, feldspar, and plagioclase and minor muscovite and occasional pyrite. Hand sample observations

from core revealed areas with large amounts of cubed and aggregated pyrite. No sulfides or other phases that might contain Au, Ag mineralization were observed within this unit.

Lower Basalt (Tlb)

The Lower Basalt unit was seen in the core that was extracted and logged at the deposit only in hole FM-4 at 719 ft and hole FM-11 at 392.5 ft. This basalt is composed of olivine, pyroxene, and plagioclase. There are highly oxidized areas; in thin section, oxidation occurs in erratic patches that comprise 30-50% of a sample (Fig. 13). There are small amounts of pyrite and ilmenite throughout the unit. The pyrite occurs in small clusters or aggregates (Fig. 14).

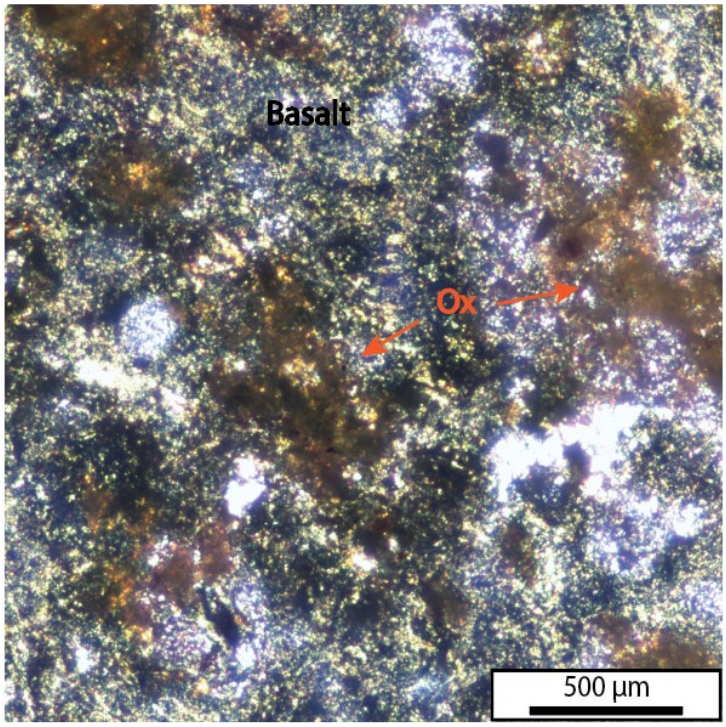

Figure 13. The rarely seen Lower Basalt unit (Tlb) sampled from hole FM-4 at 719 ft.

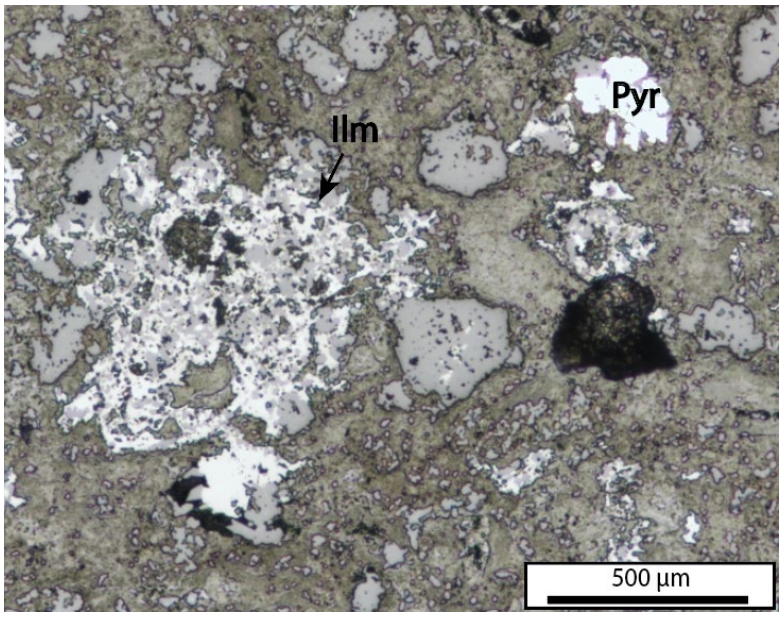

Figure 14. Pyrite (Pyr) cluster and ilmenite (Ilm) in the Tlb unit from hole FM-4 at 719.0 ft.

Quartz Latite (Tql)

The matrix of the quartz latite unit has approximately equal parts orthoclase and plagioclase (Table 1). Oxidation of the Tql samples varied from moderate to high. The oxidation was observed on the surface of grains and in a vein-like pattern through different grains, which was not mineral-specific. The sample collected from hole FM-11 at 298 ft also contained a collection of nodules that were not seen in any other samples (Fig. 15). Oxidation occurred on these nodules in addition to the oxidation occurring with the rest of the sample. The amount of quartz eyes (anhedral phenocrysts) observed ranged up to ~12%.

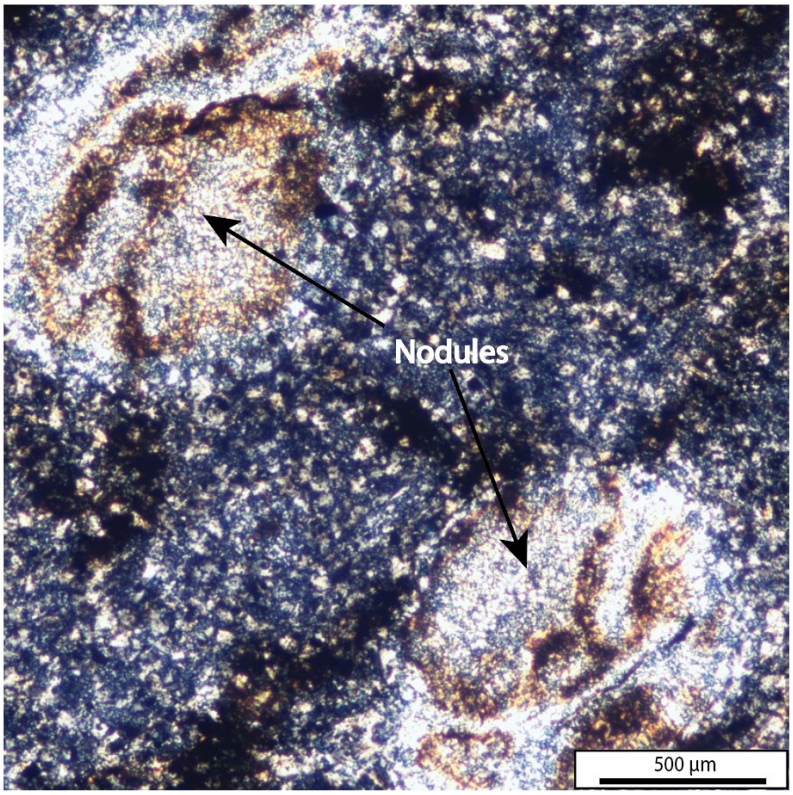

Figure 15. Representative nodules seen in the FM-11 Tql unit at 298 ft.

Pyrite in this unit is dominantly cubic, which makes up <1 up to ~20% of the thin sections examined (Figs. 16B and 16D; Table 1). Some grains are shards rather than perfect cubes. Other minerals occur included within the pyrite grains, such as sphalerite, galena, electrum, and silver phases. Thin sections of Tql had overall the highest amount of pyrite of all the units.

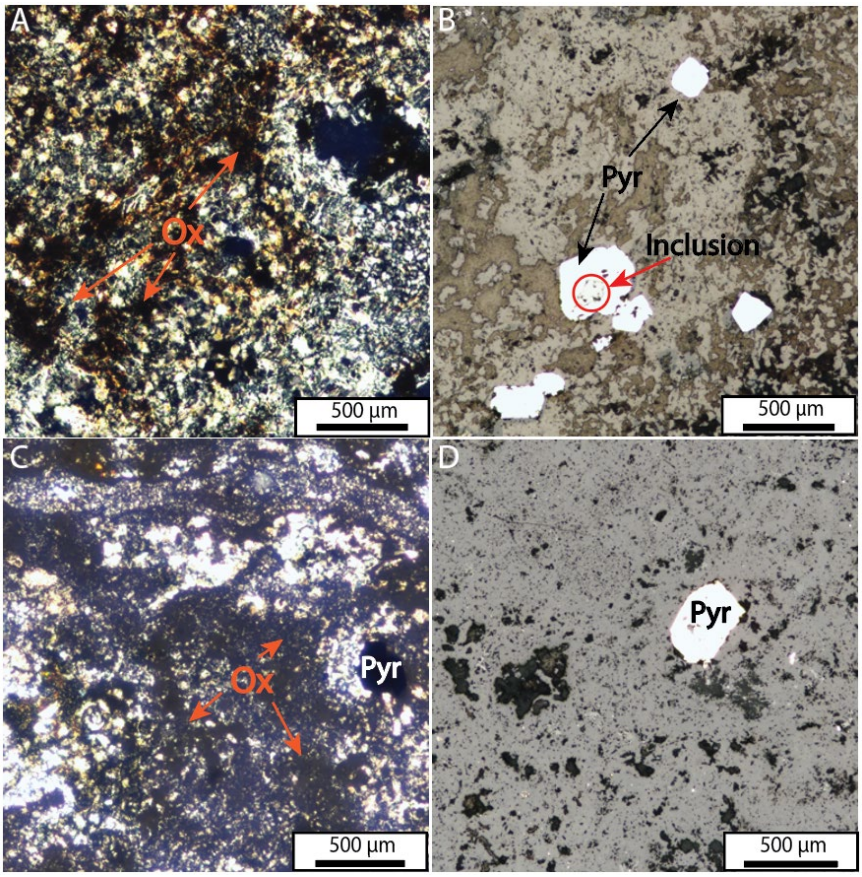

Figure 16. There is a range of pyrite (pyr) abundance and extent of oxidation (ox) throughout Tpl. Panels **A** and **B** are photomicrographs from the FM-2 Tql unit at 331.5 ft. in XPL (**A**) and RL (**B**). The sample had a high proporiton of pyrite and high oxidaiton. **C** and **D** show photomicrographs from the FM-12 Tql unit at 312 ft. in XPL (**C**) and RL (**D**). This sample has less pyrite and moderate oxidation.

Tql	Low = 0-15%, Low-Mod = 15-30%, Mod = 30-45%, Mod-High = 45-60%, High = 60-100%, NP = Not Present									
				Percentages						
Drill Hole	Depth (ft)	Qtz (Matr)	Qtz (Eyes)	Plag	Orth	Cal	Pyr	Ilm	Acc	Oxidation
FM-1	342.5	~10	~8	32	33	<1	~12	~4	~2	Mod
FM-2	331.5	~8	~1	35	34	<1	~16	~5	~3	High
FM-4	542.5	~12	~12	33	33	~4	~2	~2	<1	Mod-High
FM-10	303.0	~9	~2	33	35	<1	~16	~3	~2	Mod
FM-11	298.0	~5	<1	41	42	<1	~3	~5	<1	Mod-High
FM-12	312.0	~10	~2	37	41	~3	~6	<1	<1	Mod
FM-25	213.0	~8	~5	35	37	~4	~8	<1	~1	Mod-High
FM-26	*131.5	~9	~3	37	39	~2	~7	<2	~3	Mod-High
	302.5	~7	~6	38	40	<1	~8	<1	~1	Mod-High
FM-51	652.0	~5	~4	48	43	0	<1	0	0	Mod-High

Table 1. Proportions of minerals present in the thin sections of the Tql unit. Abbreviations: Qtz (Matr)=Quartz matrix; Qtz (Eyes)=Quartz eyes; Plag=Plagioclase; Orth=Orthoclase; Cal=Calcite; Pyr=Pyrite; Ilm=Ilmenite; Acc=Accessory minerals. Asterisk (*) indicates the sample was analyzed by EMPA.

Porphyritic Latite (Tpl)

In the field, the Tpl unit is visually similar to Tql, but when observed petrographically, the Tpl appeared less oxidized overall (Fig. 17). Quartz eyes are abundant (1-10%) in some samples, but lower (<1%) in others. Pyrite mineralization in the Tpl was relatively low, within range of <1 to ~8%. Pyrite most commonly occurred as cubes in veins but also disseminated throughout the matrix (Fig. 18). Accessory minerals occur as inclusions in the larger cubic pyrite. See Table 2 for the mineralogical observations of Tpl.

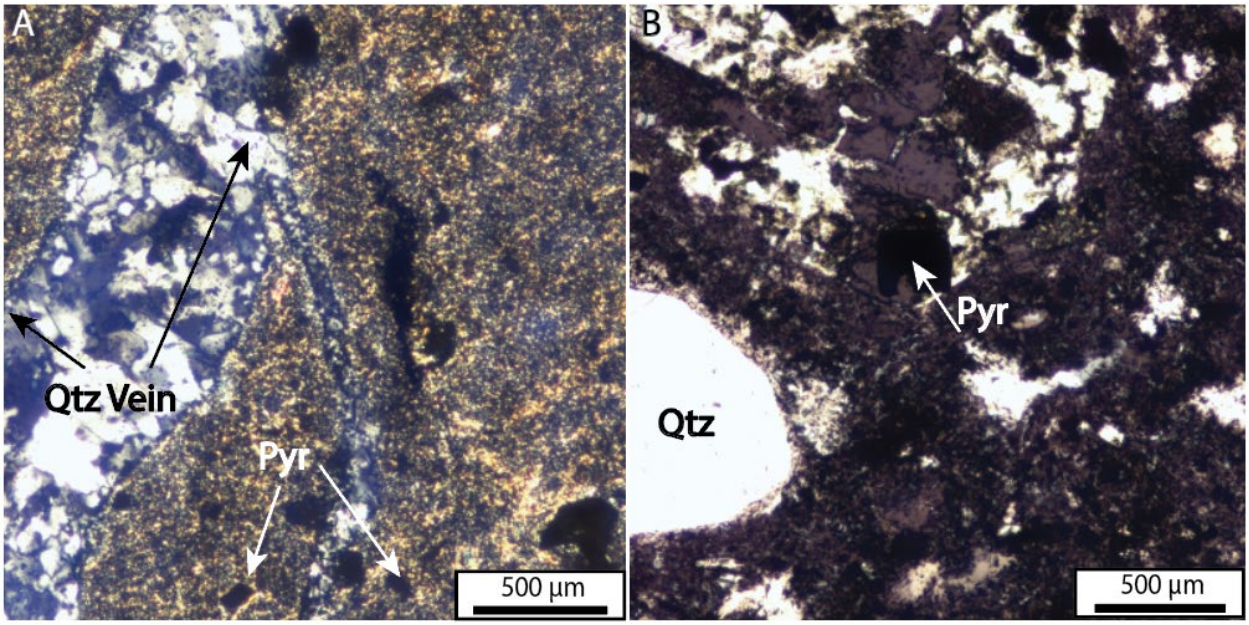

Figure 17. **A)** XPL photomicrograph of FM-26 Tpl unit at 377.5 ft showing moderate oxidation of the unit. **B)** PPL photomicrograph of FM-3 Tpl unit at 910 ft showing moderate oxidation of the unit.

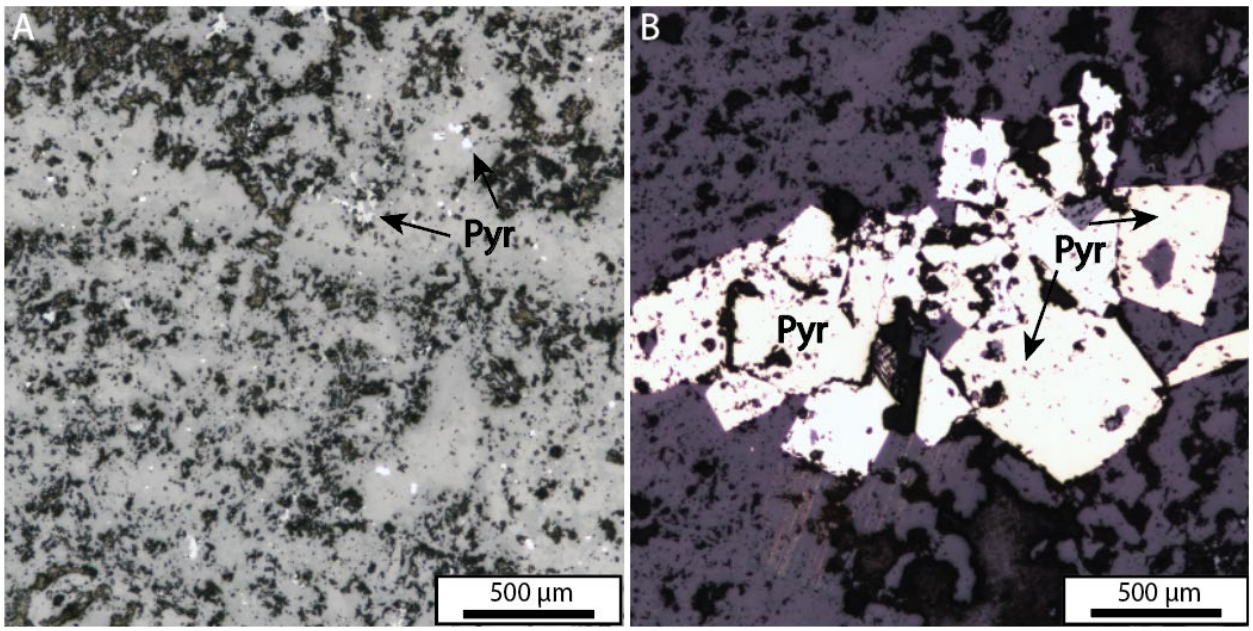

Figure 18. Reflected light photomicrographs of FM-2 Tpl unit at 749.5 ft. **A)** disseminated pyrite; **B)** clusters of cubic pyrite with the darker voids and some replacement (gray).

Tpl		Low = 0-15%, Low-Mod = 15-30%, Mod = 30-45%, Mod-High = 45-60%, High = 60-100%, NP = Not Present								
					Percentages					
Drill Hole	Depth (ft)	Qtz (Matr)	Qtz (Eyes)	Plag	Orth	Cal	Pyr	Ilm	Acc	Oxidation
FM-1	365.5	~5	~1	43	45	0	~3	<1	<1	High
FM-2	749.5	~5	<1	43	43	<1	~8	<1	~1	Mod
FM-3	*910.0	~4	~8	41	44	~2	~2	<1	~2	Low-Mod
FM-4	656.0	~4	~10	40	41	~2	~2	<1	~1	Low
FM-10	686.5	~5	~1	45	45	~1	~2	0	~1	Mod
FM-12	350.5	~5	~8	40	40	<1	~3	<1	~1	Low
FM-25	356.5	~5	<1	46	46	<1	~1	<1	<1	Mod
FM-26	377.5	~5	<1	47	47	<1	<1	0	0	Mod

Table 2. Proportions of minerals present in the thin sections of the Tpl unit. Abbreviations: Qtz (Matr)=Quartz matrix; Qtz (Eyes)=Quartz eyes; Plag=Plagioclase; Orth=Orthoclase; Cal=Calcite; Pyr=Pyrite; Ilm=Ilmenite; Acc=Accessory minerals. Asterisk (*) indicates the sample was analyzed by EMPA.

Tuff Breccia (Ttb)

The clasts of the Ttb unit consist primarily of fragments from Tql and Tpr with smaller amounts of Kdg (Table 3). Elsewhere in the Silver City area, the Ttb also includes Tlt (Tertiary Lower Tuff) and Ts (Tertiary Lacustrine sediments) but these units

are also not observed in the field at Florida Mountain (Table 3). The unit is highly oxidized, likely due to its permeability and heterogeneity.

Pyrite abundance in this unit was relatively low (<1- ~3%) apart from a sample taken from FM-51 at 509.0 ft, which contained ~10%. Cubic pyrite dominates the and often exists in clusters with smaller shards in the vicinity (Fig. 19).

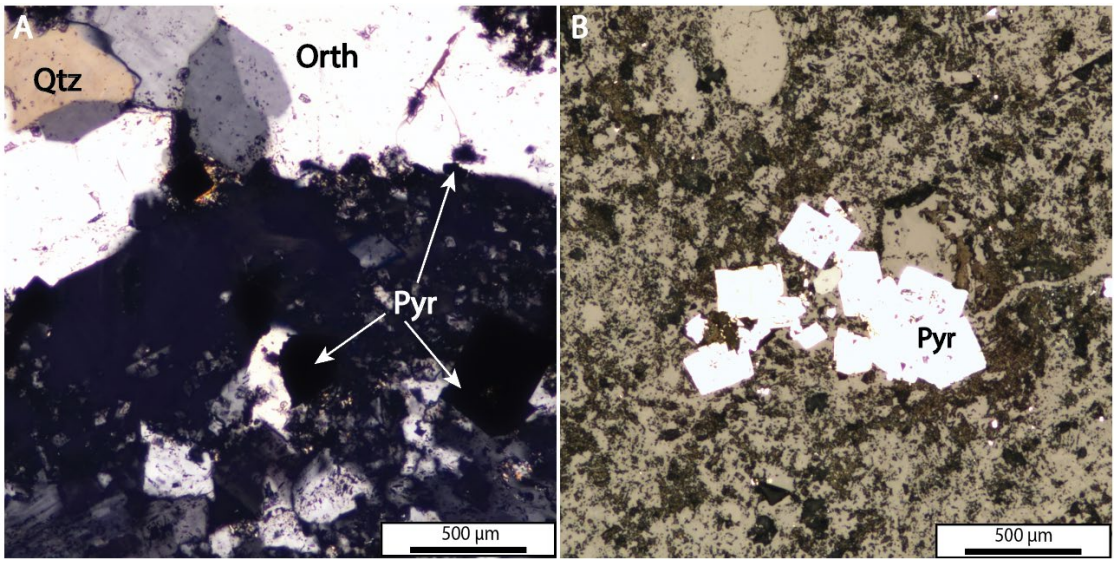

Figure 19. Photomicrographs of FM-51 Ttb unit at 509 ft. in XPL **A)** and RL **B)**.

Ttb	Low = 0-15%, Low-Mod = 15-30%, Mod = 30-45%, Mod-High = 45-60%, High = 60-100%, NP = Not Present									
					Percentages					
Drill Hole	Depth (ft)	Kgd	Tlt	Ts	Tql	Tpr	Pyr	Ilm	Acc	Oxidation
FM-1	*291.5	Low	NP	NP	Mod-High	Mod-High	~3	<1	<1	High
FM-2	270.5	Low	NP	NP	Mod-High	Mod-High	~1	<1	~1	High
FM-10	268.0	Low	NP	NP	Mod-High	Mod-High	<1	~3	<1	High
	387.5	Low	NP	NP	Mod-High	Mod-High	<1	~2	~1	High
FM-11	783.0	Low	NP	NP	Mod-High	Mod-High	~2	~1	<1	High
FM-51	509.0	Low	NP	NP	Mod-High	Mod-High	~10	<1	~2	High

Table 3. Proportions of minerals and rocks present as clasts in the thin sections of the Ttb unit. Abbreviations: Kgd=Granodiorite; Tql=Quartz latite; Tpr=Porphyritic rhyolite; Pyr=Pyrite; Ilm=Ilmenite; Acc=Accessory minerals. Asterisk (*) indicates the sample was analyzed by EMPA.

Porphyritic Rhyolite (Tpr)

The matrix of the Tpr is about equal parts quartz and orthoclase (Table 4). The oxidation of this unit overall is low to moderate. There is one exception: FM-4 at 495.5 ft represents a highly oxidized vein. Euhedral quartz coincides with a finer matrix of quartz and orthoclase (Fig. 20). Some vein structures are show comb quartz as well.

Pyrite abundance ranges from <1 – 12% and exists mainly as cubes and shards (Fig. 21). Fine-grained minerals are included within or attached to the rim of some pyrite grains seen in this unit. Some pyrite infills voids or cracks in the rock.

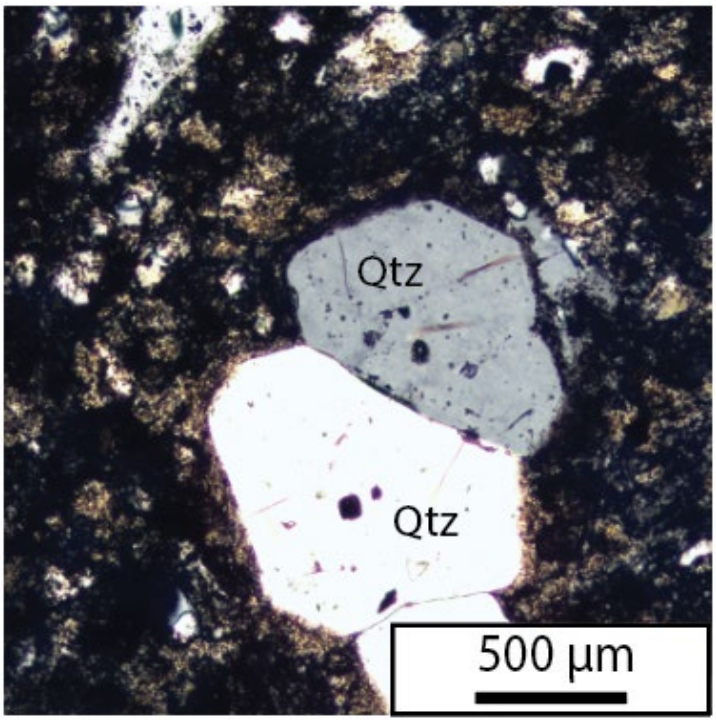

Figure 20. XPL photomicrograph showing euhedral quartz within a finer matrix sampled from hole FM-2 in the Tpr unit at 248 ft.

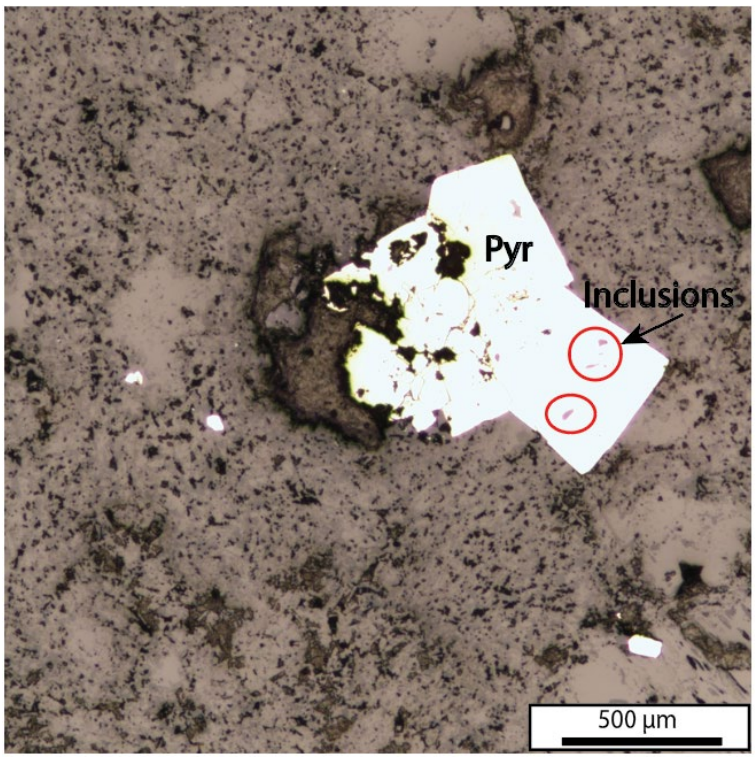

Figure 21. RL photomicrograph from hole FM-10 in the Tpr unit at 461 ft. The darker spots on the pyrite grain are inclusions, voids or replacement (e.g., red circles).

Tpr	Low = 0-15%, Low-Mod = 15-30%, Mod = 30-45%, Mod-High = 45-60%, High = 60-100%, NP = Not Present									
				Percentages						
Drill Hole	Depth (ft)	Qtz (Matr)	Qtz (Eyes)	Plag	Orth	Cal	Pyr	Ilm	Acc	Oxidation
FM-1	*253.0	35	~6	~4	45	0	~8	<1	<1	Low
FM-2	*248.0	35	~8	~8	40	~2	~7	<1	~1	Low
FM-3	102.0	43	~8	~1	45	~1	<1	~2	0	Mod
	*336.0	35	~12	~5	40	~2	~4	~2	<1	Low
FM-4	495.5	30	~15	~8	38	~3	~4	~4	<1	High
FM-10	461.5	32	~5	~5	43	~3	~10	<1	~3	Low
FM-50	*179.5	53	~1	~1	55	<1	~1	0	0	Mod
	345.0	52	~1	<1	56	~1	<1	0	0	Mod
FM-51	485.5	44	~10	~3	44	~2	~12	0	~1	Mod

Table 4. Proportions of minerals present in the thin sections of the Tpr unit. Abbreviations: Qtz (Matr)=Quartz matrix; Qtz (Eyes)=Quartz eyes; Plag=Plagioclase; Orth=Orthoclase; Cal=Calcite; Pyr=Pyrite; Ilm=Ilmenite; Acc=Accessory minerals. Asterisk (*) indicates the sample was analyzed by EMPA.

Banded Rhyolite (Tbr)

The Tbr unit matrix is composed of approximately equal amounts of quartz and orthoclase (Table 5). The oxidation of this unit overall is low to moderate, although a few samples showed a higher amount of oxidation (FM-11 at 179.5 ft. and FM-25 at 88.5 ft.). These samples had especially severe oxidation within the fine matrix and pyrite grains (Fig. 22).

The pyrite abundance of the Tbr unit ranges from <1 to ~8% and occurs as smaller disseminated cubes and shards or larger, fractured grains (Fig. 23). Few accessory minerals were observed in this unit and many of those occurred as inclusions in the pyrite grains.

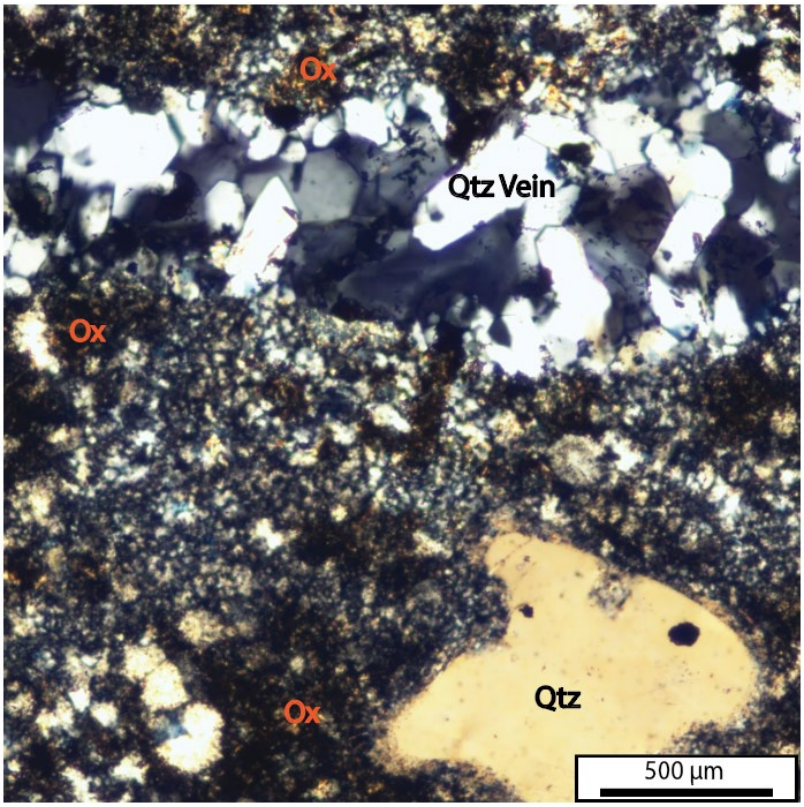

Figure 22. This sample from hole FM-25 in the Tbr unit at 20.5 ft shows high amounts of oxidation on the finer matrix material (photomicrograph in XPL). Also seen is an embayed and partially resorbed quartz (Qtz) grain next to a quartz vein.

Tbr	Low = 0-15%, Low-Mod = 15-30%, Mod = 30-45%, Mod-High = 45-60%, High = 60-100%, NP = Not Present									
		Percentages								
Drill Hole	Depth (ft)	Qtz (Matr)	Qtz (Eyes)	Plag	Orth	Cal	Pyr	Ilm	Acc	Oxidation
FM-1	86.5	40	<1	~2	55	~2	<1	<1	0	Mod
FM-2	59	35	~10	~5	45	~2	<1	~2	0	Low
FM-4	102	35	~8	~8	40	~5	~1	~1	<1	Low
	538	35	~7	~10	45	~1	~1	~2	0	Mod
FM-10	*21.5	42	~10	~10	45	~2	~1	<1	0	Low
	142.5	43	~4	~5	43	<1	<1	~3	0	Mod
FM-11	*179.5	40	~4	~4	42	~2	~6	~2	~3	High
FM-12	11.5	30	~15	~10	35	~2	~3	~3	<1	Mod
FM-25	20.5	34	~10	~6	36	~5	~5	~2	<1	Mod
	88.5	35	~8	~5	45	~1	~6	~2	~1	Mod-High
FM-26	61.5	42	~10	~8	46	~2	~1	~1	0	Low

Table 5. Table with the percentages of minerals present in the thin sections of the Tpr unit. Abbreviations: Qtz (Matr)=Quartz matrix; Qtz (Eyes)=Quartz eyes; Plag=Plagioclase; Orth=Orthoclase; Cal=Calcite; Pyr=Pyrite; Ilm=Ilmenite; Acc=Accessory minerals. Asterisk (*) indicates the sample was analyzed by EMPA.

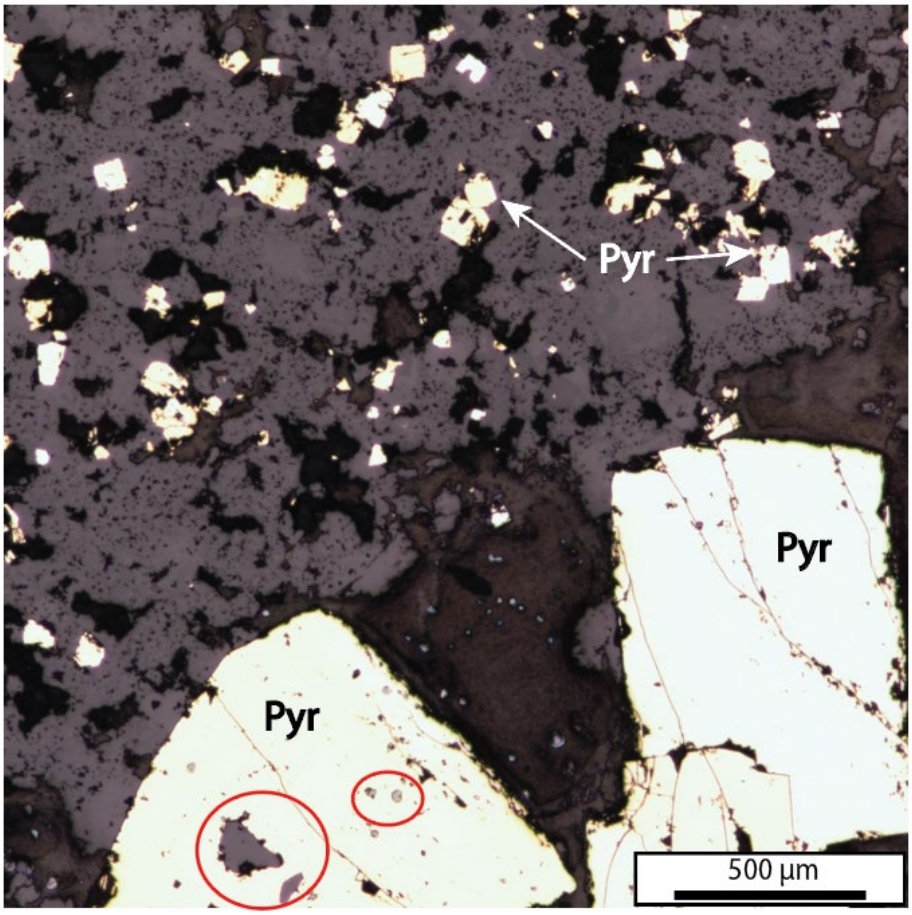

Figure 23. RL photomicrograph of a sample from hole FM-11 in the Tbr unit at 61.5 ft. Disseminated pyrite is seen next to larger, fractured pyrite grains. The left large grain shows accessory minerals as inclusions and replacement (red circle).

Summary: Petrographic Results

- Pyrite occurs in a range of size and texture (small, disseminated cubes or shards; large, fractured grains; aggregates of smaller cubes).
- Other sulfides are present in the drill core from Florida Mountain as well. Galena and sphalerite were observed in the banded rhyolite (Tbr) and quartz latite (Tql) units.
- Silver phases with a spectrum of Ag-Se-S contents were observed in samples from Tql, the porphyritic rhyolite (Tpr), and Tbr.
- The Tql unit had the highest amount of pyrite.
- Tql also had the highest proportion of accessory minerals including inclusions or replacement within pyrite.
- Oxidation was moderate to high for the samples with more pyrite and accessory minerals and oxidized nodules occur in the latite unit.
- The Tbr was the most oxidized sample characterized.

Trace Element Geochemistry and Imaging

Electron Microprobe Analysis

A selection of thin sections was chosen for EMPA to cover a range of oxidation, composition, and stratigraphic location. The suite of elements measured included S, Ti, Au, Ag, Fe, Cu, As, and Se. EDS spectra determined whether WDS would be useful. EDS investigations showed that the minerals within, between, or at the rim of the pyrite grains were electrum, sphalerite, silver phases, and galena. Silver phases are within a spectrum of Ag-Se-S.

There were a few unusual grains analyzed by EDS to observe the spectra. For example, the sample from hole FM-50 within Tpr contained pyrite cubes that did not have sulfur concentrations measurable by EMPA (Table 7); the grains appeared to be normal pyrite grains, none were found with any significant amount of sulfur. The samples from FM-26 Tql and FM-3(b) Tpr each contained a mineral with sole Cu peaks (Table 6 & 7 respectively). These grains seemed to be pure Cu filling a void (Fig. 24). FM-11 Tbr contained some grains with only Cu and S, indicating the presence of chalcocite. Future studies should consider the role of Cu in this system as this study was only able to evaluate the relative timing of Cu phases without more extensive analysis (see Discussion)

Label	Depth (ft)	Point #	S (wt. %)	Ti (wt. %)	Au (wt. %)	Ag (wt. %)	Fe (wt. %)	Cu (wt. %)	As (wt. %)	Se (wt. %)	Total (wt. %)	Grain
FM-26 Tql	131.5	1	51.57	0.02	0.06	0.00	43.99	0.00	0.11	0.02	95.76	Pyr
FM-26 Tql	131.5	2	0.04	0.00	0.03	0.00	2.08	59.41	0.00	0.08	61.64	Cu
FM-26 Tql	131.5	3	51.17	0.00	0.00	0.01	45.64	0.00	0.00	0.04	96.86	Pyr
FM-26 Tql	131.5	4	46.61	0.01	0.00	0.00	43.46	0.00	0.40	0.08	90.56	Pyr
FM-26 Tql	131.5	5	0.24	0.02	55.69	44.72	0.49	0.00	0.00	0.11	101.27	AuAg
FM-26 Tql	131.5	6	51.06	0.00	0.00	0.01	45.15	0.04	0.07	0.00	96.33	Pyr
FM-26 Tql	131.5	7	52.01	0.00	0.02	0.03	45.17	0.04	0.32	0.05	97.63	Pyr
FM-26 Tql	131.5	8	2.44	0.00	53.77	41.68	2.37	0.01	0.42	0.07	100.77	AuAg
FM-11 Tbr	179.5	1	48.37	0.00	0.00	0.00	44.76	0.07	0.36	0.01	93.58	Pyr
FM-11 Tbr	179.5	2	50.60	0.03	0.00	0.00	45.09	0.00	0.31	0.00	96.03	Pyr
FM-11 Tbr	179.5	3	20.91	0.00	0.08	66.81	12.77	0.11	0.58	5.54	106.80	Ag Phase
FM-11 Tbr	179.5	4	49.99	0.03	0.00	0.00	44.24	0.00	0.40	0.00	94.66	Pyr
FM-11 Tbr	179.5	5	28.93	0.00	0.00	0.08	15.18	49.87	0.25	0.00	94.30	Cpy
FM-11 Tbr	179.5	6	50.10	0.04	0.00	0.00	43.88	0.03	0.00	0.00	94.05	Pyr
FM-11 Tbr	179.5	7	8.86	0.05	0.04	82.38	1.59	0.00	0.10	7.60	100.62	Ag Phase
FM-11 Tbr	179.5	8	51.27	0.00	0.06	0.02	44.73	0.05	0.11	0.00	96.24	Pyr
FM-11 Tbr	179.5	9	50.86	0.00	0.00	0.00	45.19	0.14	0.02	0.04	96.25	Cc
FM-11 Tbr	179.5	10	20.32	0.00	0.03	0.05	0.39	70.50	0.41	0.10	91.80	Cc
FM-11 Tbr	179.5	11	25.12	0.00	0.00	0.03	0.45	64.50	0.00	0.00	90.11	Pyr
FM-11 Tbr	179.5	12	51.67	0.03	0.00	0.00	45.13	0.00	0.39	0.00	97.22	Pyr
FM-11 Tbr	179.5	13	16.91	0.00	0.60	63.24	9.25	0.55	0.31	6.49	97.35	Ag Phase
FM-11 Tbr	179.5	14	50.22	0.00	0.06	0.01	45.10	0.00	0.15	0.04	95.59	Pyr

Table 6. EMPA data for FM-26 Tql and FM-11 Tbr. Minerals names were given based off the percentages seen during the analysis of the samples. Pyr = pyrite, Cpy = chalcopyrite, Cu = copper, Cc = Chalcocite, AuAg = electrum, Ag phase = silver phase.

Label	Depth (ft)	Point #	S (wt. %)	Ti (wt. %)	Au (wt. %)	Ag (wt. %)	Fe (wt. %)	Cu (wt. %)	As (wt. %)	Se (wt. %)	Total (wt. %)	Grain
FM-3(b) Tpr	538.0	1	47.83	0.00	0.00	0.05	42.71	0.00	0.00	0.00	90.59	Pyr
FM-3(b) Tpr	538.0	2	50.76	0.05	0.00	0.03	42.58	0.02	0.25	0.09	93.77	Pyr
FM-3(b) Tpr	538.0	3	0.00	46.11	0.00	0.01	0.46	0.03	0.00	0.00	46.61	Pyr
FM-3(b) Tpr	538.0	4	49.65	0.03	0.06	0.05	43.21	0.00	0.65	0.01	93.66	Pyr
FM-3(b) Tpr	538.0	5	50.68	0.03	0.03	0.04	42.80	0.03	0.45	0.02	94.08	Pyr
FM-3(b) Tpr	538.0	6	50.29	0.00	0.00	0.00	41.83	0.00	0.31	0.01	92.43	Pyr
FM-3(b) Tpr	538.0	7	0.00	0.00	0.00	0.03	0.19	89.50	0.00	0.00	89.72	Cu
FM-3(b) Tpr	538.0	8	51.13	0.00	0.06	0.00	43.74	0.00	0.02	0.02	94.97	Pyr
FM-3(b) Tpr	538.0	9	13.01	0.11	0.50	74.46	3.29	6.08	0.00	6.14	103.61	Ag Phase
FM-1 Tpr(b)	253.0	1	50.83	0.03	0.00	0.00	46.19	0.00	0.50	0.00	97.55	Pyr
FM-1 Tpr(b)	253.0	2	51.30	0.00	0.00	0.01	45.71	0.00	0.02	0.00	97.03	Pyr
FM-1 Tpr(b)	253.0	3	38.72	0.04	0.04	7.39	30.37	0.06	2.65	1.26	80.54	Ag w/ Pyr
FM-1 Tpr(b)	253.0	4	51.35	0.02	0.09	0.00	45.89	0.08	0.00	0.00	97.44	Pyr
FM-1 Tpr(b)	253.0	5	51.36	0.00	0.00	0.02	45.41	0.00	0.29	0.00	97.08	Pyr
FM-1 Tpr(b)	253.0	6	50.98	0.02	0.00	0.00	45.79	0.00	0.07	0.00	96.86	Pyr
FM-2 Tpr(a)	248.0	1	52.48	0.00	0.08	0.04	45.87	0.00	0.08	0.00	98.56	Pyr
FM-2 Tpr(a)	248.0	2	50.05	0.00	0.04	0.04	45.80	0.00	1.42	0.00	97.35	Pyr
FM-2 Tpr(a)	248.0	3	50.64	0.03	0.00	0.03	45.71	0.05	0.66	0.00	97.12	Pyr
FM-2 Tpr(a)	248.0	4	50.23	0.01	0.05	0.04	45.22	0.03	0.00	0.00	95.58	Pyr
FM-2 Tpr(a)	248.0	5	50.63	0.00	0.00	0.00	45.41	0.06	0.00	0.00	96.10	Pyr
FM-2 Tpr(a)	248.0	6	51.63	0.01	0.05	0.01	45.94	0.00	0.00	0.05	97.69	Pyr
FM-2 Tpr(a)	248.0	7	48.62	0.00	0.00	0.00	42.41	0.00	0.17	0.10	91.30	Pyr
FM-2 Tpr(a)	248.0	8	52.41	0.00	0.00	0.02	45.13	0.01	0.42	0.07	98.05	Pyr
FM-50 Tpr	179.5	1	0.08	0.01	0.06	0.04	46.90	0.05	1.39	0.00	48.53	Pyr (-S)
FM-50 Tpr	179.5	2	0.08	0.00	0.00	0.03	49.37	0.03	0.30	0.00	49.80	Pyr (-S)
FM-50 Tpr	179.5	3	0.06	0.00	0.00	0.00	51.17	0.06	0.42	0.06	51.76	Pyr (-S)
FM-50 Tpr	179.5	4	32.15	0.00	0.00	0.04	48.64	0.00	0.31	0.09	81.22	Pyr (-S)
FM-50 Tpr	179.5	5	20.24	0.01	0.04	0.00	31.90	0.00	0.14	0.00	52.32	Pyr (-S)

Table 7. EMPA data for samples analyzed from the Tpr unit including FM-3(b) Tpr, FM-1 Tpr(b), FM-2 Tpr(a), FM-50 Tpr. Minerals names were given based off the percentages seen during the analysis of the samples. Pyr = pyrite, Cpy = chalcopyrite, Cu = copper, Cc = Chalcocite, AuAg = electrum, Ag phase = silver phase.

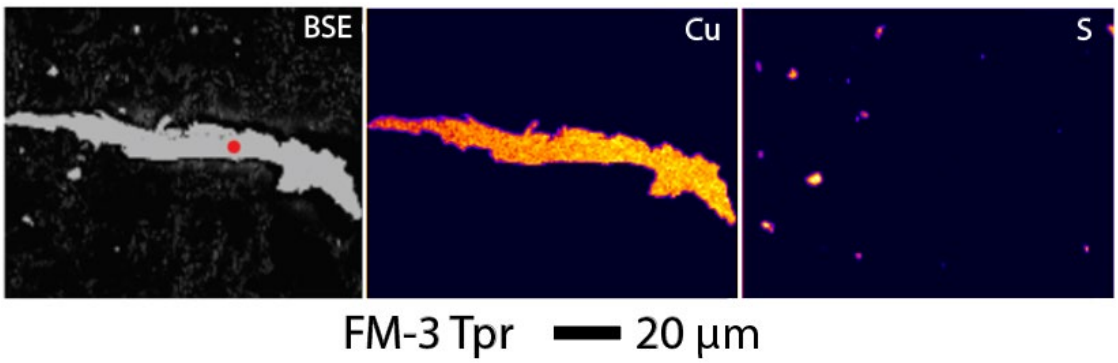

Figure 24. Elongated grain with ~89.5% Cu in FM-3 Tpr unit at 538 ft. The red dot shows point 7 on Table 7 of FM-3(b) Tpr.

Several silver phases were observed included within pyrite in the porphyritic rhyolite (Tpr) and banded rhyolite (Tbr) units in the uppermost portion of the stratigraphy (e.g., Fig. 25; sample FM-11 Tbr at 179.5 ft; Table 6). Aseto (2012) analyzed Ag phase minerals from high-grade veins at the neighboring deposit (War Eagle Mountain) and found that they contained varying proportions of Ag, S, and Se, within a continuum of Ag_2S, Ag_4SeS, and Ag_2Se (Fig. 26). The majority of the Ag phases characterized from the War Eagle samples have compositions between Ag_4SeS and Ag_2Se. Mason (2015) analyzed similar samples from the Black Jack-Trade Dollar high-grade vein at Florida Mountain with similar results. The Ag phase minerals analyzed in this study from lower-grade areas of Florida Mountain are consistent with the grains analyzed by Aseto (2012) and Mason (2015) from high-grade veins (Fig. 26).

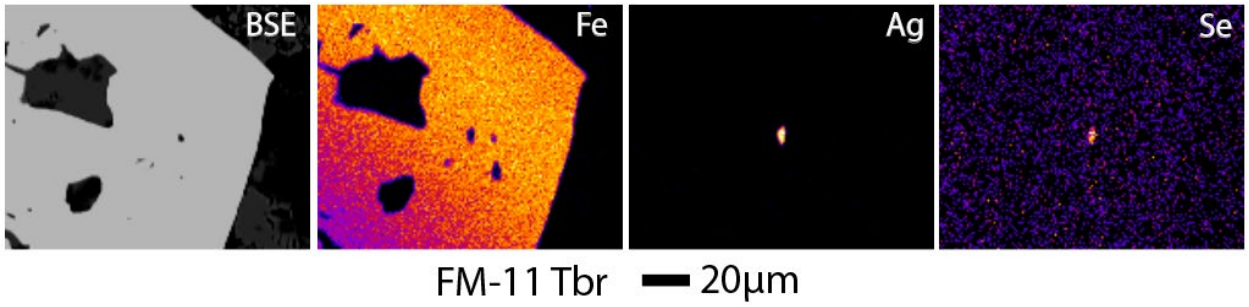

Figure 25. Back-scattered electron image and elemental maps of pyrite from the Tbr unit at hole FM-11,179.5 ft. A small silver phase containing selenium can be seen within this cubic pyrite.

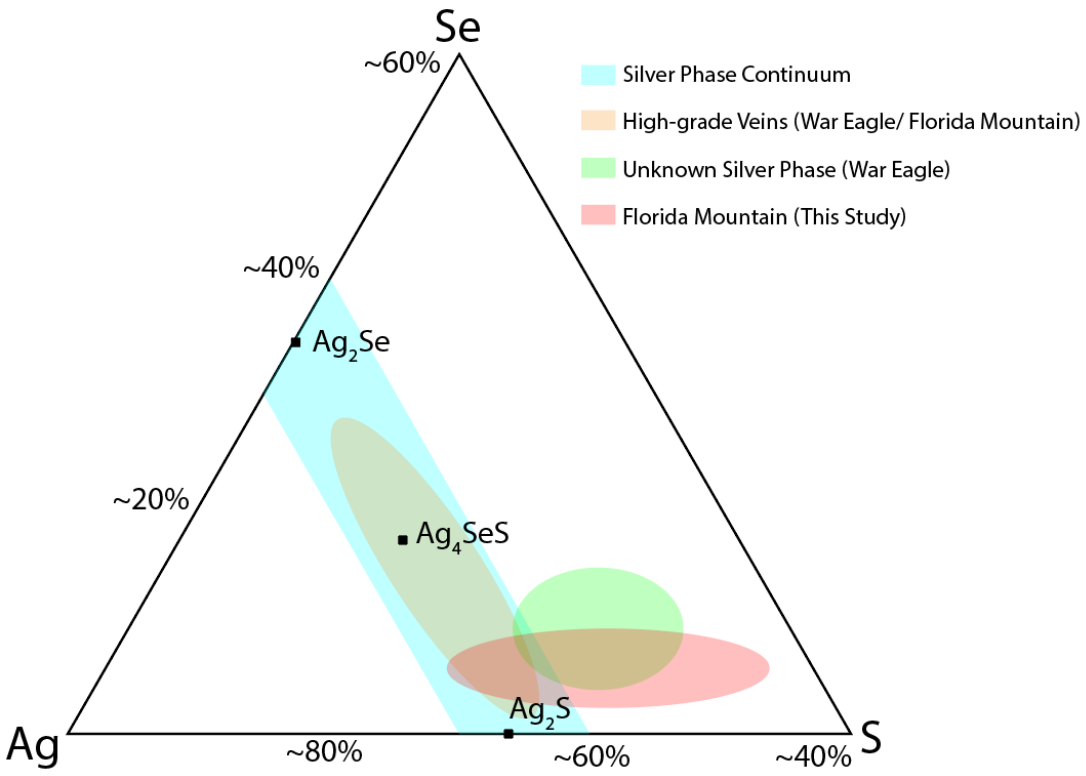

Figure 26. A schematic ternary diagram after Aseto (2012) and Mason (2015) comparing the composition of Ag phases containing Se and S from War Eagle (Aseto, 2012) and Florida Mountain (Mason, 2015; this study). Blue field represents the Ag-Se-S phase continuum described by (Petruk et al., 1974).

Electrum exists both as inclusions within pyrite but also between the grains of cubic pyrite clusters (e.g., FM-26 Tql at 131.5 ft; Figs. 27 & 28). Electrum grains analyzed by EMPA contain ~55% Au and ~45% Ag (Table 6, point 5 of the Tql group).

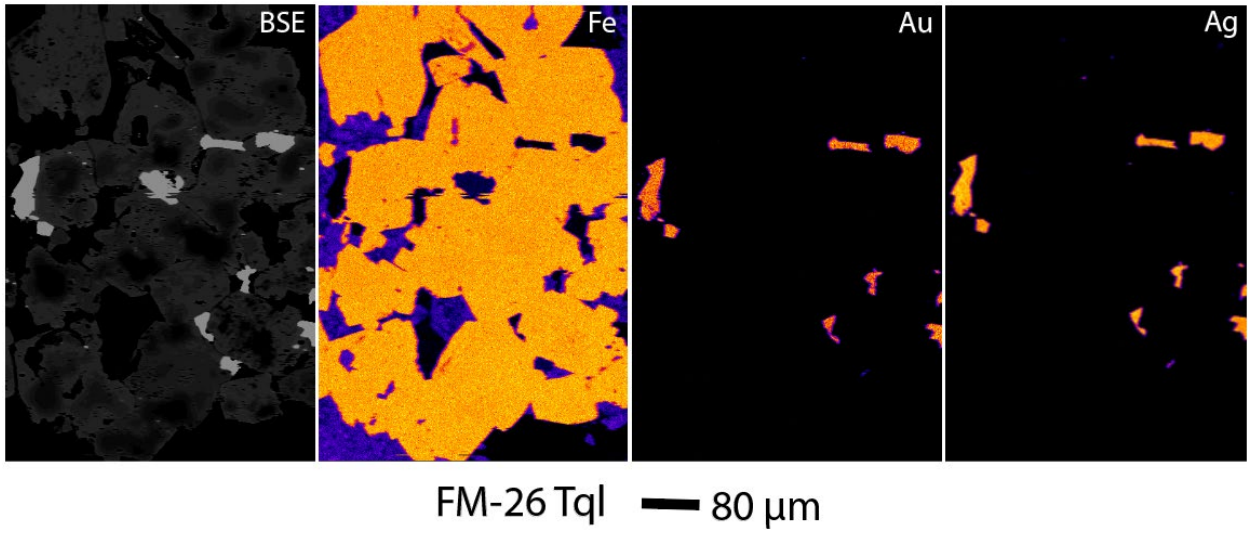

Figure 27. Electrum between the grains of a cluster of cubic pyrite in sample FM-26 Tql (131.5 ft).

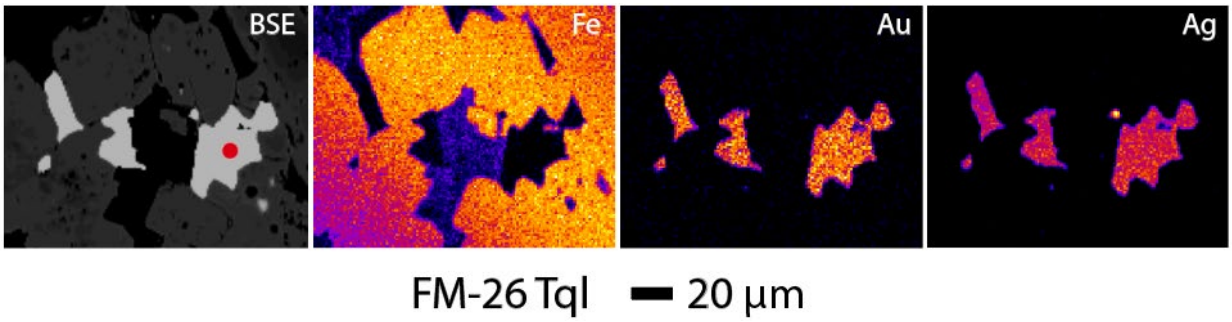

Figure 28. Electrum within a pyrite cluster in the Tql unit from sample FM-26 (131.5 ft). Red dot in the BSE shows the location of an WDS analysis. Electrum contains ~55% Au and ~45% Ag (Table 6, Point 5 of FM-26 Tql).

Trace Element Concentrations Measured by LA-ICP-MS

Additional trace element measurements were performed by LA-ICP-MS to further characterize the pyrite and its associated phases. Metal concentrations along line scans are reported in Figures 30, 32, 34, 36, 38; spot and line locations are illustrated in the images of Figures 29, 31, 32, 33, 35, 37. Appendix B contains detailed tables of LA-ICP-MS results. The pyrites analyzed (n=9) contained a wide range of concentrations of Au, Ag, Pb, Cu, Zn, As, and Se. Some pyrite grains (e.g., FM-25(b) Tbr, Fig. 29) with no

inclusions contained low concentrations (<0.5 ppm) of Au (e.g., FM-25(b) Tbr, Fig. 30) while others with relatively large metal-rich inclusions (e.g., FM-4 Tpr, Fig. 31 & 32) had a higher concentration (>1.0 ppm) of Au and Ag within the pyrite itself (e.g., FM-4 Tpr, Fig. 34). The pyrite grain from the FM-12 Tpl unit (Fig. 35) contained multiple inclusions with elevated levels of Au and Ag, but the pyrite itself had relatively low Au and Ag (e.g., FM-12 Tpl, Fig. 36).

There are three main observations from the LA-ICP-MS trace element data: 1) there are trace amounts of Au and Ag in many pyrite grains, which can vary between the core and rim of an individual grain; 2) some grains have inclusions rich in Au, Ag, Cu, Pb, Zn and the surrounding pyrite only contains trace amounts of Au and Ag; 3) there are pyrite grains with inclusions rich in Au, Ag, Cu, Pb, Zn but the surrounding pyrite grain has elevated concentrations of Au and Ag near the inclusion.

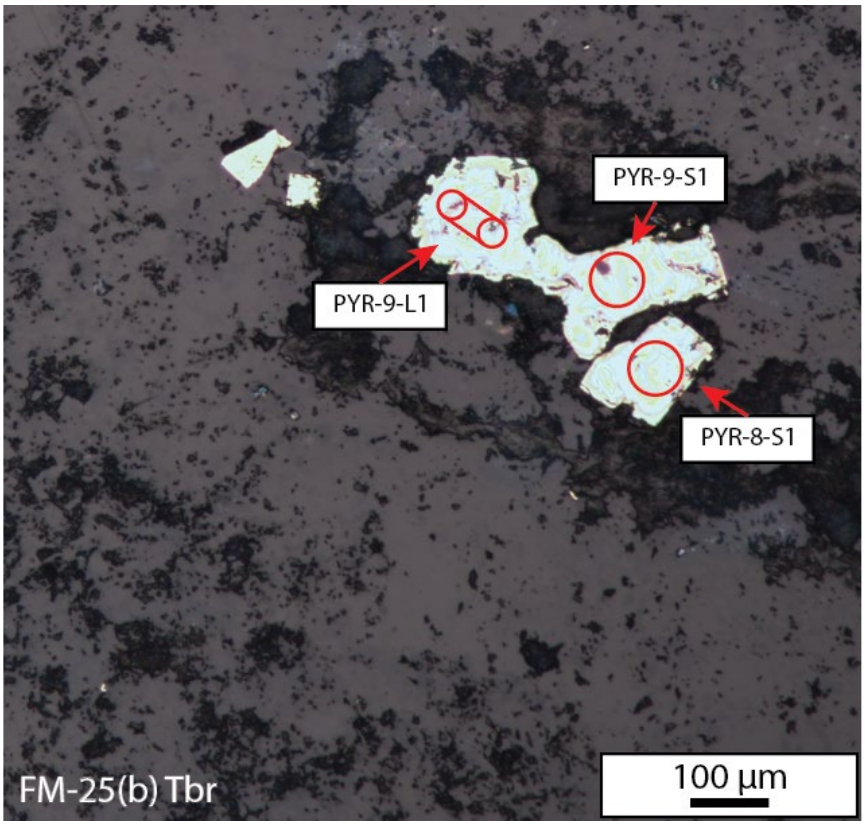

Figure 29. FM-25(b) Tbr unit (88.5 ft) pyrite grains that were analyzed by LA-ICP-MS. Label PYR-9-L1 corresponds with graphs in Figure 29; PYR = pyrite grain, # = number or grain analyzed, S = spot, L = line.

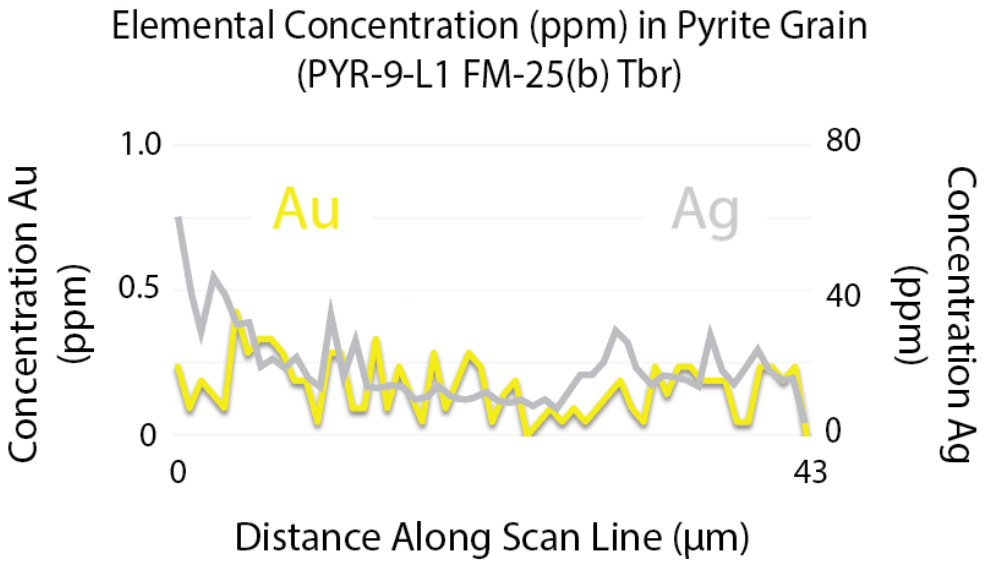

Figure 30. Au and Ag concentrations along the line scan done on a pyrite grain in FM-25(b) (Fig. 29; PYR-9-L1). The left y-axis is ppm Au and the right y-axis is ppm Ag.

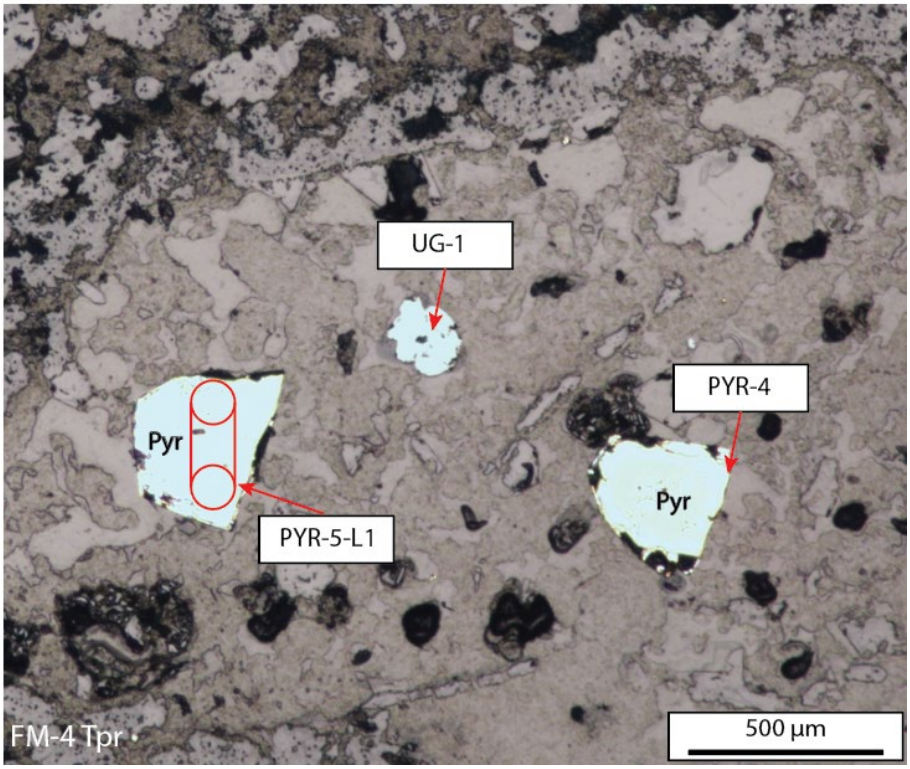

Figure 31. FM-4 Tpr unit (498.5 ft) pyrite grains that were analyzed by LA-ICP-MS. Label PYR-5-L1 corresponds with graphs in Figure 32; PYR = pyrite grain, # = number or grain analyzed, S = spot, L = line.

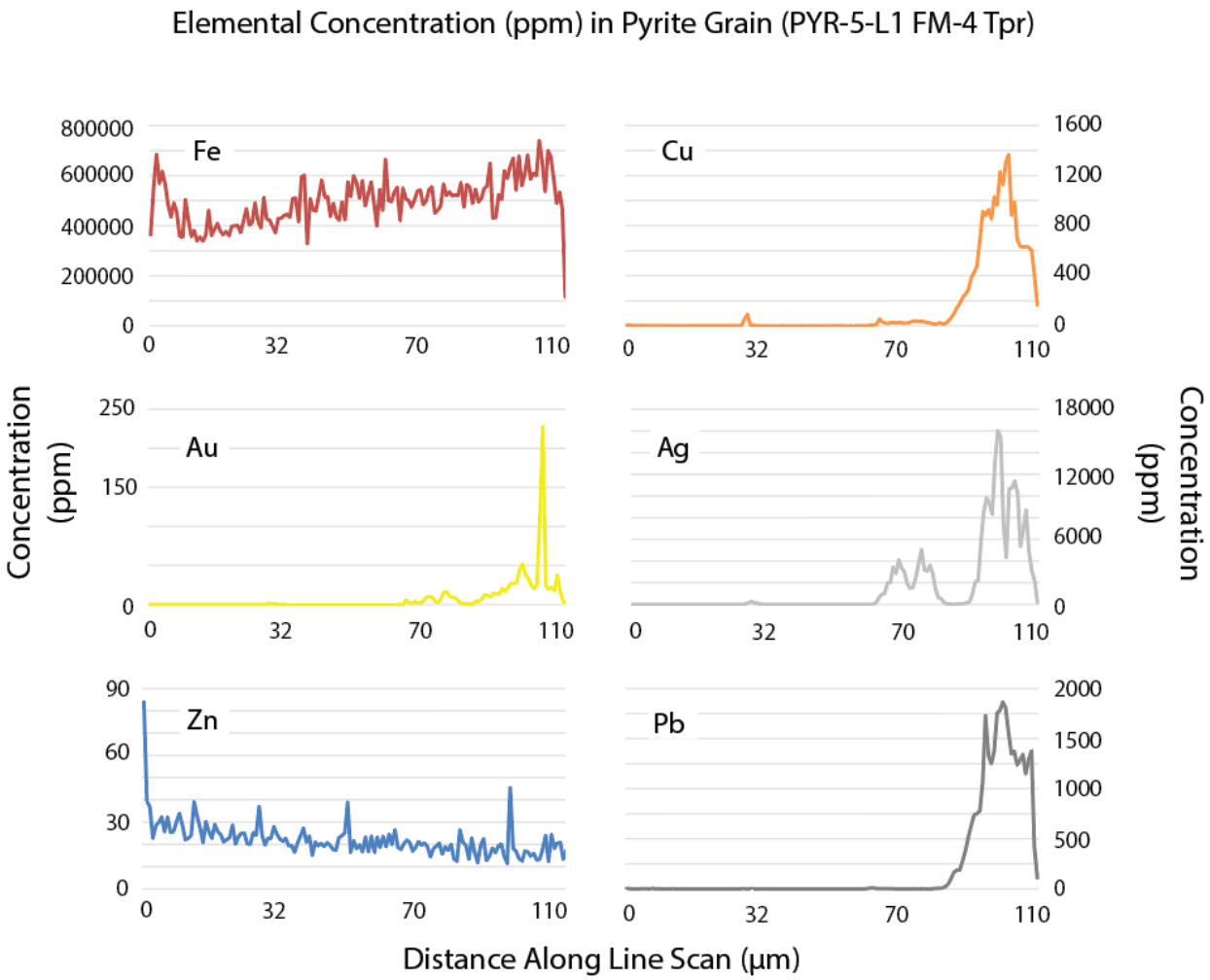

Figure 32. Elemental concentrations measured by line scan on PYR-5-L1 in the Tpr unit (Fig. 31). Note the different scales in y-axis between each panel.

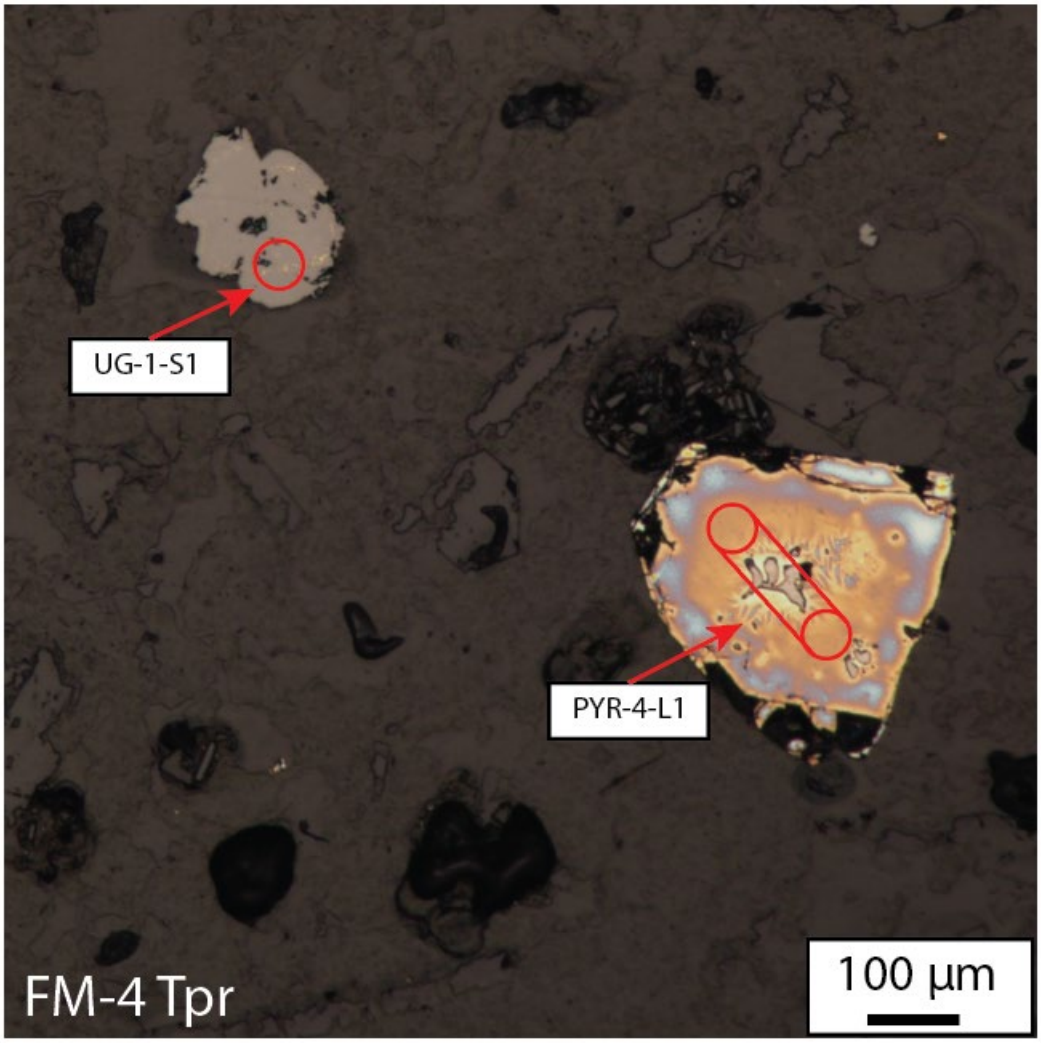

Figure 33. FM-4 Tpr unit (498.5 ft) pyrite grains that were analyzed by LA-ICP-MS. Label PYR-4-L1 corresponds with graphs in Figure 34; PYR = pyrite grain, # = number or grain analyzed, S = spot, L = line. Tarnish on PYR-4-L1 was removed by a single pre-ablation pass prior to analysis.

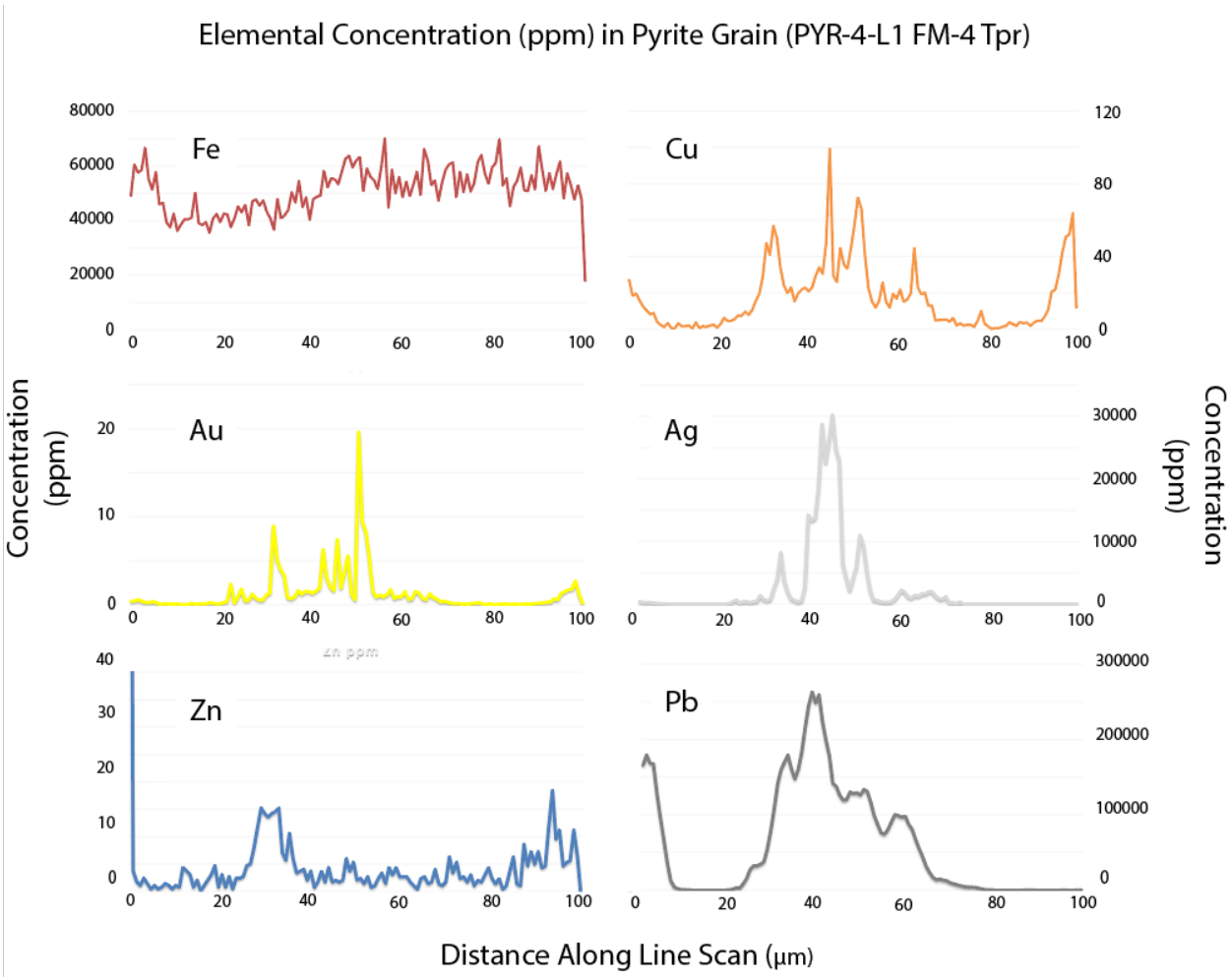

Figure 34. Elemental concentrations measured by line scan on PYR-4-L1 in the Tpr unit (Fig. 33). Note the different y-axis scales between each panel.

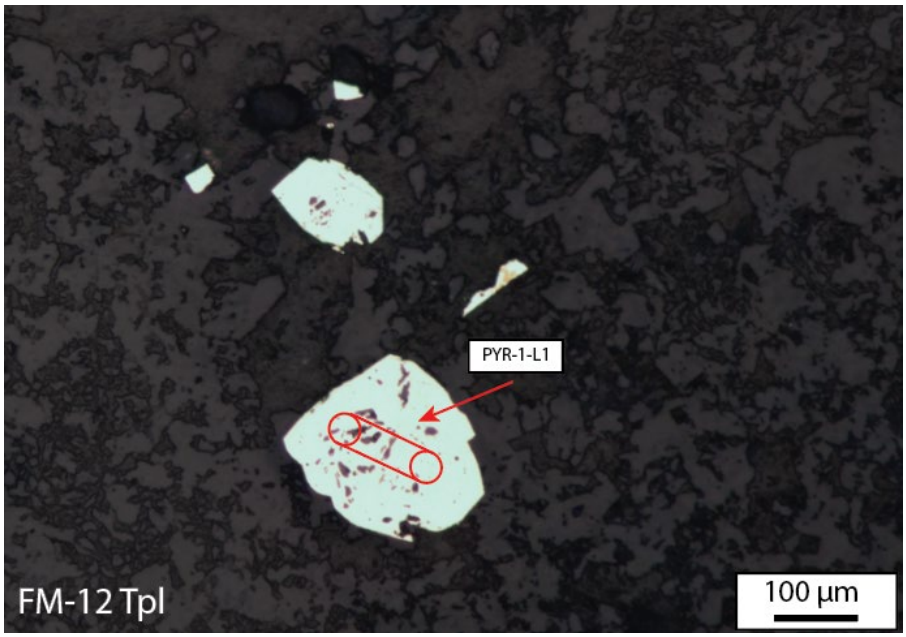

Figure 35. FM-12 Tpl unit (350.5 ft) pyrite grains that were analyzed by LA-ICP-MS. Label PYR-1-L1 corresponds with graphs in Figure 36; PYR = pyrite grain, # = number or grain analyzed, S = spot, L = line.

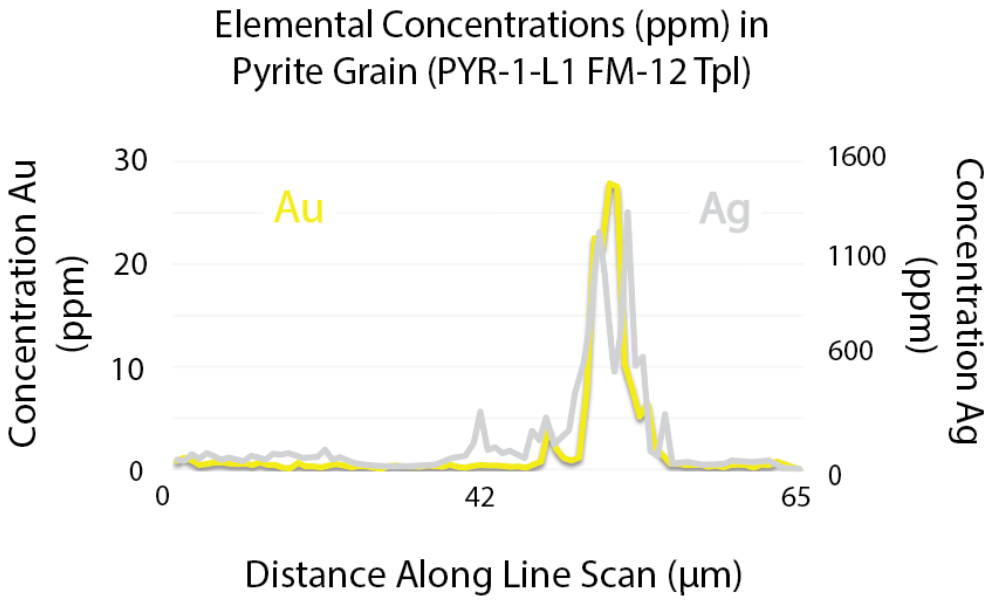

Figure 36. Au and Ag concentrations along the line analyzed in PYR-1-L1 from thin section FM-12 within the Tpl unit (Fig. 35). Labeled as PYR-1-L1. The left y-axis is Au and the right y-axis is Ag.

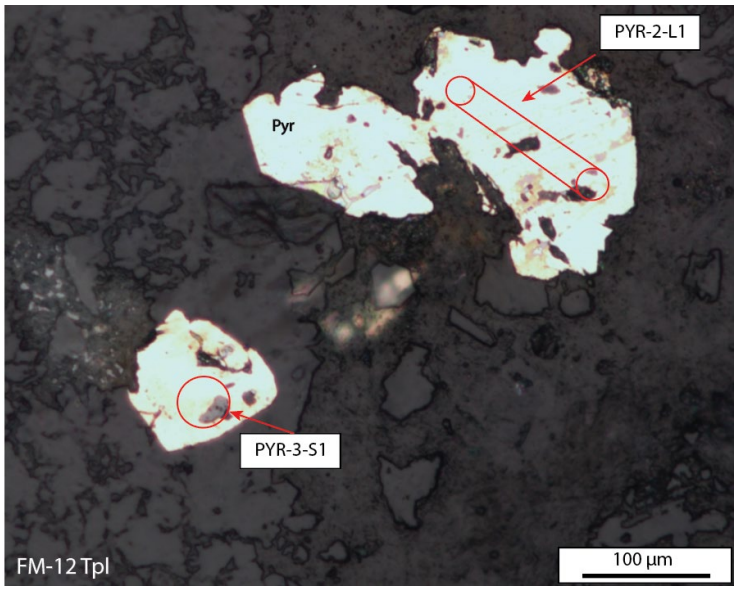

Figure 37. FM-12 Tpl unit (350.5 ft) pyrite grains that were analyzed by LA-ICP-MS. Label PYR-2-L1 corresponds with graphs in Figure 38; PYR = pyrite grain, # = number or grain analyzed, S = spot, L = line.

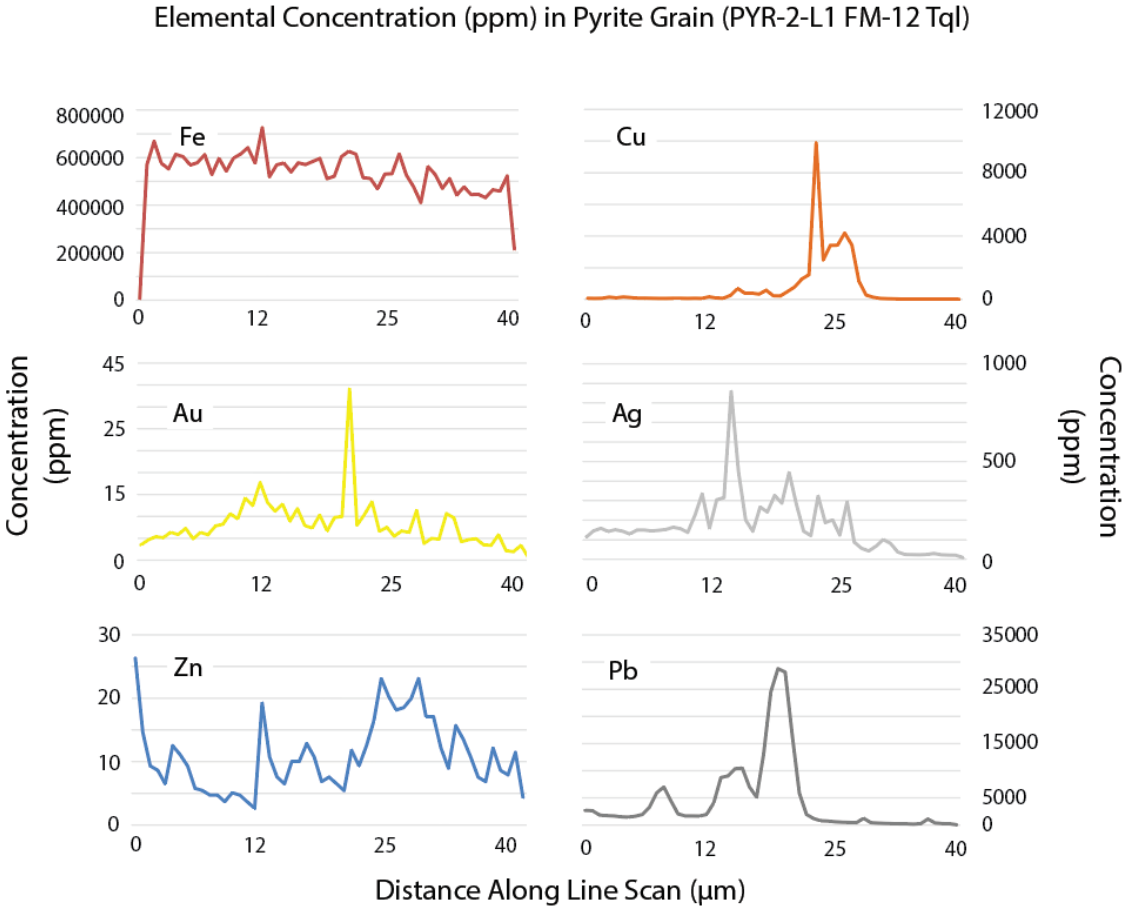

Figure 38. Elemental concentrations measured by line scan on PYR-2-L1 in the Tql unit (Fig. 37). Note the different scales in y-axis between each panel.

Summary of Geochemical (EMPA, LA-ICP-MS) Results

- Accessory minerals include galena, sphalerite, chalcocite, electrum, silver phases.
- Au and Ag (electrum, silver phases, and/or metal rich inclusions) can either be found within the matrix of pyrite grains, within pyrite inclusions, or on the edges of pyrite grains.
- Pyrite grains with inclusions containing elevated Au, Ag, Pb, Cu, and Zn can have higher amounts of those metals within the pyrite grain.
- Replacement and inclusions in pyrite grains contain Au, Ag, Pb, Cu, and/or Zn.

Preliminary Geochronology

Geochronological analysis of four samples from Florida Mountain was completed by Raeann Garcia and Dr. Bill Hames in the Auburn Noble Isotope Mass Analysis Lab (ANIMAL). The Florida Mountain samples contained adularia, which can be used for $^{40}Ar/^{39}Ar$ dating. Adularia was identified in hand samples by staining with sodium cobaltinitrite, and small cores, rich in adularia, were obtained with a diamond core drill for analysis. Results and ages are reported in Fig. 39. The ages obtained for the Florida Mountain adularia range from ~15.352 ±0.134 Ma to 15.95 ±0.20 Ma.

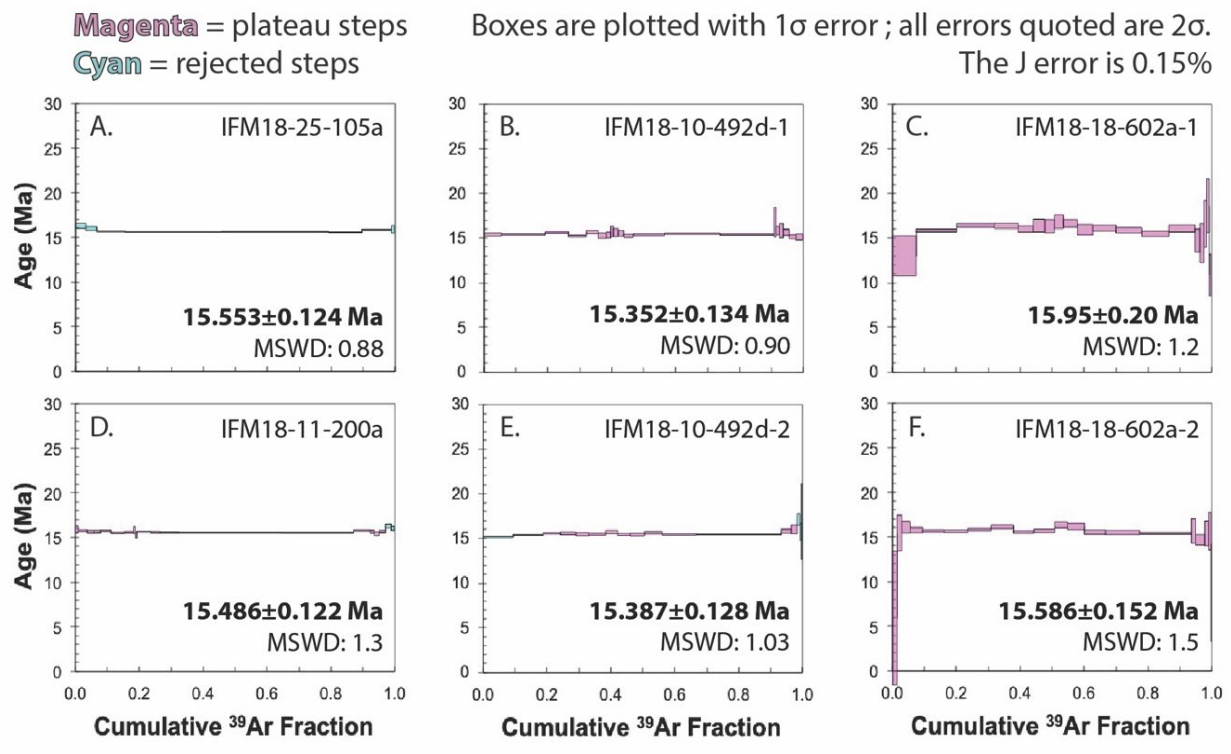

Figure 39: Results and sample age from $^{40}Ar/^{39}Ar$ geochronology. The boxes are plotted with 1σ error; all errors quoted are 2σ. The J error is 0.15%. Cyan indicates data not used. Figure by Raeann Garcia.

Discussion

Relationship with the Yellowstone Hotspot

The age range of adularia grains from Florida Mountain is ~15.352 Ma to ~15.95 Ma. These dates correspond with the timing for the duration of bimodal magmatism that has been reported in the region (Camp, 1995; Pierce and Morgan, 2012) and previous studies in the Silver City district and Northern Great Basin (Unger, 2008; Hames et al., 2009). These data support the hypothesis that the Yellowstone hotspot was the source of the fluids that formed the Florida Mountain deposit and that the Au and Ag were transported into the system from a magmatic source (c.f., Saunders et al., 2008).

Paragenesis of the Florida Mountain Deposit

Based on petrographic and trace element analyses, at least three stages of fluid input can be identified (Fig. 40). The primary mineral associated with higher grades of Au and Ag is pyrite. The variable grain sizes and textures observed in the pyrite (disseminated, cubic, aggregates) reflect multiple fluid events.

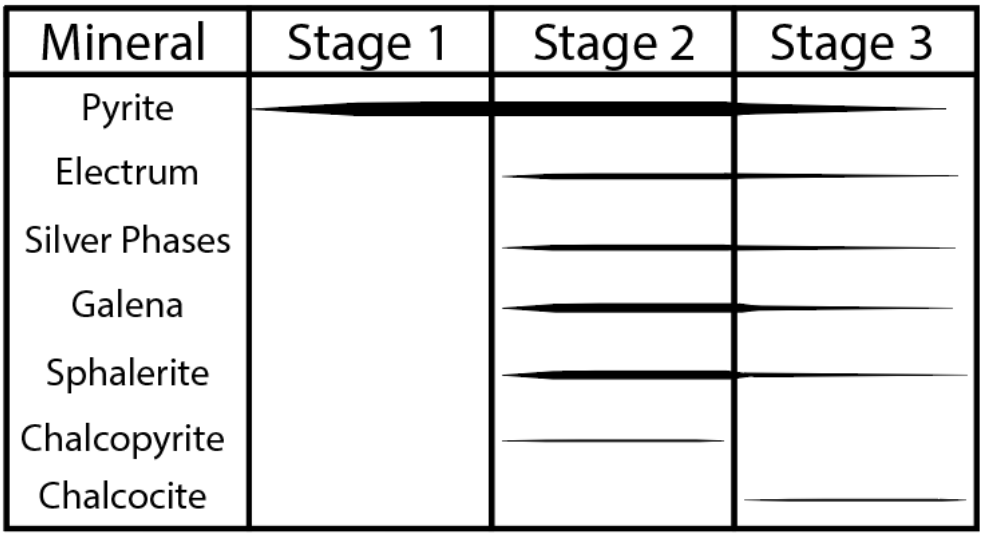

Figure 40. Paragenesis of the Florida Mountain deposit.

The first fluid stage primarily resulted in the deposition of iron sulfide (i.e., pyrite). The second stage can be discerned from the first by the introduction of Au, Ag, Pb, Cu and Zn into the system. Electrum, silver phases, and other accessory minerals such as galena and sphalerite appear as inclusions and or replacement within the pyrite grains (Fig. 41), as well as separate singular grains. The pyrite grains with inclusions contain higher concentrations of Au in the structure of the pyrite as well. There are also inclusions within pyrite grains that do not have any kind of fracturing or alteration that would lead to the inclusion being brought in, also indicating they were present during formation. The composition of the silver phases seen in lower-grade samples of Florida

Mountain are closer to that of aguilarite (Ag_4SeS) and acanthite (Ag_2S) than naumannite (Ag_2Se) (Fig. 24); this is similar to observations by Aseto (2012) and Mason (2015) at War Eagle Mountain and the Florida Mountain veins, respectively. The role of Se in the Silver City district ore systems remains unconstrained.

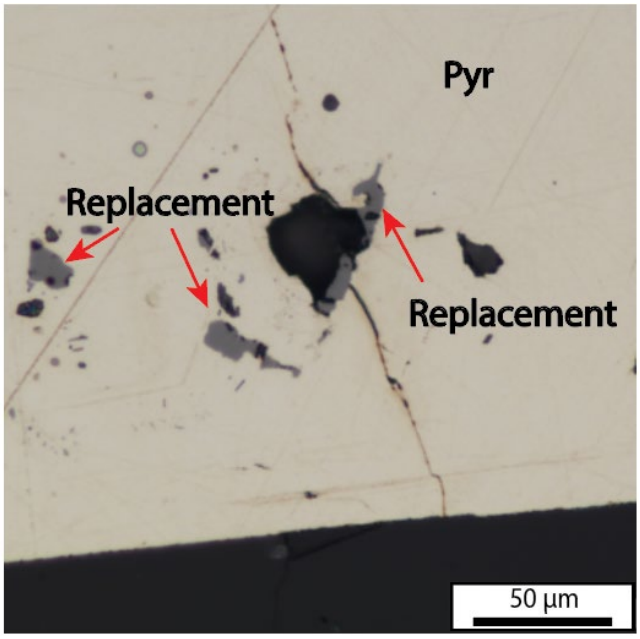

Figure 41. Photomicrograph from FM-10 Tpr at 142.5 ft showing fractures and voids that facilitated replacement of pyrite.

During the third stage, electrum and silver phases infilled open spaces in pyrite clusters and attached to the rims of pyrite grains (Fig. 26 & 27). At the same time, base metals were introduced into the system and resulted in the deposition of galena, sphalerite, and the silver phases. These minerals are always located near pyrite or replacing pyrite rims or edges adjacent to fractures and voids (Fig. 42 & 43). Zinc and lead are the dominant base metals during this stage, as indicated by the presence of sphalerite and galena. There is a lesser proportion of copper in the system as well, indicated by the presence of chalcopyrite, chalcocite, and the rare occurrence of metallic copper (Fig. 28, Table 7).

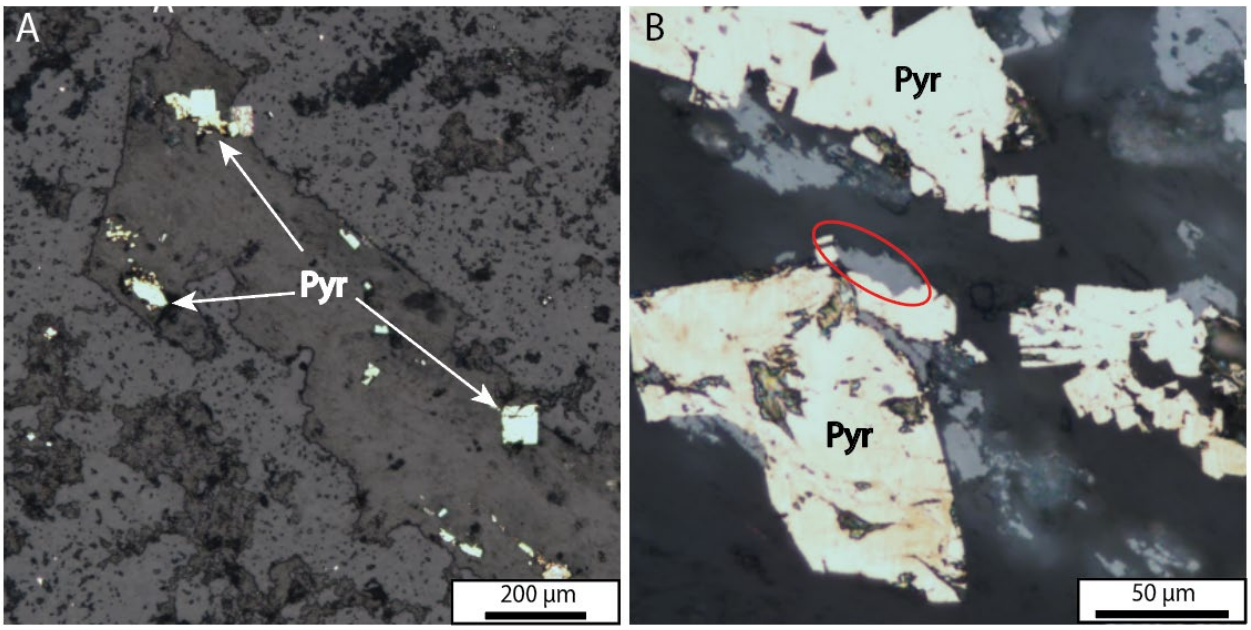

Figure 42. Replacement occurring at two different scales in the FM-4 Tbr unit at 105.5 ft. **A)** Pyrite grains replacing within plagioclase. **B)** Replacement (red circle) at the edge of a pyrite grain within **A).**

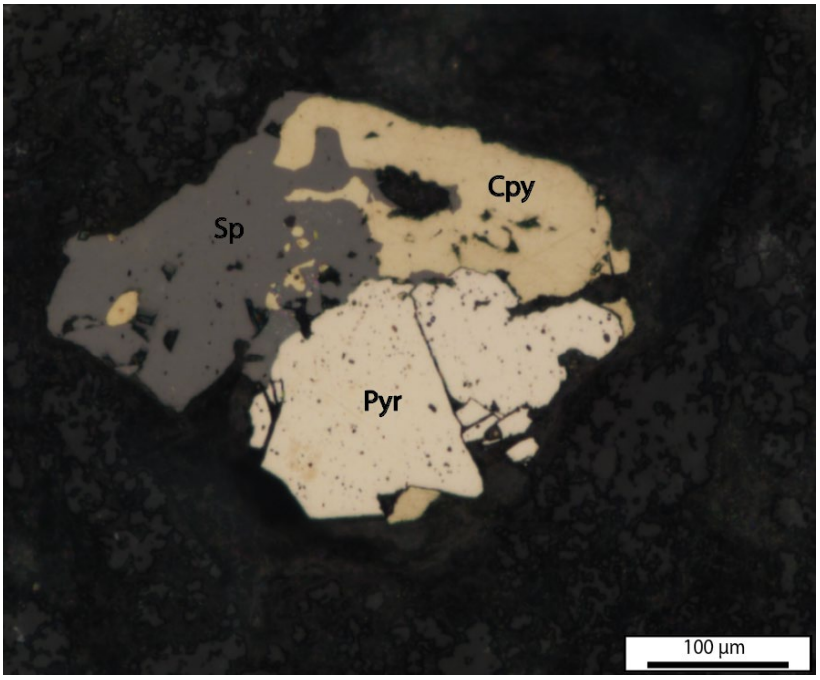

Figure 43. Replacement of the pyrite by chalcopyrite (Cpy) and later sphalerite (Sp), which also replaced Cpy. FM-10 Ttb unit at 387.5 ft.

The main introduction of Au and Ag to the system occurred during the second stage, and the third stage provided additional electrum and base metals. The observed differences in metal occurrence across the deposit (i.e., precious and base metals)

could be due to different fluid events and the proximity to the main pathway (Fig. 44 & 45). Figure 45 illustrates the correlation of higher Au grades and the transitionally oxidized areas (rather than unoxidized areas), which correspond with relatively shallow depths within the drill holes. This relationship outlines a preferred ore fluid pathway, trap, boiling level (Fig. 44), and/or height of neutral buoyancy that existed during the genesis of Florida Mountain at current depths of ~115.0 ft.

Overall, the paragenetic sequence closely follows that of Mason (2015) who focused on the high-grade veins at Florida Mountain. However, when examining the Florida Mountain deposit as a whole from drill core samples, it appears that electrum, silver phases, and base metal sulfides were introduced earlier. Furthermore, the later stages (2 and 3) include both electrum and silver phases rather than silver phases alone. The difference could be attributed to the proximity to the high-grade veins to concentrated fluid pathways since previous studies such as Mason (2015) focused on high-grade veins. Alternatively, it is possible that the lower grade samples obtained from the drill core offer a different timeline of ore transport and deposition that overlaps with that of the Black Jack-Trade Dollar vein at Florida Mountain.

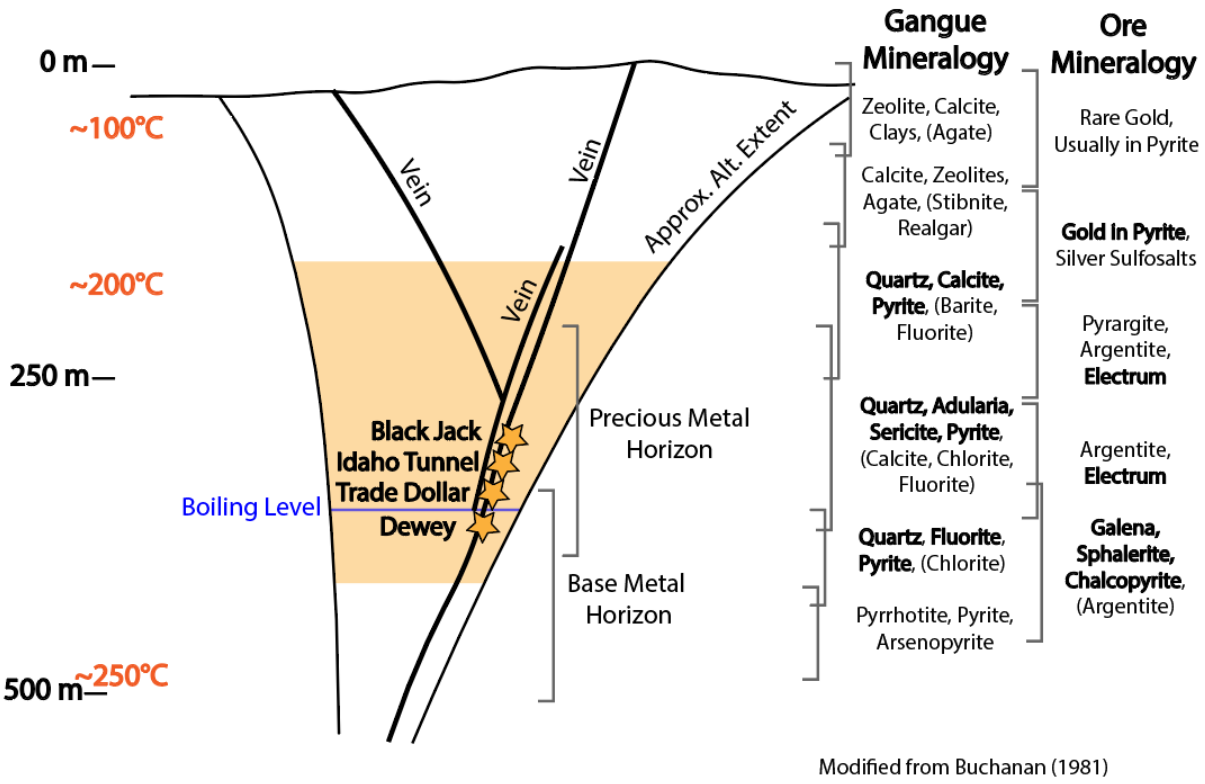

Figure 44. Approximate location of the Florida Mountain deposit (yellow shading) within an idealized cross-section of an epithermal system (after Mason, 2015 and modified from Buchanan, 1981). Stars represent the approximate locations of the high-grade vein samples studied in Mason (2015).The bolded minerals in right column to are those observed in this study.

Figure 45 presents a set of ArcPro maps that were completed from geophysical data that Integra Resources provided with Au and Ag grades. The maps show a bird's eye view as well as a cross sectional view of the drill core. This three-dimensional visualization allows for the interpretation of fluid flow in the deposit including the fluids' ability to branch out horizontally within a unit. The higher grades are generally found at shallower depths.

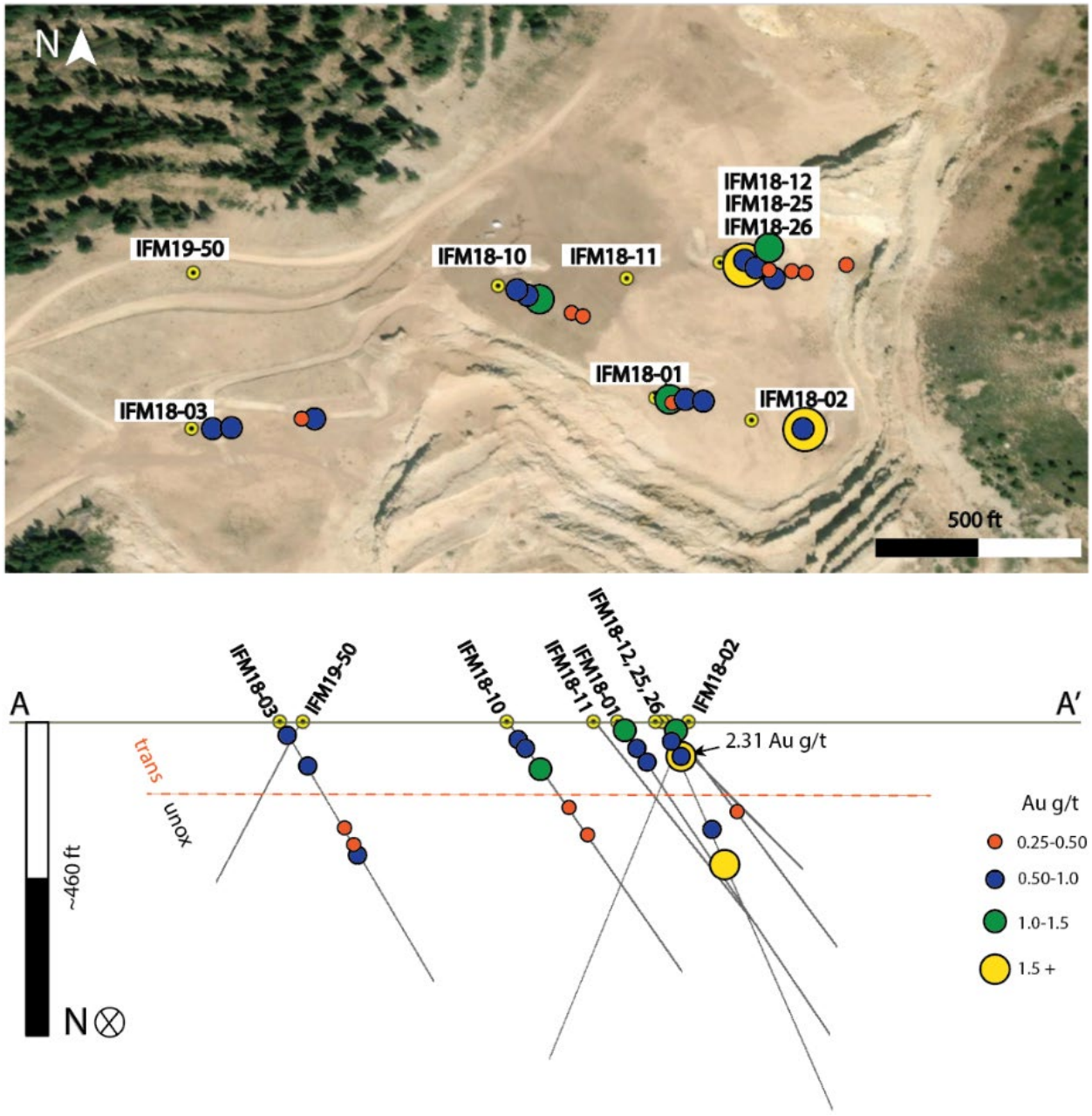

Figure 45. Spatial distribution of Au grade along drill core in map view (top) and cross section (bottom). Cross-sectional view can be manipulated using ArcPro in the x-, y-, and z-directions for three-dimensional visualization (see Appendix C for details). Size and color of circles indicate Au grade as reported by Integra Resources. Note that the drill holes drawn in the bottom panel are not along a single plane. Trans = transitionally oxidized samples; unox = unoxidized samples; classification determined by Integra Resources.

In the field, faulted areas with darker, more oxidized or “transitional” rock (Fig. 46) are targets for exploration as they are associated with higher grades as well as easier processing of the material. Typically, the moderate to highly oxidized samples in

this study had a higher proportion of accessory minerals, some of which included Au and Ag (Table 6). Pyrite grains within the oxidized zone are also typically more altered and fractured, which led to a higher amount of alteration and/or replacement and resulted in higher concentrations of Au and Ag. In general, these samples were extracted from relatively shallow depths within the drill holes (Fig. 45), suggesting that the ore fluid did not react as extensively with the rocks that currently lie below ~115 feet. This could be due to changes in lithology, structure (faults, fractures), or controlled by the buoyancy and changing temperature of the ore fluid at the time of transport.

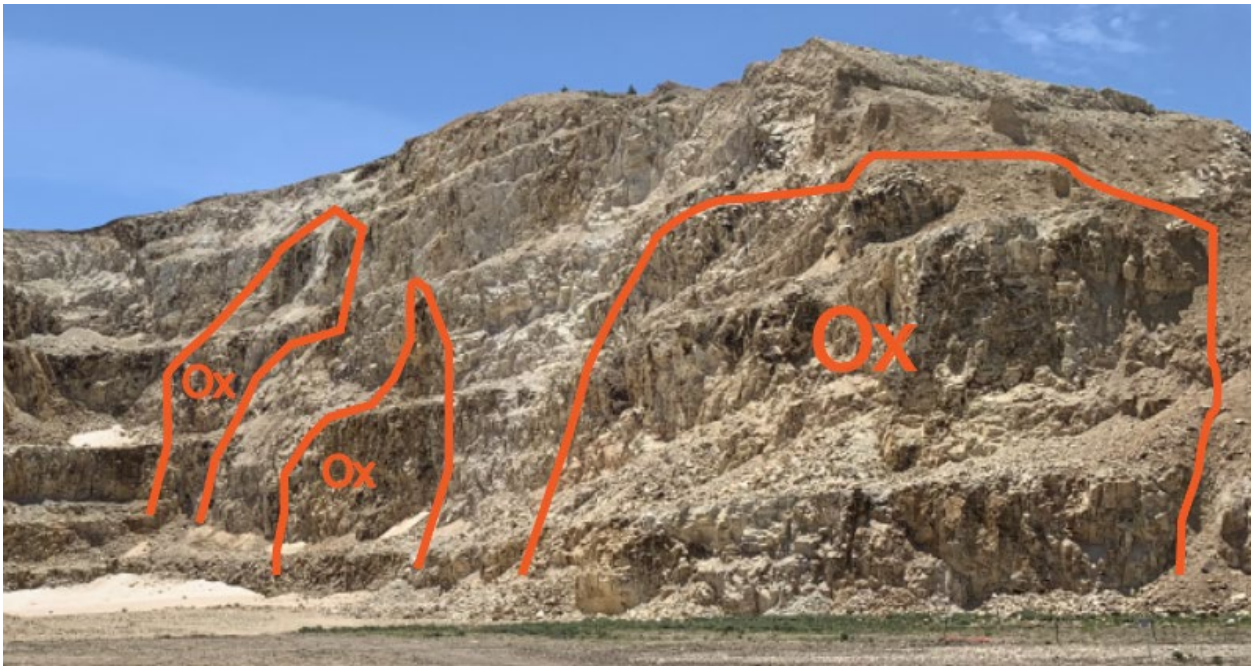

Figure 46. The wall of Stone Cabin open pit. The orange lines outline the more oxidized rock (darker). This area of oxidation is controlled by fractures and faulting.

Exploration Indicators

When looking for indicators in samples or on a pit wall, there are two groups to consider: macroscopic and microscopic. Veins or areas that are more altered indicate

that ore fluid flowed through the area and likely deposited Au and Ag. Another macroscopic indicator is a discoloration of pyrite bearing veins. For example, the veins in Figure 47 have a yellow color that is easily recognizable, and it contains the electrum grains seen in Figures 26 and 27.

Microscopically, identifying gold-colored grains on the edges of pyrite grains within veins is likely to reveal Au-rich samples. These grains were deposited from a fluid that came through after the deposition of pyrite grains in the vein. Also looking for pyrite grains that have replacement, darker inclusions, or a brighter gold color could also point to higher grades of Au and Ag. LA-ICP-MS analyses show that such inclusions can contain elevated levels of Au and Ag and higher amounts of Au in the structure of the pyrite grain. Pyrite grains that were not altered did not contain elevated Au and Ag.

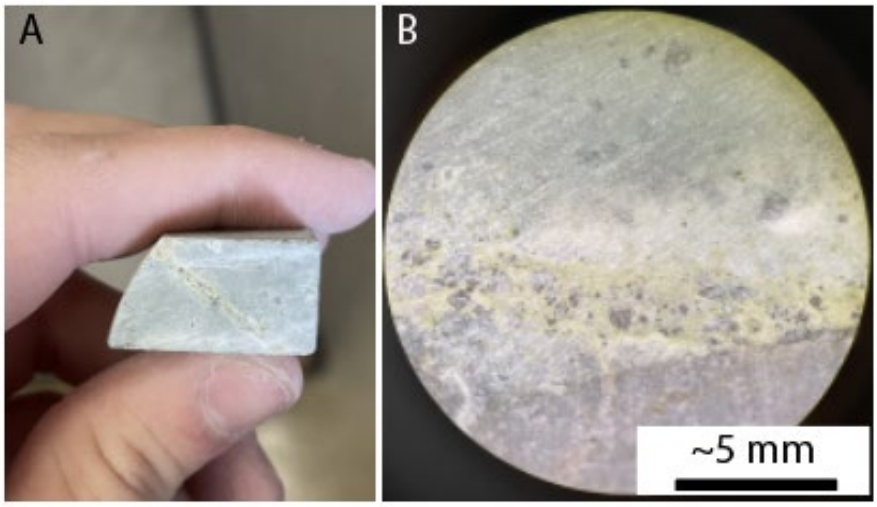

Figure 47. A) Billet from the FM-26 Tql unit at 131.5 ft that contained electrum grains: pencil for scale. **B)** is a closer view taken through a stereoscope.

Future Research/Outstanding Questions

For future research, there are several additional field and analytical investigations that would 1) constrain ore-fluid pathways to aid in exploration; 2) characterize the

transport and mobility of the metals observed in the Florida Mountain system; 3) establish the relationship between all of the Silver City district epithermal deposits, to be applied to other epithermal Au-Ag districts (e.g., within the NGB).

Close analysis of the alteration across the Florida Mountain deposit would help shed light on the extent and relative timing of individual events. This could also develop a more precise way of field observation identification of higher grades. Additionally, our understanding of localized ore fluid flow would be improved through detailed characterization of structural features (e.g., faults, veins) exposed and intersected by drilling at Florida Mountain. The structure of the deposit should be considered in the context of the high-grade and low-grade areas as well as the extent of oxidation and alteration.

From the geochemical perspective, the composition of the fluid(s) should be better constrained and one useful approach would be fluid inclusion analysis. Quantifying salinity and metal content of microscopic pockets of preserved ore fluid will inform the question of how the Au and Ag (in addition to Se and other metals) were transported within the deposit during each stage of the deposit's formation. This knowledge would also contribute to our understanding of anomalous mineralogy observed at Florida Mountain, e.g., pyrite grains depleted of their S, chalcopyrite with low Cu, and the rare occurrence of metallic Cu.

Originally, this research included plans for analysis of the S isotope composition of pyrite in lower grade drill core samples for a comparison to previous isotopic work used to constrain ore fluid and metal source. However, this was no longer possible due to the COVID-19 pandemic. Sulfur and additional isotope data from the low-grade

samples of Florida Mountain would be valuable to test the magmatic source invoked by Mason et al. (2015) and Mason (2015) in the context of the entire Florida Mountain deposit. Similarly, Se isotope analysis could be used to understand the role of Se in the transport of Ag.

At the district-scale, a study comparing the detailed mineralogy, host lithology, geochemistry, and structure of Florida Mountain with its neighboring deposits, DeLamar Mountain and War Eagle Mountain, would offer novel insight into fluid flow and metal source and metal mobility on the local and district scales. Thus far, differences in host lithology have been recognized, which will not only influence ore fluid transportation and trapping, but also the ingredients available to the ore system(s).

Conclusions

The Silver City district and the Northern Great Basin are areas with great potential for the mineral industry, but few detailed studies exist. On a regional scale, a better understanding of Florida Mountain and the Silver City district contribute to our understanding of similar systems within the NGB. The goal of this study was to develop a deposit-scale view of Florida Mountain beyond the high-grade veins and, in doing so, evaluate the conditions of metal and fluid transport and deposition, which could be applied to similar deposits. Specifically, we aimed to constrain the timing of the formation of Florida Mountain relative to the Yellowstone hotspot, determine the likely source of the ore, and identify possible exploration indicators. All of the previous studies on Florida Mountain produced data from surface samples targeting the high-grade veins, providing a limited view of this deposit. This opportunity to utilize the extensive drill core collection with Integra Resources allowed us to build a thorough

characterization of low-grade samples across the entire deposit at Florida Mountain. By using petrographic and geochemical analyses, this study confirms the timing and controls on the formation of the Au-Ag epithermal deposit at Florida Mountain:

- Ar-Ar geochronology of adularia at Florida Mountain revealed ages of ~15.352 to ~15.95 Ma. This range is consistent to other studies within the NGB and confirms a likely genetic relationship with the Yellowstone hotspot.
- Multiple fluid events contributed to mineralization at Florida Mountain in at least three stages. The second stage was most likely responsible when the majority of Au and Ag was transported and deposited in the deposit; the fluids of the third stage provided supplemental Au and Ag.
- The paragenesis of the larger Florida Mountain deposit is similar, but not identical, to that of the high-grade veins studied before: pyrite → electrum → silver phases + base metal sulfides → copper phases (metallic copper and copper sulfides).
- The consistency in age, mineralogy, geochemistry, and paragenesis of the lower grade samples analyzed here to the high-grade veins previously studied supports the hypothesis that the source of the ore fluids and metals is magmatic. Additional isotopic studies could be utilized in future work to confirm this.
- Target mineralization (Au, Ag) can be seen as individual grains (electrum, Ag-Se sulfides), inclusions, replacement, and within the structure of pyrite.

References Cited

Aseto, C.O., 2012, Geology, geochemistry, and geochronology of the mid-Miocene, low-sulfidation epithermal gold-silver ores on War Eagle Mountain, Silver City District, Idaho: Unpublished M.Sc. thesis, Auburn, Alabama, Auburn University.

Buchanan, L.J., 1981, Precious metal deposits associated with volcanic environments in the southwest: Arizona Geological Society Digest, v. 14, p. 237-262.

Camp, V.E., 1995, Mid-Miocene propagation of the Yellowstone mantle plume head beneath the Columbia River Basalt source region: Geology, v. 23, p. 435- 438.

Camp, V.E., and Wells, R.E., 2021, The Case for a Long-Lived and Robust Yellowstone Hotspot: GSA Today, v. 31, No.1, p. 4-10.

Halsor, S.P., Bornhorst, T.J., Beebe, M., Richardson, K., and Strowd, W., 1988, Geology of the DeLamar silver mine, Idaho: A volcanic dome complex and genetically associated hydrothermal system: Economic Geology, v. 83, p. 1159-1169.

Hames, W.E., Unger, D.L., Saunders, J.A., Kamenov, G.D., 2009, Early Yellowstone hotspot magmatism and gold metallogeny, Journal of Volcanology and Geothermal Research, v. 188 p. 214-224.

Hanan, B.B., Shervais, J.W., and Vetter, S.K., 2008, Yellowstone plume – continental lithosphere interaction beneath the Snake River Plain: Geology, v. 36, no. 1, p. 51-54

Hasten, Z.E.L., 2012, Mid-Miocene magmatism in the Owyhee Mountains, ID: Origin and petrogenesis of volcanic rocks in the silver city district: Unpublished M.Sc. thesis, Manhattan, Kansas, Kansas State University.

Hedenquist, J.W., and Houghton, B.F., 1987, Epithermal gold mineralization and its volcanic environments: Earth Resources Foundation, The University of Sydney, p. 422.

Hedenquist, J.W., 1992, Recognition of magmatic contributions to active and extinct hydrothermal systems, in Hedenquist, J.W., ed., Magmatic contributions to hydrothermal systems: Geological Survey of Japan, Report 279, p. 68-79.

Hedenquist, J.W., and Lowenstern, J.B., 1994, The role of magmas in the formation of hydrothermal ore deposits: Nature, v. 370, p. 519-527.

Hedenquist, J.W., Arribas, A.R., and Gonzalez-Urien, E., 2000, Exploration for epithermal gold deposits: Reviews in Economic Geology, v. 13, p. 245-277.

“Idaho.” *Suretypedia*, 2019, www.suretypedia.com/state/idaho/.

Integra Resources, 2019, Florida Mountain Project, Project History, integraresources.com/project/florida-mountain-project/project-history.

Integra Resources, 2019, The DeLamar Project, Corporate Presentation: September 2019, integraresources.com/investors/corporate-presentation.

John, D.A., 2001, Miocene and early Pliocene epithermal gold-silver deposits in the northern Great Basin, western USA: Characteristics, distribution, and relationship to magmatism: Economic Geology, v. 96, p. 1827–1853.

Kamenov, G.D., Saunders, J.A, Hames, W.E., and Unger, D.L., 2007, Mafic magmas assources for gold in middle Miocene epithermal deposits of the northern Great Basin, United States: Evidence from Pb-isotope compositions of native gold: Economic Geology, v. 102, p.1191-1195.

Lindgren, W., 1900, The gold and silver veins of the Silver City, DeLamar, and other mining districts in Idaho, in U.S. Geological Survey 20th Annual Report, Part 3, p. 65-256.

Lindgren, W., 1933, Mineral deposits: New York, McGraw-Hill, 4th ed., 930 p.

Mason, M.S, 2015, Ore petrography, geochemistry, and genesis of epithermal silver-gold veins on Florida Mountain, Silver City District, Idaho: Unpublished M.Sc. Thesis, Auburn, Alabama, Auburn University.

Mason M.S., Saunders J. A., Aseto C., Hames W. E., Brueseke M.E., 2015, Epithermal Au-Ag ores of War Eagle and Florida Mountains, Silver City District, Owyhee County, Idaho: Geological Society of Nevada Publication.

Markl, G., Lahaye, Y., and Schwinn, G., 2006, Copper isotopes as monitors of redox processes in hydrothermal mineralization: Geochimica et Cosmochimica Acta, v. 70, p. 4215-4228.

Mathur, R., Ruiz, J., Titley, S., Liermann, L., Buss, H., and Brantley, S., 2005, Cu isotopic fractionation in the supergene environment with and without bacteria: Geochimica et Cosmochimica Acta, v. 69, p. 5233-5246.

"Owyhee County, Idaho." *Wikipedia*, Wikimedia Foundation, 31 Oct. 2019, en.wikipedia.org/wiki/Owyhee_County,_Idaho.

Okamoto, A., and Tsuchiya, N., 2009, Velocity of vertical fluid ascent within vein-forming fractures: Geology, v. 37, no. 6, p. 563-566.

Pansze, A.J., 1975, Geology and Ore Deposits of the Silver City –DeLamar –Flint Region, Owyhee County, Idaho: Idaho Bureau of Mines and Geology Pamphlet no. 161, p. 79.

Petruk, W., Owens, D.R., Stewart, J.M., and Murray, E.J., 1974, Observations on acanthite, aguilarite, and naumannite: Canadian Mineralogist, v. 12, p. 365-369.

Pierce, K.L., and Morgan, L.A., 1992, The track of the Yellowstone hot spot: volcanism, faulting, and uplift, in: Link, P.K., Kuntz, M.A., Platt, L.B., eds., Regional Geology of Eastern Idaho and Western Wyoming: Geological Society of America Memoir, v. 179, p. 1-53.

Saunders, J.A., 1990, Colloidal transport of gold and silica in epithermal precious-metal systems: evidence from the Sleeper deposit, Nevada: Geology, v. 18, p. 757-760.

Saunders, J.A., 1994, Silica and gold textures in bonanza ores of the Sleeper deposit, Humboldt County, Nevada: Evidence for colloids and implications for epithermal ore-forming processes: Economic Geology, v. 89, p. 628-638.

Saunders, J.A., Cook, R.B., and Schoenly, P.A., 1996, Electrum disequilibrium crystallization textures in volcanic-hosted bonanza epithermal gold deposits in northern Nevada, in Coyner, A.R., and Fahey, P.L., eds., Geological Society of

Nevada Symposium 1995: Geology and Ore Deposits of the American Cordillera, Reno, Nevada, May 1995, p. 173-179.

Saunders, J.A., Unger, D.L., Kamenov, G.D., Fayek, M., Hames, W.E., and Utterback, W.C., 2008, Genesis of Middle Miocene Yellowstone hotspot-related bonaza epithermal Au-Ag deposits, Northern Great Basin, USA: Mineralium Deposita, v. 43, p. 715-734.

Seal, R.R., 2006, Sulfur isotope geochemistry of sulfide minerals: Reviews in Mineralogy & Geochemistry, v. 61, p. 633-677.

Sillitoe, R.H. and Hedenquist, J.W., 2003, Linkages between Volcanotectonic Settings, Ore-Fluid Compositions, and Epithermal Precious Metal Deposits: Society of Economic Geologists, Special Publication 10, p. 315-343.

Simmons, S.F., White, N.C., and John, D.A., 2005, Geological characteristics of epithermal precious and base metal deposits: Economic Geology 100th Anniversary Volume, p. 485-522.

Unger, D.L., 2008, Geochemistry, geochronology and ore petrology of low-sulfidation Au-Ag ores in the northern Great Basin region of Nevada-Idaho: Unpublished M.Sc. thesis, Auburn, Alabama, Auburn University.

Vikre, P.G., 1985, Precious metal vein systems in the National District, Humboldt County, Nevada: Economic Geology, v. 80, p.360-393.

Vikre, P.G., 1987, Paleohydrology of Buckskin Mountain, National district, Humboldt County, Nevada: Economic Geology, v. 82, p.934.

Appendix A: Electron Microprobe Analysis Energy Dispersive Spectroscopy Spectra

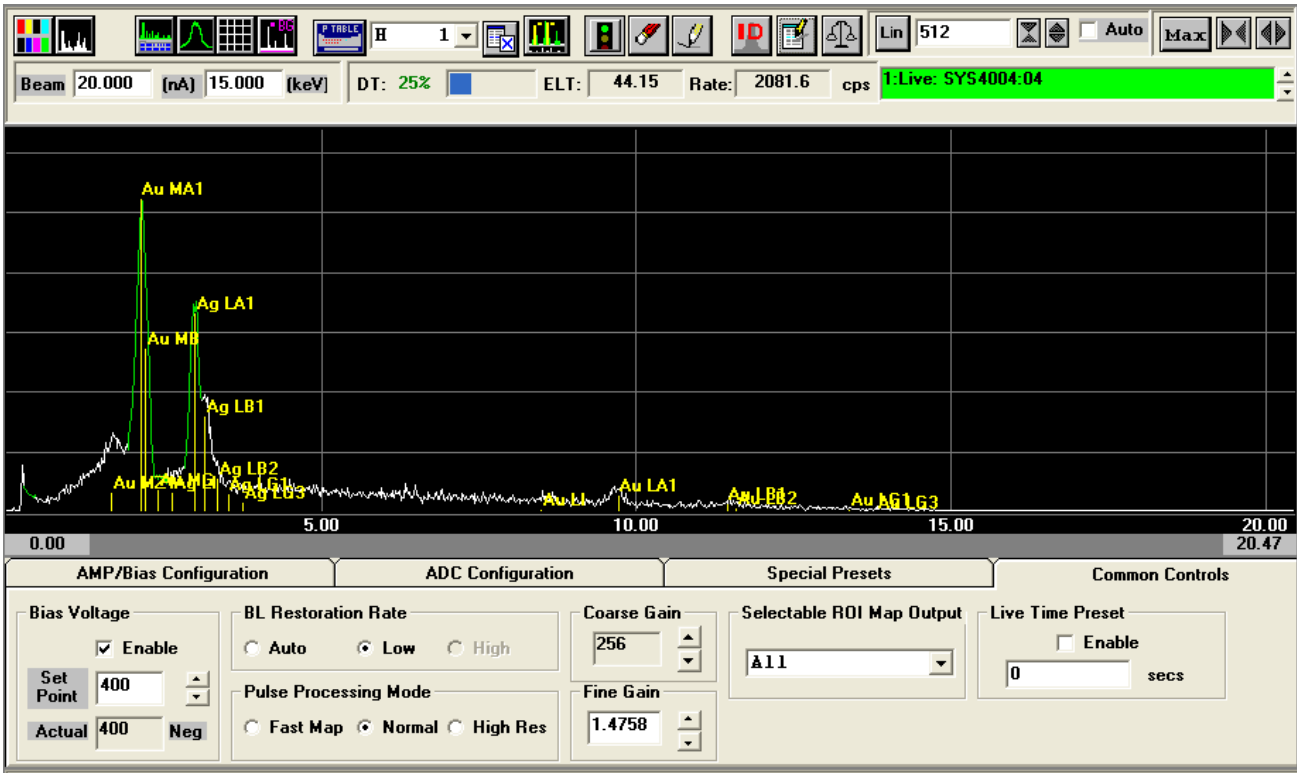

Figure A1. Spectrum of electrum grain (above) (FM-26 Tql).

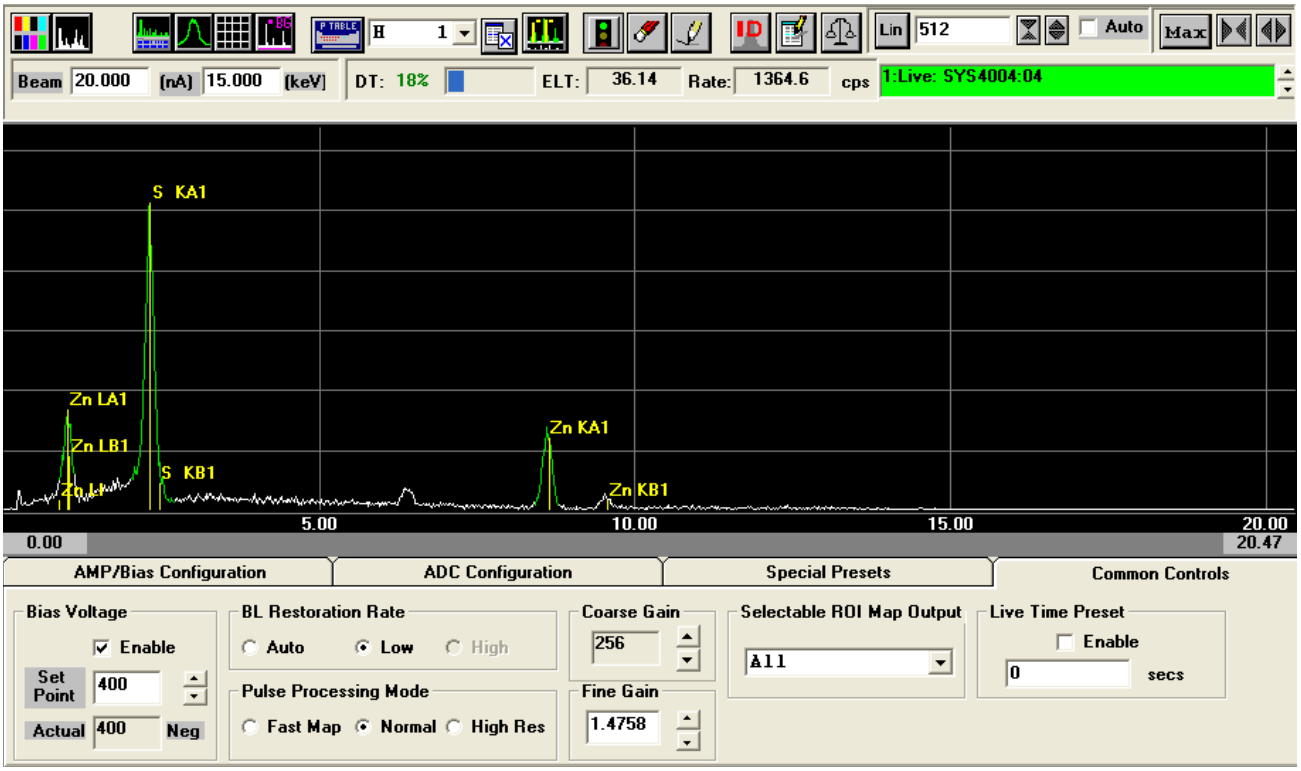

Figure A2. Spectrum of sphalerite grain (above) (FM-26 Tql).

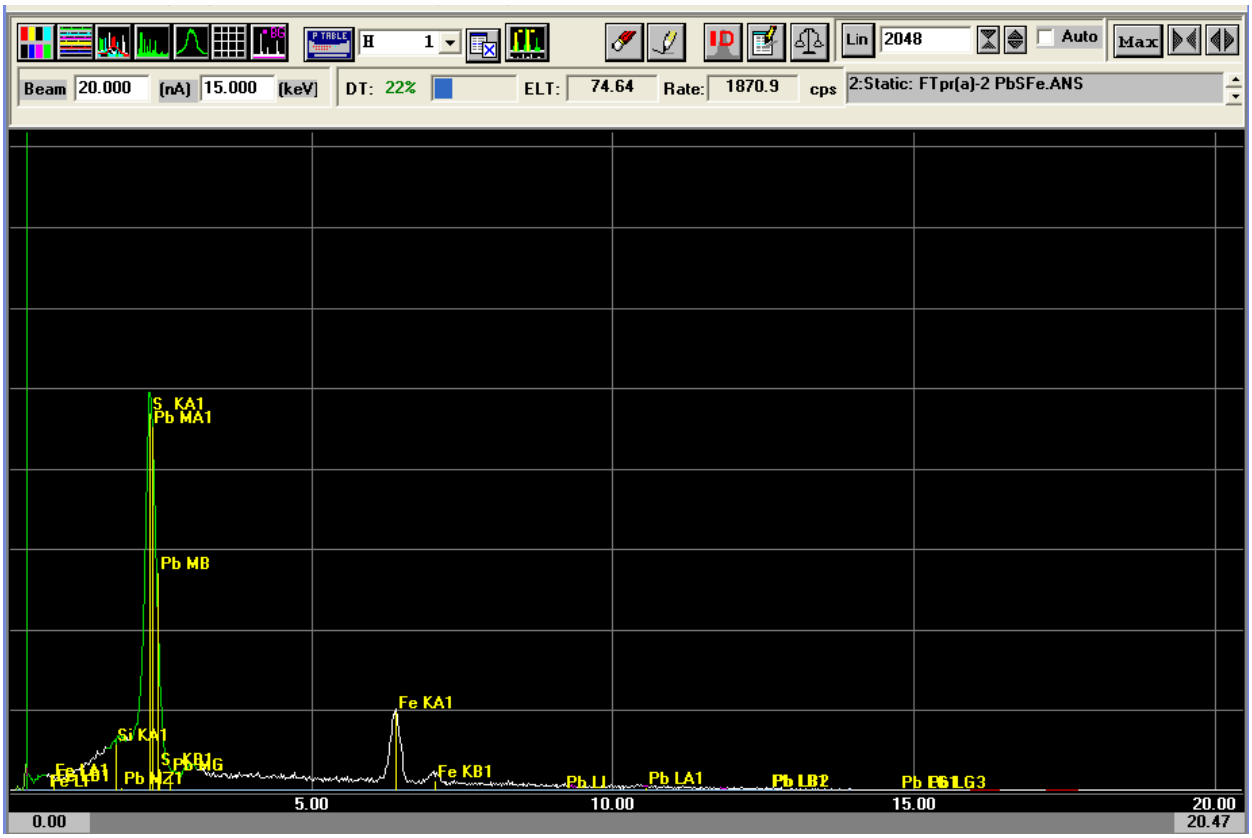

Figure A3. Spectrum of galena (above) (FM-2 Tpr(a)). Iron peak reflects interference from adjacent pyrite grain.

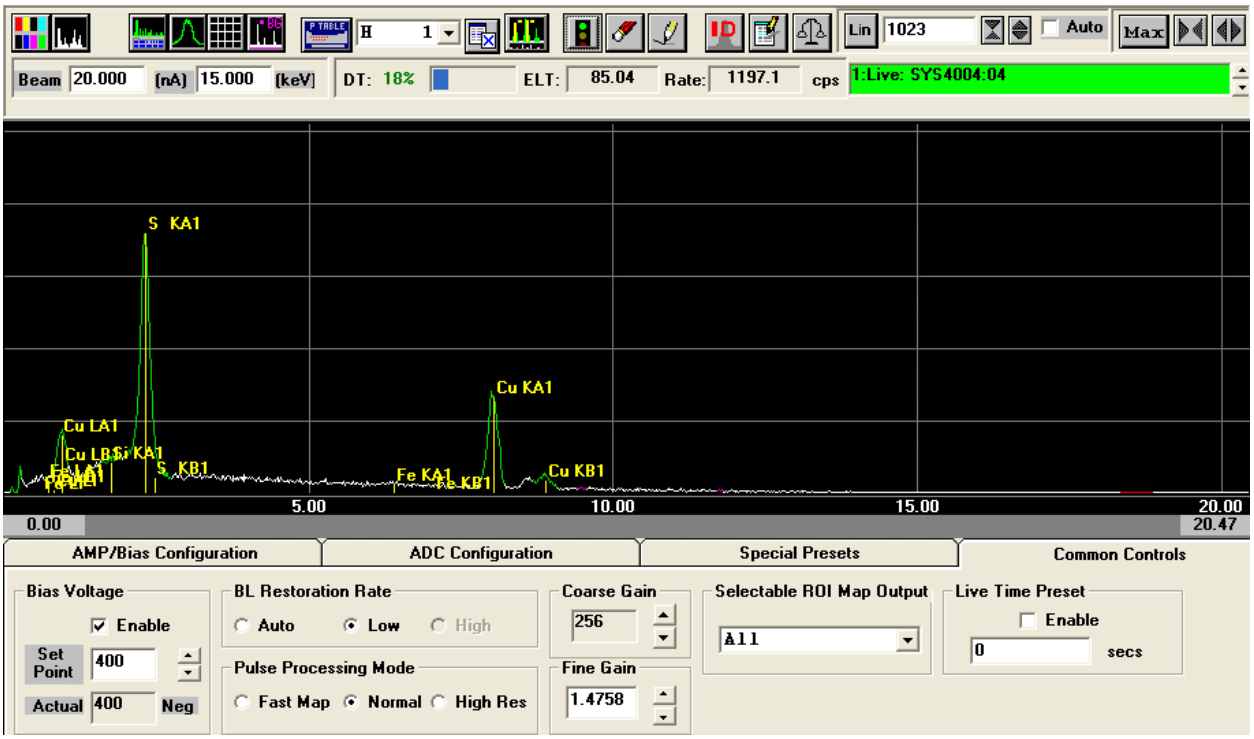

Figure A4. Spectrum of chalcocite (above) (FM-11 Tbr).

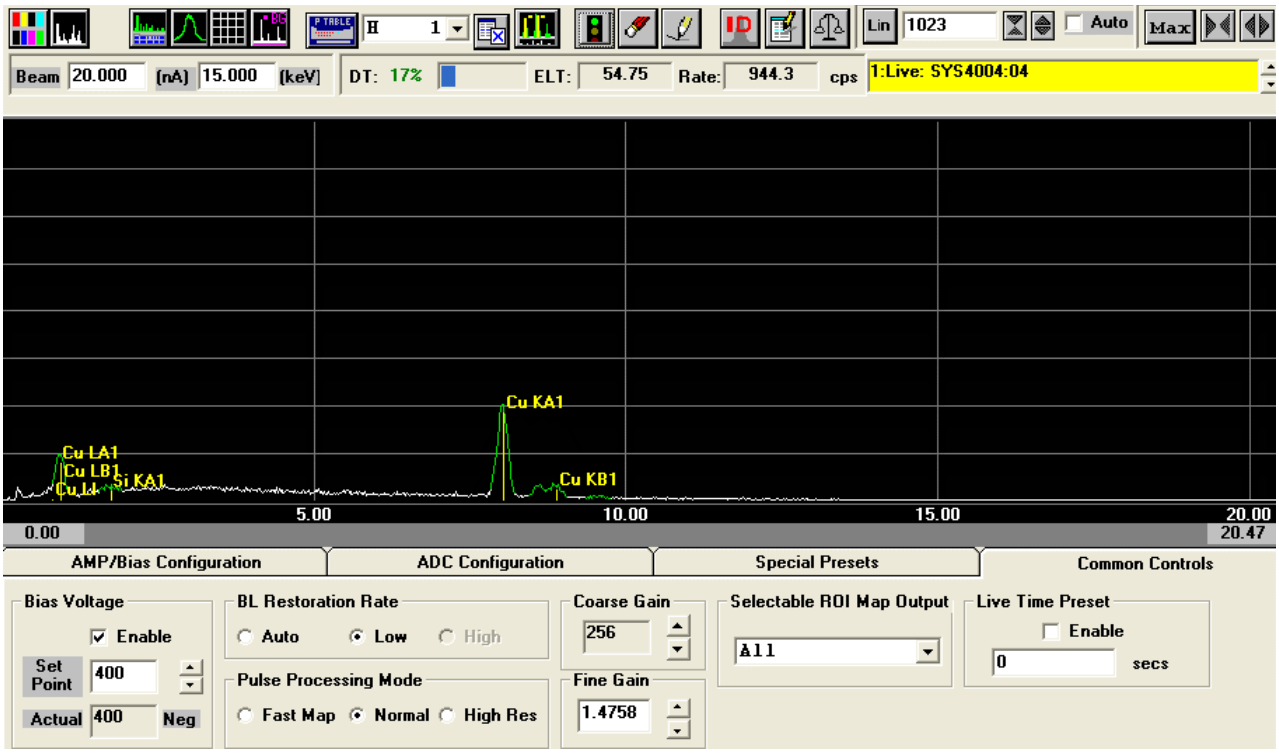

Figure A5. Spectrum of >90%(copper grain (above) (FM-3b Tpr).

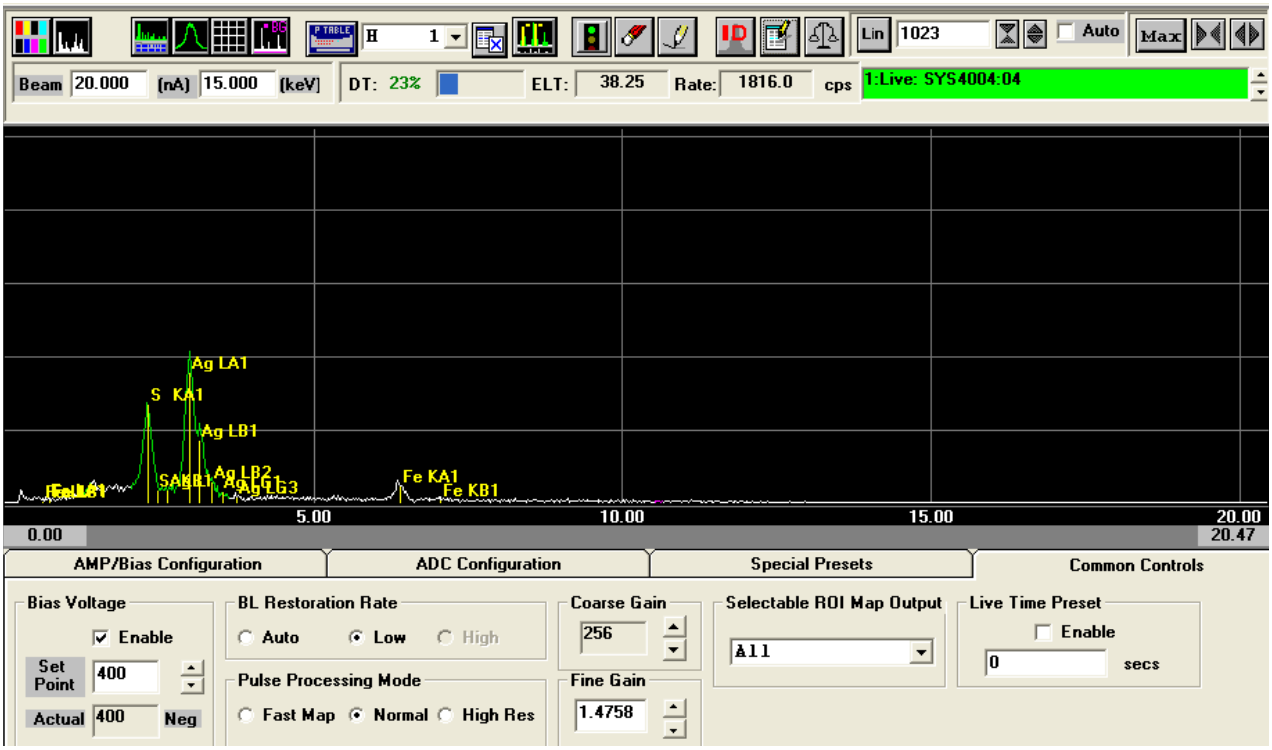

Figure A6. Spectrum of a silver phase grain (above) (FM-11 Tbr). Selenium does not appear in spectrum but was measured.

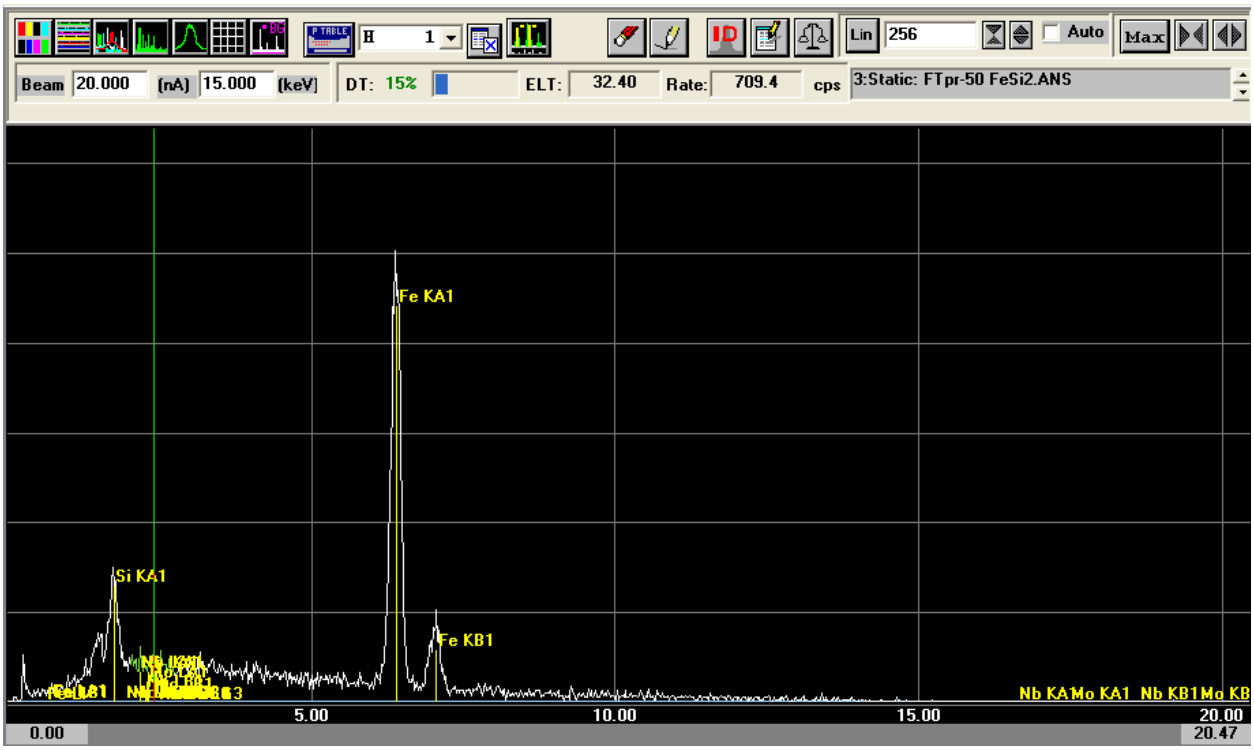

Figure A7. Spectrum of low-sulfur pyrite grain (above) (FM-50 Tpr).

Appendix B: Laser Ablation-Inductively Coupled Plasma-Mass Spectrometry Raw Data

PYR-1- L1-FM-12 Tpl

t (sec)	Ti (ppm)	Fe (ppm)	Ni (ppm)	Cu (ppm)	Zn (ppm)	As (ppm)	Ag (ppm)	Sb (ppm)	Au (ppm)	Pb (ppm)
0.00	2.07	702577.48	3.15	22.19	5.55	4659.33	50.14	10.11	0.81	96.40
0.16	1.27	706215.02	4.23	17.38	3.77	4808.13	44.02	9.30	1.15	103.30
0.32	2.47	717697.32	5.72	17.65	3.77	4883.38	79.59	10.21	0.86	113.04
0.47	0.07	660260.82	6.80	13.53	0.19	5082.96	55.15	10.21	0.43	122.72
0.63	2.07	661354.42	4.37	14.55	1.62	4904.57	86.91	11.83	0.52	123.86
0.79	0.87	645634.02	4.37	15.99	1.62	4625.03	62.66	11.88	0.67	1086.89
0.95	11.66	737827.30	2.21	19.20	3.41	4208.46	51.31	11.18	0.67	4053.20
1.11	1.67	718418.10	6.94	13.64	13.40	3597.38	62.23	10.38	0.57	6418.29
1.26	2.47	557679.42	4.50	10.49	0.55	3717.25	50.19	10.00	0.52	6971.17
1.42	1.67	535306.69	5.86	9.74	0.91	3147.82	43.91	8.98	0.57	7974.07
1.58	4.07	547608.45	6.40	10.06	3.05	3015.55	71.30	14.73	0.43	8170.16
1.74	1.27	561351.53	7.88	13.26	1.98	2896.91	64.25	14.25	0.67	8663.49
1.90	5.27	598042.12	4.50	13.00	1.98	2758.81	52.32	15.92	0.43	9337.94
2.05	4.47	541919.51	5.32	18.77	2.69	2739.30	82.24	18.34	0.43	10267.15
2.21	6.07	586165.87	2.88	22.46	3.40	2611.85	77.06	15.59	0.14	12547.28
2.37	9.66	594797.48	3.69	14.49	1.26	2553.03	85.02	15.70	0.09	13724.24
2.53	5.27	494076.03	5.45	17.91	1.98	2401.15	72.15	14.41	0.62	11399.04
2.69	4.07	507725.31	3.29	16.15	2.33	2433.24	60.78	11.23	0.28	12360.39
2.84	8.07	613374.91	2.34	10.11	1.98	2390.99	65.26	13.55	0.28	9967.31
3.00	6.07	497535.62	2.61	11.87	2.33	2436.75	65.37	11.23	0.19	8536.03
3.16	7.27	460389.96	2.07	10.00	2.33	2310.79	103.05	8.55	0.38	5573.88
3.32	10.86	540507.47	1.67	10.22	3.05	2292.67	52.47	9.03	0.52	4866.42
3.48	12.06	516516.58	0.99	8.78	1.62	2318.15	64.46	6.39	0.38	2592.10
3.63	18.05	491179.77	1.12	10.00	5.54	2300.33	44.17	5.59	0.19	1953.51
3.79	12.86	527983.53	1.40	9.95	2.69	2214.70	32.69	6.50	0.33	1235.64
3.95	13.66	578532.05	1.39	10.54	4.47	2237.17	23.88	6.13	0.28	630.76
4.11	12.06	683653.09	1.12	11.29	1.97	2151.37	22.18	6.77	0.14	235.77
4.27	9.67	497322.86	1.39	6.85	2.33	2255.77	16.45	13.01	0.04	148.51
4.42	9.67	544946.26	1.26	9.42	4.83	2130.94	18.52	6.39	0.33	128.31
4.58	4.47	623863.65	2.07	9.42	2.69	2279.42	14.81	6.23	0.38	153.44
4.74	28.04	550363.61	1.12	10.80	3.76	2358.59	19.15	6.18	0.28	418.37
4.90	37.63	500120.51	2.07	14.06	3.04	2400.44	17.88	8.22	0.28	1051.71
5.06	14.06	564592.53	2.34	14.65	2.69	2397.74	18.52	7.20	0.24	844.78
5.21	16.46	514276.37	1.39	12.62	3.04	2350.19	19.90	7.95	0.38	1409.13
5.37	22.85	601374.73	0.72	12.67	2.69	2215.92	23.71	8.97	0.33	2782.44
5.53	19.65	499773.35	2.61	12.46	1.97	2288.15	26.26	7.90	0.24	5143.77
5.69	17.26	537486.61	2.48	9.68	3.76	2299.98	35.76	10.16	0.48	9280.26
5.85	20.45	496682.94	1.53	11.18	3.40	2289.88	58.37	7.79	0.24	15723.58
6.00	17.26	444765.22	1.94	9.63	4.47	2076.09	56.50	9.24	0.14	22221.88
6.16	19.25	456765.88	4.10	12.46	4.47	2044.23	71.37	10.43	0.33	21463.12
6.32	19.65	487646.54	6.12	14.17	3.40	1849.84	117.07	7.79	0.43	26201.51
6.48	23.65	504013.78	8.42	15.24	3.75	1785.91	299.65	9.35	0.38	33526.74
6.64	18.05	407520.95	7.75	11.71	2.68	1777.10	102.32	8.60	0.38	38608.34
6.79	22.85	549192.62	5.18	15.02	6.96	1783.53	116.26	9.46	0.33	36769.29

PYR-1- L1-FM-12 Tpl

t (sec)	Ti (ppm)	Fe (ppm)	Ni (ppm)	Cu (ppm)	Zn (ppm)	As (ppm)	Ag (ppm)	Sb (ppm)	Au (ppm)	Pb (ppm)
6.95	30.04	532452.75	10.86	14.81	1.97	1764.18	85.36	10.48	0.24	35512.56
7.11	26.84	426234.31	16.67	12.46	6.61	1708.27	96.80	10.10	0.28	33303.26
7.27	26.84	501825.02	15.18	13.95	5.54	1891.10	77.61	9.24	0.14	22997.56
7.43	25.24	564313.24	16.67	12.78	2.33	1814.80	58.94	6.98	0.48	14644.02
7.58	28.84	506301.01	14.91	13.21	3.39	1862.87	201.76	7.84	0.76	20395.97
7.74	34.03	606898.32	8.96	16.04	2.32	2095.59	152.28	9.08	3.98	17976.20
7.90	30.83	565327.00	9.37	12.78	5.53	2518.31	281.89	8.43	1.96	23497.17
8.06	26.84	544007.58	11.53	19.78	6.60	2598.49	131.87	9.19	1.10	32316.28
8.22	27.64	478745.33	10.18	23.95	6.25	2888.02	173.37	9.62	0.86	40094.14
8.37	32.03	558359.22	6.66	21.17	4.46	3191.57	203.69	9.72	1.15	41404.13
8.53	27.24	527186.43	4.91	102.51	3.75	2982.39	439.52	15.00	7.73	37915.50
8.69	28.04	644900.40	3.83	48.42	3.04	2697.87	552.92	7.74	22.54	30432.98
8.85	30.43	448927.00	3.29	53.90	2.68	2580.74	795.87	7.47	21.58	25728.29
9.01	30.83	560996.89	3.83	43.60	6.96	2403.58	1266.38	6.98	27.89	22899.44
9.16	38.02	464076.14	2.61	46.76	5.17	2523.44	960.91	6.71	27.55	9117.13
9.32	29.24	599148.96	2.75	41.61	5.53	2470.12	468.58	6.45	10.27	5230.87
9.48	35.63	494982.66	2.48	28.33	3.75	2611.65	704.42	5.75	7.82	4868.64
9.64	27.64	529893.78	1.53	22.66	4.46	2874.80	1367.58	6.07	5.13	3727.64
9.80	23.25	570399.51	2.20	26.41	4.10	3147.70	536.86	4.46	6.43	3327.81
9.95	32.03	556481.86	1.66	15.88	5.53	3245.07	585.33	4.62	2.20	3288.01
10.11	28.84	530891.55	0.85	16.73	3.39	3044.40	95.47	4.03	1.39	3268.96
10.27	30.83	564733.97	1.53	12.51	5.89	2832.35	70.60	3.97	0.57	2085.07
10.43	32.83	620054.85	0.99	13.10	6.60	2576.86	287.79	3.87	0.57	1826.95
10.59	26.44	510596.19	3.42	12.46	4.46	2540.16	30.86	4.13	0.43	1598.74
10.74	22.45	537737.95	2.20	11.82	6.60	2460.94	32.24	4.83	0.43	1486.44
10.90	40.02	482677.90	1.66	13.69	4.81	2373.84	40.04	4.13	0.48	1258.14
11.06	91.95	535768.57	0.99	10.48	5.17	2249.61	24.60	5.21	0.24	966.04
11.22	106.74	511058.44	1.12	10.86	8.02	2240.41	25.34	4.99	0.38	535.60
11.38	84.35	538943.77	0.72	13.42	5.53	2237.42	29.80	4.56	0.19	377.16
11.53	46.40	476464.74	2.07	14.91	6.24	2294.25	28.36	5.96	0.43	278.87
11.69	28.44	465313.84	3.56	12.83	6.59	2262.83	28.36	7.30	0.48	216.60
11.85	30.43	579110.20	2.20	14.86	4.46	2316.42	47.16	8.92	0.43	176.46
12.01	26.84	540803.27	2.34	14.86	4.81	2401.26	39.24	7.41	0.14	114.60
12.17	20.45	431945.55	2.61	13.69	1.60	2374.81	39.72	7.84	0.48	100.63
12.33	27.24	541459.66	3.28	14.91	4.46	2403.88	37.91	6.28	0.38	142.25
12.48	28.43	592182.59	3.42	12.72	3.74	2504.96	38.18	5.96	0.76	182.30
12.64	28.83	490753.11	2.61	13.69	3.39	2809.66	46.52	5.75	0.52	126.82
12.80	46.00	515858.32	3.69	13.95	8.37	2169.19	34.67	2.68	0.24	48.11
12.96	8.08	125937.39	0.85	2.59	1.60	442.66	7.39	0.70	0.04	15.73

PYR-2-L1-FM-12 Tpl

t (sec)	Ti (ppm)	Fe (ppm)	Ni (ppm)	Cu (ppm)	Zn (ppm)	As (ppm)	Ag (ppm)	Sb (ppm)	Au (ppm)	Pb (ppm)
0.00	2.60	7083.46	16.21	79.29	26.32	5790.07	114.18	171.90	3.50	2715.57
0.16	3.02	569726.34	19.72	66.35	14.64	6959.72	145.09	221.08	4.65	2660.39
0.32	3.75	667804.89	25.65	75.04	9.33	7650.25	158.77	233.42	5.37	1849.77
0.47	3.60	576231.63	25.52	154.28	8.63	8310.77	142.46	231.93	5.13	1719.08
0.63	3.48	552444.76	25.65	106.15	6.50	9219.71	151.30	248.38	6.38	1687.19
0.79	3.47	613535.20	28.21	160.52	12.52	9238.82	144.06	239.65	5.85	1524.79
0.95	3.61	603858.98	30.78	119.74	11.10	8731.80	129.56	244.12	7.29	1463.93
1.11	3.51	568559.06	26.59	89.99	9.33	9169.91	149.90	244.12	4.89	1610.21
1.26	3.52	578799.92	21.06	87.19	5.80	9062.12	149.63	241.74	6.33	1957.31
1.42	3.50	612449.20	26.32	72.78	5.44	9038.56	144.91	232.58	5.80	3303.10
1.58	4.82	529273.55	26.73	69.88	4.73	9460.22	148.29	250.13	7.82	5916.93
1.74	4.13	596249.42	33.88	67.36	4.73	9828.14	152.52	250.85	8.20	7021.65
1.90	4.65	542652.23	26.32	75.04	3.67	10339.85	164.16	246.98	10.60	4428.34
2.05	4.45	597673.78	24.16	81.27	5.09	10757.60	156.22	235.44	9.45	2063.60
2.21	5.08	615161.28	26.32	70.63	4.73	10921.64	137.99	247.85	14.16	1684.78
2.37	5.24	641534.88	25.11	79.33	3.67	12095.28	225.95	257.69	12.48	1679.46
2.53	5.25	577101.35	20.93	71.49	2.61	13102.69	334.63	260.01	17.72	1639.84
2.69	5.69	725569.05	22.41	165.12	19.23	13024.90	159.10	242.77	13.15	1945.15
2.84	5.88	519111.83	21.74	98.81	10.74	11682.01	304.28	229.86	11.18	4083.30
3.00	5.77	569113.84	20.12	75.41	7.56	10478.98	315.60	212.18	12.81	8754.41
3.16	5.67	577508.75	22.27	265.82	6.50	10600.94	857.92	199.93	8.92	9034.78
3.32	6.13	539492.09	20.66	696.59	10.04	10193.43	448.09	188.74	11.76	10352.83
3.48	5.38	577983.17	20.93	399.56	10.04	10305.59	200.58	178.93	7.87	10495.85
3.63	5.67	570460.75	23.08	402.91	12.86	9075.64	143.92	155.36	7.34	7010.80
3.79	5.69	583363.45	21.60	334.77	10.74	9444.01	267.05	154.16	10.31	5125.22
3.95	5.78	596241.58	24.70	587.56	6.85	8737.50	241.90	148.75	6.71	13099.22
4.11	5.76	511503.18	23.62	235.79	7.56	8388.70	326.41	141.06	9.74	24523.15
4.27	5.91	521553.94	24.57	225.99	6.50	9411.96	287.25	134.42	9.98	28781.74
4.42	7.97	603762.76	29.55	501.75	5.44	8783.03	443.36	105.13	39.10	28168.52
4.58	6.31	626377.26	21.33	795.09	11.80	8608.99	283.48	114.73	8.01	16617.14
4.74	6.75	614070.06	22.27	1288.24	9.33	8338.01	143.58	126.52	10.41	5858.42
4.90	6.07	515511.17	22.54	1569.12	12.51	8185.90	121.49	124.67	13.34	1953.46
5.06	6.15	512193.19	24.70	9885.57	16.40	7802.88	322.98	109.68	6.62	1201.61
5.21	5.47	468262.44	20.92	2498.22	23.11	7023.73	187.93	97.91	7.53	800.07
5.37	5.61	530404.27	15.13	3417.39	20.28	7221.95	201.08	85.51	5.47	739.25
5.53	5.29	532464.98	15.13	3420.71	18.16	6535.61	123.89	88.70	6.67	611.15
5.69	5.63	615720.50	14.72	4192.59	18.52	6130.75	293.38	82.75	6.33	518.25
5.85	5.64	526180.84	9.74	3445.22	19.93	6017.19	87.70	77.02	11.37	495.63
6.00	5.18	477028.09	13.51	1161.12	23.11	5937.21	56.23	76.96	3.83	430.73
6.16	5.15	410708.86	14.32	279.19	17.10	5764.20	42.42	78.26	4.99	1246.70
6.32	5.23	561987.50	29.55	140.64	17.10	5916.34	67.25	72.85	4.79	433.02
6.48	5.04	528836.73	12.03	70.78	12.15	5900.77	100.78	63.35	10.65	367.86
6.64	5.02	470911.13	11.89	51.43	8.97	5774.01	81.53	50.85	9.64	301.30
6.79	5.33	511092.03	11.49	35.54	15.68	5517.63	37.51	50.47	4.22	262.40

PYR-2-L1-FM-12 Tpl

t (sec)	Ti (ppm)	Fe (ppm)	Ni (ppm)	Cu (ppm)	Zn (ppm)	As (ppm)	Ag (ppm)	Sb (ppm)	Au (ppm)	Pb (ppm)
6.95	4.79	442604.95	8.79	31.96	13.56	5197.91	24.58	43.58	4.70	225.94
7.11	4.75	476792.73	8.25	28.44	10.74	4530.30	23.94	37.28	4.89	211.88
7.27	4.64	443951.29	8.39	22.73	7.55	4619.61	23.05	31.00	3.50	177.71
7.43	4.28	445655.13	8.12	26.57	6.85	4717.62	24.42	23.37	3.40	241.06
7.58	4.47	431356.28	10.81	27.05	12.15	4828.54	30.01	17.09	5.80	1115.28
7.74	4.19	464501.50	10.68	20.65	8.61	4938.96	23.05	12.97	2.20	394.90
7.90	3.95	458711.62	9.74	27.48	7.91	4706.73	21.25	14.41	1.91	284.72
8.06	3.81	522757.73	7.04	25.18	11.44	4643.04	20.41	9.91	3.40	255.96
8.22	2.16	214950.26	2.46	8.55	4.37	1342.44	8.40	1.72	0.62	64.32

PYR-4-L1-FM- Tpr

t (sec)	Ti (ppm)	Fe (ppm)	Ni (ppm)	Cu (ppm)	Zn (ppm)	As (ppm)	Ag (ppm)	Sb (ppm)	Au (ppm)	Pb (ppm)
0.00	2.08	489436.87	1.45	27.25	158.11	1925.66	423.53	91.76	0.37	166039.66
0.16	2.17	605159.73	0.15	18.26	3.72	2194.14	232.15	94.39	0.42	179226.77
0.32	2.25	576438.33	0.02	19.57	1.74	2359.26	279.34	94.50	0.56	168366.83
0.47	2.49	585543.81	0.28	15.76	1.08	2487.33	257.06	85.14	0.37	167573.42
0.63	2.76	666840.26	0.15	12.37	2.40	2428.09	165.87	73.86	0.23	127864.06
0.79	2.49	551231.44	0.28	10.23	1.41	2612.30	115.90	54.07	0.23	96750.66
0.95	2.48	514743.88	0.15	8.09	0.42	2395.87	72.16	40.01	0.33	67038.02
1.11	2.05	577088.79	-0.12	8.77	1.08	2047.99	52.97	21.04	0.23	36886.09
1.26	2.19	460489.27	0.15	3.92	0.42	1905.32	23.17	7.77	0.04	12426.76
1.42	2.31	465147.84	-0.12	2.25	0.75	1825.10	5.57	3.67	0.09	4279.90
1.58	2.24	393901.42	0.54	1.05	1.41	1647.94	3.36	1.44	0.09	1840.70
1.74	2.36	375945.40	0.15	3.29	1.08	1567.37	1.69	0.45	0.04	677.76
1.90	2.48	425533.20	-0.12	0.43	0.42	1610.70	1.95	0.24	0.04	289.42
2.05	2.05	363371.14	-0.25	0.37	1.08	1479.08	1.19	0.50	0.09	309.56
2.21	2.33	385009.09	1.06	3.14	0.75	1574.06	0.64	0.76	-0.01	105.57
2.37	2.49	405126.82	-0.25	1.52	4.37	1689.58	9.20	0.35	-0.01	113.27
2.53	2.39	404731.55	0.80	1.52	3.71	1782.49	0.23	0.61	-0.01	48.41
2.69	2.18	411345.31	0.15	1.88	3.05	1901.70	0.13	0.30	0.14	31.87
2.84	2.63	503680.04	0.15	0.32	0.75	1936.29	0.08	0.35	0.04	15.84
3.00	2.58	390938.34	0.15	3.66	2.06	1834.49	0.23	0.19	0.09	15.19
3.16	2.22	384192.21	0.15	0.37	0.09	1824.85	0.03	0.09	0.09	30.46
3.32	15.40	394519.94	0.80	1.57	1.08	1873.26	0.43	0.40	0.09	17.95
3.48	2.71	355842.73	0.54	1.10	2.06	1881.45	0.64	0.35	0.23	53.27
3.63	2.55	408465.09	0.67	2.04	3.05	1844.03	5.47	0.50	0.14	130.05
3.79	2.51	423945.63	0.15	2.30	4.69	1793.35	0.69	0.76	0.09	119.04
3.95	2.68	394199.33	0.67	0.79	0.74	1820.20	0.99	0.50	0.09	184.85
4.11	2.46	426051.82	0.93	2.77	3.05	1892.13	54.58	0.71	0.23	891.65
4.27	2.64	422213.37	0.28	6.16	0.74	2178.02	367.40	2.53	0.37	3041.09
4.42	2.46	376521.71	0.02	4.33	2.72	2108.11	693.21	2.11	2.31	2577.84
4.58	2.74	408971.47	1.72	4.49	0.41	2077.32	133.82	4.45	0.18	8230.58
4.74	2.52	452271.56	-0.12	5.43	2.39	2014.98	379.54	11.62	0.85	15153.83
4.90	2.73	431334.39	0.54	7.41	2.39	2102.62	391.72	14.84	1.74	27033.48
5.06	2.91	458126.31	0.01	7.35	2.71	1965.77	197.50	17.70	0.47	31990.50
5.21	2.75	383010.50	0.67	9.54	4.69	1894.80	385.35	20.36	0.47	32201.49
5.37	2.75	471771.43	0.67	7.87	5.02	1873.52	427.09	19.21	1.18	34164.88
5.53	2.77	477655.80	2.11	10.64	7.98	1810.07	1360.15	21.55	0.75	37265.34
5.69	3.37	455426.48	2.37	15.49	11.60	1750.11	753.06	31.50	0.51	54095.21
5.85	3.78	474082.34	1.06	19.45	15.22	1906.33	570.65	49.87	0.51	78846.95
6.00	3.87	432358.13	0.41	29.01	14.23	2136.07	766.27	147.34	1.08	107323.45
6.16	3.97	408809.98	0.80	47.27	13.57	2430.20	2634.71	105.50	1.27	141125.76
6.32	3.52	367670.35	1.06	41.04	14.23	2280.26	4042.34	143.32	8.94	159831.90
6.48	3.45	479272.11	0.41	56.76	14.56	2400.00	8218.21	113.18	5.15	170058.17
6.64	3.56	408004.60	0.93	50.15	15.21	2557.51	3714.56	117.29	4.01	179133.98
6.79	3.48	419642.42	1.32	33.77	6.99	2344.60	1987.25	127.84	3.35	160604.30

PYR-4-L1-FM- Tpr

t (sec)	Ti (ppm)	Fe (ppm)	Ni (ppm)	Cu (ppm)	Zn (ppm)	As (ppm)	Ag (ppm)	Sb (ppm)	Au (ppm)	Pb (ppm)
6.95	3.84	438586.55	0.41	24.04	5.67	2487.52	835.10	100.18	0.80	147860.37
7.11	4.20	503930.52	0.67	19.66	10.60	2428.59	589.25	105.44	0.66	160533.49
7.27	3.45	466504.17	0.80	22.90	6.00	2363.15	328.77	112.65	0.89	183363.34
7.43	3.07	545047.99	0.41	15.22	3.36	2336.47	503.42	125.35	1.60	216620.34
7.58	2.93	450311.77	0.28	19.55	3.69	2343.31	2689.86	133.58	1.18	244971.25
7.74	3.39	484520.83	0.41	21.69	4.02	2368.79	14246.10	136.38	1.51	263058.12
7.90	3.45	404016.34	0.15	22.84	2.05	2590.10	13352.54	143.30	1.46	248738.26
8.06	3.22	478875.05	-0.12	20.75	3.69	2649.77	13713.91	152.61	1.27	259137.37
8.22	3.54	487520.97	0.41	22.95	0.73	2571.60	18760.07	129.62	1.55	223882.33
8.37	2.86	492061.26	0.28	29.27	1.72	2516.00	28726.99	113.43	1.84	199486.06
8.53	2.80	583267.24	1.58	33.86	3.69	2630.92	22582.31	99.38	6.24	178189.76
8.69	3.05	522207.68	0.15	30.47	1.71	2488.05	26006.22	86.25	3.02	141811.29
8.85	3.61	554244.05	0.54	47.63	4.35	2691.48	30209.50	75.34	2.03	137705.14
9.01	3.55	552496.38	-0.12	99.28	1.71	2837.58	24737.26	70.62	1.60	126018.05
9.16	3.37	533815.12	0.54	29.47	2.04	2823.64	23007.38	60.15	7.42	119375.21
9.32	3.46	580537.49	0.54	25.71	1.71	2654.42	6484.88	84.25	1.89	119979.12
9.48	3.98	627106.48	0.28	44.59	2.04	2542.84	4247.38	69.41	3.68	130057.59
9.64	3.53	638467.56	1.58	35.53	5.99	2670.52	2183.03	69.05	5.53	128204.63
9.80	3.36	595679.25	1.32	33.23	3.68	2580.79	4140.73	69.83	1.13	129184.98
9.95	3.41	620379.59	0.80	44.17	5.33	2536.13	6039.76	77.95	0.56	126064.94
10.11	3.37	634283.36	0.41	57.00	2.04	2660.03	10973.82	118.89	19.59	133550.31
10.27	3.24	508645.38	0.67	72.43	2.37	2947.89	9384.45	115.47	9.45	130889.77
10.43	3.57	590486.85	1.06	66.29	1.38	3114.12	5235.82	85.97	8.27	116299.78
10.59	3.44	561456.65	0.15	40.66	2.69	2918.18	2145.68	58.73	5.24	98753.22
10.74	3.61	547636.05	0.15	22.05	0.72	2997.21	654.45	45.41	1.46	86947.54
10.90	3.40	515575.67	0.54	15.11	1.05	3064.15	567.17	44.68	0.85	76070.09
11.06	2.97	596459.84	0.15	11.83	2.36	3067.02	367.37	42.75	1.08	73995.26
11.22	3.28	700619.37	0.28	15.42	3.35	3051.84	266.84	43.69	0.89	80494.22
11.38	2.81	449224.09	0.41	25.60	1.38	2955.78	279.83	52.56	1.13	90452.54
11.53	2.97	586361.82	0.80	14.90	4.33	3086.15	363.55	56.64	1.70	100131.05
11.69	3.06	501673.88	0.67	11.72	3.02	3162.57	739.58	54.08	0.70	98788.89
11.85	3.36	558905.85	1.06	19.34	4.33	3219.52	1384.29	50.53	0.89	96644.57
12.01	3.34	486939.07	0.28	16.68	2.69	3350.12	2223.18	57.79	0.89	98082.73
12.17	2.94	543516.98	0.01	21.68	2.69	3228.22	1894.08	53.61	1.46	87361.43
12.32	3.20	489876.72	0.41	15.01	2.69	3003.83	1130.54	58.05	0.61	80489.02
12.48	3.08	532559.84	0.01	16.26	1.70	3003.51	973.22	41.29	0.66	67152.61
12.64	3.08	579766.96	0.41	19.75	1.04	3063.45	1413.91	55.07	1.46	55201.87
12.80	3.29	494274.88	0.67	44.58	0.38	3169.02	1224.66	49.95	1.32	44621.81
12.96	3.70	661972.73	0.28	23.04	2.35	3199.07	1661.37	42.01	0.70	31954.70
13.12	3.75	620691.65	1.06	19.02	2.68	3003.65	1644.14	29.35	0.56	23429.28
13.27	3.31	530568.79	0.41	20.06	1.37	3001.00	1970.43	21.39	1.22	17139.77
13.43	3.21	547501.89	0.14	12.87	1.70	2794.04	1959.63	14.42	0.80	13558.42
13.59	3.53	473317.97	-0.12	12.87	4.00	2761.88	1275.99	12.13	0.66	14436.55
13.75	3.53	538989.50	0.01	4.74	1.37	2752.31	829.75	10.73	0.33	13239.69

PYR-4-L1-FM- Tpr

t (sec)	Ti (ppm)	Fe (ppm)	Ni (ppm)	Cu (ppm)	Zn (ppm)	As (ppm)	Ag (ppm)	Sb (ppm)	Au (ppm)	Pb (ppm)
13.91	3.42	588027.70	0.54	4.95	1.04	2601.58	816.83	7.67	0.37	12423.61
14.06	3.51	606914.22	0.93	5.00	1.69	2410.35	1169.02	7.67	0.28	9622.03
14.22	3.38	613119.65	0.80	5.36	6.29	2290.88	160.80	7.67	0.14	8211.93
14.38	3.75	486015.03	1.06	4.01	3.33	2229.40	245.64	6.52	0.09	6927.49
14.54	3.70	579523.93	1.06	6.09	5.31	2090.23	36.72	5.07	0.14	5823.04
14.70	3.05	505884.41	0.54	1.98	2.35	1925.14	332.16	3.15	0.04	4703.26
14.85	3.23	569939.90	0.41	3.12	2.67	1803.38	17.49	3.05	0.09	3915.95
15.01	3.48	507937.70	0.41	1.92	1.69	1750.52	12.31	3.20	0.04	3760.08
15.17	3.29	537968.15	0.41	2.24	3.00	1822.28	12.00	2.53	0.14	3883.95
15.33	3.74	615472.18	0.80	2.29	1.03	1601.11	6.01	3.25	0.14	2604.76
15.49	3.53	640770.43	0.01	1.25	2.01	1487.03	4.91	1.23	0.23	1583.49
15.64	3.47	571868.75	0.28	4.48	1.69	1492.35	2.54	1.13	0.04	668.20
15.80	3.20	536215.87	0.14	9.74	3.00	1295.83	1.59	0.66	-0.01	319.38
15.96	3.54	595658.20	0.54	2.91	4.31	1148.91	0.83	0.51	0.09	179.13
16.12	3.57	611969.65	0.28	1.30	2.34	1053.29	0.33	0.25	-0.01	102.96
16.28	3.36	698029.86	-0.12	0.05	1.35	1022.20	0.33	0.19	-0.01	61.39
16.43	3.54	529920.90	0.41	0.52	2.34	890.91	0.33	0.04	0.09	35.95
16.59	3.42	555366.06	0.80	0.41	0.37	827.35	0.38	0.09	0.04	133.09
16.75	3.12	454057.07	1.97	1.25	1.02	792.02	5.31	0.35	0.04	24.01
16.91	3.71	523870.78	0.41	1.66	3.65	741.56	0.13	0.14	-0.01	29.50
17.07	3.67	546935.30	1.19	3.74	6.28	739.35	0.38	0.45	0.09	23.14
17.22	3.44	593859.07	0.54	2.55	1.35	650.45	0.28	0.61	-0.01	16.94
17.38	3.24	511752.94	0.54	1.77	1.02	607.31	0.53	0.45	0.04	11.61
17.54	2.95	509242.63	0.41	3.90	8.57	660.88	2.09	0.71	0.09	9.12
17.70	3.52	566707.87	0.01	3.12	4.63	651.53	1.14	0.25	0.04	11.19
17.86	3.48	515317.36	0.67	3.54	7.26	733.51	2.54	0.82	0.09	9.04
18.01	3.58	673975.86	-0.12	1.71	4.96	714.23	0.38	0.35	0.14	14.17
18.17	3.34	587726.91	-0.12	3.54	7.26	707.61	1.64	0.66	0.14	14.78
18.33	3.71	508624.44	0.27	4.78	4.30	757.18	0.88	0.77	0.18	14.10
18.49	3.28	574228.63	0.27	4.32	4.63	724.94	0.53	0.14	0.28	12.85
18.65	3.47	516542.98	2.10	6.82	11.85	1402.32	5.11	2.11	0.28	16.63
18.80	4.58	572582.88	2.63	10.46	18.42	1703.18	2.09	0.87	0.66	9.49
18.96	4.14	616199.37	1.45	20.52	9.55	2459.08	13.61	2.37	0.56	10.81
19.12	4.12	482389.85	3.15	21.62	11.19	3247.85	6.21	1.65	1.27	16.85
19.28	5.45	573061.74	2.76	29.92	4.62	4672.80	2.29	1.44	1.46	9.15
19.44	3.98	529496.65	2.37	41.62	5.28	7603.47	2.79	2.01	1.70	12.81
19.59	3.92	478496.63	1.58	50.62	5.61	7572.10	2.95	2.68	1.74	26.45
19.75	3.86	530071.32	2.76	52.14	11.19	8862.41	4.50	3.20	2.69	20.97
19.91	3.55	477399.71	3.28	63.72	6.59	5410.29	1.89	1.13	1.18	5.56
20.07	1.57	176405.88	0.14	11.55	-0.31	1316.95	0.48	0.25	0.18	21.04

PYR-5-L1-FM-4 Tpr

t (sec)	Ti (ppm)	Fe (ppm)	Ni (ppm)	Cu (ppm)	Zn (ppm)	As (ppm)	Ag (ppm)	Sb (ppm)	Au (ppm)	Pb (ppm)
0.00	1.86	363050.69	0.79	4.72	83.97	420.48	1.88	3.77	-0.01	7.94
0.16	2.12	552047.88	3.65	5.23	39.39	320.23	0.58	6.09	-0.01	2.09
0.32	2.28	684403.71	0.53	3.78	36.79	297.99	-0.02	0.31	0.04	0.82
0.47	2.37	569170.27	0.02	2.75	22.80	281.45	0.13	0.00	-0.01	0.33
0.63	1.97	616701.20	0.15	2.18	28.32	287.14	0.13	0.16	-0.01	0.56
0.79	2.54	565972.66	0.02	2.75	29.95	296.08	0.08	0.11	-0.01	1.68
0.95	2.14	482901.77	0.28	1.81	32.22	271.95	0.03	0.11	-0.01	1.94
1.11	2.59	434998.20	0.41	2.28	25.72	281.71	0.18	0.26	-0.01	1.16
1.26	2.58	490192.82	0.15	1.76	32.22	229.43	0.13	-0.05	-0.01	1.01
1.42	2.34	453421.64	0.41	1.66	25.38	225.91	0.08	0.16	-0.01	5.28
1.58	2.23	356823.96	-0.11	1.30	25.71	226.18	-0.02	0.11	-0.01	0.03
1.74	1.89	353695.34	0.15	1.87	29.93	271.67	0.08	0.11	-0.01	2.02
1.90	2.23	504082.65	-0.11	2.02	33.83	219.13	-0.02	0.31	-0.01	0.63
2.05	2.27	422764.29	0.28	1.35	28.62	226.98	-0.02	0.05	-0.01	0.60
2.21	2.13	356938.34	0.15	1.04	22.12	236.45	0.08	0.05	-0.01	0.22
2.37	1.99	380744.15	0.02	0.83	22.77	208.58	0.08	-0.05	0.04	0.33
2.53	2.14	339348.09	0.28	1.40	24.06	190.99	0.08	0.11	-0.01	1.27
2.69	2.32	354310.65	0.02	1.30	39.02	197.21	-0.02	0.00	-0.01	0.34
2.84	2.22	338146.74	-0.11	0.78	32.84	197.21	0.03	0.00	-0.01	0.48
3.00	2.27	363244.93	-0.24	0.73	27.31	191.53	-0.02	0.00	-0.01	0.60
3.16	2.42	460856.82	-0.24	1.19	20.80	199.37	0.28	0.26	-0.01	0.49
3.32	2.77	361266.48	-0.24	0.62	30.23	186.93	0.13	0.00	-0.01	0.11
3.48	2.28	385554.03	16.53	1.61	25.67	188.82	0.08	-0.05	-0.01	0.15
3.63	2.25	408303.23	-0.11	1.40	22.75	162.87	0.08	0.00	-0.01	0.15
3.79	2.28	378684.23	0.02	1.19	28.92	185.03	0.08	0.21	0.04	0.49
3.95	2.53	363147.14	0.28	1.82	25.66	187.73	0.48	0.11	-0.01	0.82
4.11	2.20	377200.31	0.41	0.83	24.36	209.10	0.23	0.21	-0.01	0.64
4.27	2.27	360608.47	0.02	0.47	21.11	189.35	0.08	0.11	0.04	0.34
4.42	2.75	397492.42	-0.11	1.66	22.08	162.59	0.03	0.00	-0.01	0.22
4.58	2.55	399810.05	-0.11	1.09	23.05	177.73	-0.02	0.00	-0.01	0.56
4.74	2.58	400813.30	-0.24	0.99	28.57	195.03	0.08	0.05	-0.01	0.94
4.90	2.29	372720.88	0.02	1.25	20.12	170.70	0.08	0.11	-0.01	0.79
5.06	2.71	417010.21	0.02	1.51	23.37	167.45	0.03	0.21	-0.01	1.05
5.21	2.52	466853.73	0.02	1.30	24.99	175.83	0.03	-0.05	-0.01	0.04
5.37	2.53	401976.79	0.02	1.77	24.99	186.10	-0.02	0.00	0.04	0.75
5.53	2.55	414087.34	0.02	1.20	20.11	173.39	2.42	-0.05	0.04	0.08
5.69	2.76	490816.96	0.15	1.61	20.11	192.58	4.57	0.16	-0.01	-0.11
5.85	2.36	417289.29	0.28	1.35	25.31	178.53	1.63	0.11	-0.01	0.00
6.00	2.59	392115.51	-0.11	1.35	24.00	172.04	0.43	0.16	-0.01	0.79
6.16	2.94	511938.57	-0.11	0.99	37.00	159.07	0.33	0.16	-0.01	1.05
6.32	2.69	427720.24	0.67	4.77	24.00	139.35	59.40	0.05	-0.01	2.02
6.48	2.73	422391.46	0.28	55.03	19.77	116.14	145.21	0.21	2.02	1.42
6.64	2.94	397640.06	0.15	91.57	22.69	108.05	266.75	0.00	0.32	0.11
6.79	2.92	371962.93	-0.11	7.10	22.69	104.81	121.43	0.21	1.26	1.50

PYR-5-L1-FM-4 Tpr

t (sec)	Ti (ppm)	Fe (ppm)	Ni (ppm)	Cu (ppm)	Zn (ppm)	As (ppm)	Ag (ppm)	Sb (ppm)	Au (ppm)	Pb (ppm)
6.95	2.62	428454.73	0.02	4.72	27.88	86.74	127.57	0.00	0.09	1.16
7.11	2.56	428881.97	-0.11	1.92	24.63	76.76	30.63	0.00	0.04	0.83
7.27	3.06	440854.54	-0.11	0.63	22.36	85.39	6.77	0.16	0.37	0.27
7.43	2.94	445127.21	-0.24	-0.15	21.38	67.87	2.12	0.21	-0.01	1.28
7.58	3.06	434390.48	-0.11	0.06	22.68	69.75	1.18	0.26	-0.01	0.27
7.74	2.76	508035.58	0.41	0.27	19.43	55.74	0.73	0.05	-0.01	-0.07
7.90	3.03	509996.35	-0.11	0.06	19.42	57.63	0.13	0.05	-0.01	-0.07
8.06	3.06	416152.41	0.28	-0.15	16.50	58.71	0.28	0.00	-0.01	0.34
8.22	2.83	595748.22	-0.11	0.06	20.72	75.41	0.13	0.26	-0.01	0.30
8.37	2.91	600847.62	-0.11	0.06	23.64	65.44	0.33	0.21	-0.01	0.49
8.53	3.27	328923.91	0.15	0.16	27.20	63.56	-0.02	0.31	-0.01	0.34
8.69	2.48	507042.60	0.02	-0.25	21.03	56.82	0.03	0.11	-0.01	-0.11
8.85	2.90	462146.78	0.41	0.01	23.63	60.32	0.08	0.05	-0.01	0.27
9.01	2.87	459095.91	0.15	-0.35	15.18	58.98	0.03	0.00	-0.01	-0.14
9.16	3.76	519235.52	0.02	0.06	21.02	69.48	-0.02	0.05	-0.01	0.38
9.32	3.02	582637.64	0.02	-0.20	19.40	55.47	0.03	0.16	-0.01	0.34
9.48	3.14	513071.92	0.02	-0.30	20.37	59.51	0.08	0.00	-0.01	-0.18
9.64	2.92	516291.03	-0.24	0.84	19.07	43.08	0.23	0.21	-0.01	0.27
9.80	2.91	436963.49	0.54	-0.10	20.69	45.51	0.03	0.57	-0.01	0.12
9.95	2.56	488078.95	0.15	-0.09	19.71	58.44	0.03	0.00	-0.01	0.04
10.11	3.06	435635.79	-0.11	0.11	17.76	45.24	0.08	0.26	-0.01	0.01
10.27	3.09	422547.96	0.41	0.58	17.43	48.20	0.43	0.83	-0.01	0.34
10.43	3.26	494014.89	0.28	0.68	22.95	57.36	2.22	0.57	-0.01	0.76
10.59	3.27	424003.81	0.02	-0.04	23.92	64.63	0.63	0.16	-0.01	0.49
10.74	3.07	575001.49	0.02	0.32	25.22	51.16	0.33	0.26	0.04	0.38
10.90	2.79	517402.34	0.67	0.16	38.85	50.90	0.13	0.21	-0.01	-0.22
11.06	2.87	598259.79	0.02	-0.20	16.45	53.86	0.38	0.36	-0.01	0.38
11.22	2.62	570084.92	-0.24	0.06	21.64	60.59	0.08	0.00	-0.01	0.31
11.38	3.53	509879.90	0.15	0.37	18.06	63.29	0.33	0.16	-0.01	0.27
11.54	3.21	579382.46	-0.11	0.53	19.68	53.86	0.03	0.21	-0.01	-0.10
11.69	2.95	480177.96	-0.24	0.11	16.76	49.82	-0.02	0.06	-0.01	0.20
11.85	3.13	528470.33	-0.11	-0.04	23.25	58.17	0.08	0.16	-0.01	0.27
12.01	3.15	573722.53	-0.24	-0.04	16.75	52.51	-0.02	0.06	-0.01	0.20
12.17	3.10	493283.94	-0.11	-0.14	23.57	56.82	0.08	-0.05	-0.01	-0.18
12.33	3.05	399819.95	0.15	0.01	16.42	59.52	-0.02	0.06	-0.01	0.12
12.48	2.91	544697.00	0.02	0.37	23.24	52.51	-0.02	0.16	-0.01	0.31
12.64	3.46	462103.99	-0.11	0.89	18.69	71.37	0.43	0.06	-0.01	0.35
12.80	2.92	663920.28	0.02	1.20	23.55	59.25	0.33	0.00	-0.01	-0.06
12.96	3.05	500548.38	0.02	1.20	19.01	53.32	0.48	0.00	-0.01	0.20
13.12	2.98	496295.43	0.15	1.15	24.52	54.13	2.37	0.06	-0.01	0.72
13.27	3.00	534353.00	0.02	2.29	19.98	48.74	3.12	0.21	-0.01	5.02
13.43	3.15	552196.86	0.15	5.97	26.46	64.90	11.46	0.00	-0.01	9.70
13.59	3.32	420854.58	0.15	7.00	18.67	60.05	176.15	0.06	0.37	10.42
13.75	3.02	550313.37	0.02	13.69	17.70	60.32	627.94	0.11	0.28	2.74

PYR-5-L1-FM-4 Tpr

t (sec)	Ti (ppm)	Fe (ppm)	Ni (ppm)	Cu (ppm)	Zn (ppm)	As (ppm)	Ag (ppm)	Sb (ppm)	Au (ppm)	Pb (ppm)
13.91	3.10	507671.55	0.15	54.28	20.29	50.63	930.77	0.16	6.20	3.15
14.06	3.14	499054.57	-0.11	29.00	21.91	58.98	987.38	0.16	1.78	2.44
14.22	3.38	474181.73	0.02	21.47	20.93	49.02	1987.82	0.21	1.40	2.82
14.38	2.67	504525.99	-0.11	19.08	17.04	43.63	2016.37	0.06	3.90	1.81
14.54	2.96	539067.68	-0.24	25.46	18.66	53.32	3444.07	0.06	1.97	1.66
14.70	2.86	541360.88	0.28	26.61	21.25	54.94	2864.08	-0.05	2.01	1.77
14.85	2.76	483871.09	0.02	22.19	19.62	50.09	4111.91	0.06	4.55	0.72
15.01	3.09	499809.81	-0.11	28.42	20.59	47.13	3360.05	0.06	9.82	0.87
15.17	3.47	544652.12	0.15	21.21	18.97	40.13	2989.61	0.16	10.01	0.46
15.33	2.99	555936.25	-0.11	22.40	14.43	37.98	1900.08	0.11	9.59	0.13
15.49	3.20	450575.09	0.15	23.80	17.99	71.64	1489.06	0.16	4.04	0.99
15.64	3.22	461515.73	-0.11	31.70	19.29	48.48	1560.62	0.36	2.72	0.73
15.80	3.07	479545.55	0.41	38.87	20.58	54.67	2466.96	0.16	7.33	1.25
15.96	3.03	565672.92	0.02	37.26	15.71	55.21	3736.02	0.31	15.80	0.76
16.12	3.51	520129.77	0.02	36.17	18.95	49.56	5038.43	0.16	16.04	0.80
16.28	3.43	535154.57	0.41	36.89	17.33	50.36	3205.85	0.00	10.57	1.36
16.43	3.04	519204.48	0.02	27.96	19.92	51.98	3063.09	0.26	8.74	0.35
16.59	3.08	522726.76	0.41	23.96	13.43	34.75	3613.52	0.06	8.46	0.43
16.75	3.33	519941.44	0.02	20.64	12.46	63.02	2789.10	0.00	4.18	0.73
16.91	3.10	571546.80	-0.11	13.27	26.40	174.65	1350.17	0.73	1.78	3.53
17.07	2.92	475006.62	0.02	14.36	20.88	399.38	604.65	1.09	1.03	4.62
17.22	3.09	564450.04	0.15	25.05	19.58	648.30	544.07	2.12	0.75	6.75
17.38	3.46	553854.27	0.41	15.81	13.42	1011.03	161.29	4.90	0.93	9.89
17.54	3.23	489586.30	-0.24	18.04	22.82	1394.51	56.37	6.96	1.12	22.30
17.70	2.99	545897.91	0.67	39.02	16.33	2326.55	27.40	18.83	4.36	49.21
17.86	2.94	495576.22	0.41	64.54	11.79	4024.60	22.99	33.09	4.18	103.63
18.01	3.25	507376.87	0.15	100.04	19.57	6931.62	21.74	46.56	6.95	166.38
18.17	2.79	548090.76	0.02	145.02	22.48	9775.29	28.54	56.30	12.17	187.57
18.33	3.04	558817.43	0.54	179.03	12.75	12662.97	53.45	61.34	11.84	188.50
18.49	3.15	648415.69	0.41	226.59	14.70	14587.04	94.89	88.23	9.49	279.21
18.65	3.47	430397.29	1.06	253.36	18.26	17304.45	135.49	122.81	14.57	380.74
18.80	3.36	433346.61	0.41	290.25	16.31	19287.87	244.57	175.07	13.30	519.57
18.96	3.28	523797.07	0.28	385.05	19.23	22754.16	942.38	199.14	13.16	634.71
19.12	3.53	505404.59	0.41	426.42	20.20	24868.70	2107.64	225.84	20.37	737.10
19.28	3.39	620062.64	0.41	479.81	14.68	30642.27	2157.68	222.33	16.36	751.68
19.44	3.60	589724.58	0.28	695.78	11.44	31517.04	5726.37	258.16	21.07	777.81
19.59	3.45	640038.60	0.80	912.78	45.48	31966.52	8516.15	323.55	27.01	1064.51
19.75	3.24	669679.90	-0.11	883.27	18.24	32559.63	9870.00	324.62	27.15	1728.14
19.91	3.68	542642.79	0.28	931.05	16.94	32888.01	9359.65	283.55	27.81	1331.37
20.07	3.25	677650.68	0.28	853.52	13.70	41739.91	8313.46	313.92	43.83	1251.73
20.23	3.75	560492.00	0.54	1028.13	12.40	39886.73	13186.01	363.40	51.87	1372.14
20.38	3.27	606094.63	0.15	965.12	16.93	42924.58	16032.27	484.53	38.77	1753.18
20.54	3.57	681839.64	0.28	1231.88	16.61	41944.42	15440.21	465.89	32.86	1784.03
20.70	3.68	586326.75	0.28	1127.80	14.66	40785.76	7241.13	498.03	24.94	1863.32

PYR-5-L1-FM-4 Tpr

t (sec)	Ti (ppm)	Fe (ppm)	Ni (ppm)	Cu (ppm)	Zn (ppm)	As (ppm)	Ag (ppm)	Sb (ppm)	Au (ppm)	Pb (ppm)
20.86	3.74	609586.62	0.15	1303.15	15.95	40764.18	4346.32	444.02	20.22	1806.58
21.02	3.30	599255.10	0.02	1365.75	13.03	40983.51	10678.95	403.02	26.21	1554.76
21.17	3.72	738936.75	0.54	885.43	13.35	40534.40	10752.23	331.30	117.34	1348.78
21.33	3.24	657141.12	0.54	986.95	17.89	36374.20	11386.56	317.00	227.56	1372.73
21.49	3.73	537099.97	0.15	689.40	24.04	33420.09	10235.67	288.54	23.94	1238.47
21.65	3.88	698770.89	0.02	634.92	12.37	35044.06	5361.51	284.53	19.70	1287.91
21.81	3.78	676130.82	0.67	629.82	24.36	34155.89	6827.35	272.13	22.11	1341.54
21.96	4.03	585156.38	0.41	632.44	18.20	30430.68	8718.96	247.25	18.05	1149.42
22.12	3.38	489314.74	0.41	626.22	20.79	28037.59	4934.92	261.78	37.63	1291.08
22.28	5.75	534690.80	0.80	602.53	20.79	29658.59	3110.93	288.10	15.84	1378.30
22.44	2.84	463621.52	0.15	399.47	13.33	13133.60	2202.78	98.47	3.61	420.54
22.60	1.04	114705.69	-0.11	166.72	17.22	3283.37	209.71	29.20	1.26	109.74

PYR-6-L1-FM-4 Tpr

t (sec)	Ti (ppm)	Fe (ppm)	Ni (ppm)	Cu (ppm)	Zn (ppm)	As (ppm)	Ag (ppm)	Sb (ppm)	Au (ppm)	Pb (ppm)
0.00	841.13	639183.96	8.30	56.64	11.59	10343.07	62.42	20.77	6.78	163.50
0.16	1079.48	631524.98	11.02	65.21	71.14	10873.70	92.40	22.88	6.46	158.93
0.32	1073.58	625214.06	8.04	80.62	9.98	10130.54	83.46	19.94	6.74	146.97
0.47	1006.83	633290.27	8.30	69.89	4.83	10198.11	100.09	23.24	5.89	149.00
0.63	1231.95	634024.60	10.89	73.22	8.36	10058.54	101.30	19.84	6.55	171.06
0.79	1315.78	592276.70	11.66	73.06	6.75	10502.21	125.23	20.51	5.71	163.18
0.95	1139.12	532918.54	6.88	66.30	6.43	11768.45	145.19	19.74	5.38	158.42
1.11	1218.36	591391.28	7.65	72.91	5.78	11441.86	77.29	21.33	6.03	150.10
1.26	1836.38	663124.55	5.33	75.77	8.35	10418.80	74.78	19.79	6.17	144.32
1.42	1474.60	563379.22	8.04	82.75	6.42	10295.19	93.75	16.86	7.02	117.99
1.58	1159.34	475475.72	8.95	57.15	6.42	9893.07	114.43	15.31	4.68	118.75
1.74	1855.74	501663.17	7.40	59.44	6.09	9610.14	80.54	13.46	4.11	127.74
1.90	796.98	630762.08	12.57	56.79	5.12	9308.10	122.14	15.11	4.44	146.53
2.05	1107.49	557239.95	8.30	55.70	9.62	8713.43	73.92	17.01	4.11	161.48
2.21	912.02	560089.17	9.46	53.72	5.12	8606.43	119.21	19.27	4.30	203.55
2.37	942.34	551372.28	12.44	64.42	5.44	8781.87	105.40	22.46	2.80	237.67
2.53	1580.41	551922.24	18.52	55.64	9.62	8622.89	94.09	25.24	3.65	293.25
2.69	1422.44	535686.13	29.00	76.49	6.40	9288.30	101.12	27.40	5.42	316.20
2.84	1153.32	566400.81	18.91	57.88	7.68	10977.77	101.07	29.61	4.16	308.69
3.00	1455.31	586301.35	19.68	86.54	20.54	11049.92	149.61	27.86	4.68	264.40
3.16	1190.58	510825.49	18.91	58.39	7.03	9544.88	102.23	28.48	4.77	248.84
3.32	1469.68	470439.02	16.06	69.67	7.67	9313.70	84.39	28.12	4.25	266.43
3.48	1006.01	513058.76	28.09	68.42	53.67	10491.38	101.97	33.53	4.63	285.17
3.63	1038.58	491396.33	24.34	71.02	63.96	11175.28	110.63	34.66	3.88	300.91
3.79	965.89	478988.70	19.16	119.65	19.24	12135.87	120.15	37.91	5.10	360.35
3.95	1002.51	559399.38	22.53	102.71	7.02	12905.80	91.31	38.99	4.77	326.22
4.11	880.94	588940.07	21.36	82.79	7.02	13111.20	94.68	42.18	6.45	301.41
4.27	838.43	573874.58	25.50	161.42	9.58	12963.59	79.67	48.17	4.86	313.71
4.42	1181.78	574156.74	22.40	91.75	6.69	12459.41	162.86	49.05	4.39	297.73
4.58	1383.71	457256.62	23.05	129.65	8.61	13191.42	415.31	47.65	4.72	291.04
4.74	1235.42	498070.83	23.17	125.14	4.75	14140.16	135.93	48.32	7.44	302.22
4.90	1252.07	580374.20	21.23	166.57	7.97	16404.49	269.08	56.38	7.11	338.68
5.06	1095.03	587844.84	13.86	177.37	5.39	15404.66	234.49	63.72	7.44	333.00
5.21	1060.65	533761.42	23.69	150.53	8.92	15493.60	195.53	67.44	5.00	342.00
5.37	1251.87	544486.88	19.81	125.19	8.92	14379.82	427.14	67.49	5.33	358.78
5.53	1482.70	577534.56	24.73	157.83	4.74	13238.22	408.62	61.65	6.03	355.00
5.69	1724.90	510551.71	24.85	145.95	8.27	13451.76	1864.84	71.63	6.59	795.06
5.85	1103.43	629957.71	22.01	130.48	6.98	14338.25	1202.23	66.46	6.13	564.31
6.00	1074.82	559431.28	20.07	116.34	8.59	13635.34	715.12	66.92	4.16	412.21
6.16	1124.17	551396.80	31.71	144.79	5.37	14571.88	240.20	69.92	5.56	386.96
6.32	1651.06	567607.80	28.35	186.64	9.23	14408.59	245.32	72.92	6.50	382.83
6.48	1161.08	599123.77	24.08	180.15	9.87	16624.59	149.11	82.71	7.11	385.42
6.64	1016.13	498726.92	26.53	208.67	7.93	16803.23	190.97	79.81	7.44	468.36
6.79	741.54	648529.57	26.02	198.14	9.22	18977.33	183.13	91.37	6.03	528.09

PYR-6-L1-FM-4 Tpr

t (sec)	Ti (ppm)	Fe (ppm)	Ni (ppm)	Cu (ppm)	Zn (ppm)	As (ppm)	Ag (ppm)	Sb (ppm)	Au (ppm)	Pb (ppm)
6.95	779.58	545948.67	19.81	201.74	8.57	20751.10	246.38	100.93	8.84	510.23
7.11	700.55	537956.14	19.68	267.62	6.32	19904.02	158.31	114.66	8.42	523.60
7.27	1066.29	649607.52	23.43	339.49	8.89	19397.96	98.57	94.43	7.90	423.20
7.43	1487.07	512628.52	24.85	190.90	8.24	16771.40	96.41	86.86	8.09	386.71
7.58	1183.99	522540.48	32.61	182.72	9.52	16719.48	89.07	84.16	6.73	470.68
7.74	928.13	572538.91	30.41	203.37	4.70	17033.69	108.57	88.31	6.50	491.17
7.90	1126.87	639580.06	30.93	196.12	5.66	17634.93	115.67	103.42	6.45	551.02
8.06	1655.43	571682.03	24.33	256.21	5.98	21269.23	115.31	120.22	6.78	543.72
8.22	1290.01	521191.47	21.87	311.12	7.91	20762.87	102.83	126.95	6.78	526.26
8.37	1154.16	589569.71	23.17	235.57	9.83	20852.70	178.38	118.45	7.48	458.51
8.53	1033.31	711967.95	18.77	300.23	5.33	20190.38	147.86	105.59	12.26	441.32
8.69	1316.66	630232.37	18.38	247.52	8.22	18743.81	112.64	86.90	7.72	422.10
8.85	1350.45	628281.99	23.17	246.46	8.22	17884.25	73.67	84.30	7.15	414.44
9.01	1486.40	554788.31	27.31	170.90	6.29	17249.95	71.17	81.56	5.23	389.06
9.16	1343.39	551295.22	19.29	182.43	5.32	15313.48	77.08	78.39	5.56	363.77
9.32	1552.64	594701.83	22.78	159.84	11.10	12765.54	78.83	84.61	4.35	385.73
9.48	1592.11	450536.04	25.36	141.35	8.21	11210.65	74.17	65.61	3.88	317.96
9.64	1677.91	478757.04	26.66	145.08	8.85	10669.23	133.55	61.47	5.19	338.86
9.80	1698.18	603431.54	13.21	98.97	7.56	9941.80	101.36	60.85	3.78	331.28
9.95	2262.87	551133.23	17.86	105.76	11.41	10233.61	92.82	61.42	4.63	313.92
10.11	1763.19	489122.73	15.66	106.12	8.20	8992.98	63.11	48.51	4.02	297.56
10.27	1626.77	535056.94	15.15	93.91	9.80	8278.44	49.87	43.86	6.36	273.68
10.43	1582.31	607758.49	16.96	96.51	8.19	8076.24	63.81	38.66	4.86	259.70
10.59	1124.74	524151.54	15.66	88.90	7.54	9161.02	58.76	31.55	4.86	247.44
10.74	1207.83	634438.88	12.56	91.92	7.22	10397.37	78.22	30.57	5.28	230.35
10.90	1143.83	617125.34	11.14	84.16	5.93	11445.93	69.25	35.26	6.78	214.83
11.06	2169.13	554767.59	13.08	93.49	7.54	11714.31	105.12	33.15	6.45	193.80
11.22	1393.99	472923.82	16.05	82.75	6.57	10706.23	60.65	29.34	7.43	178.54
11.38	1501.81	607857.46	13.08	62.63	7.85	10957.64	71.95	28.26	6.92	182.69
11.53	1389.81	535358.39	15.15	54.32	5.60	9507.42	68.30	27.33	7.06	176.73
11.69	1581.26	520955.97	15.53	66.94	7.53	9415.88	39.69	20.80	5.61	175.42
11.85	1420.30	531681.63	12.95	56.29	8.16	8991.93	58.25	23.68	5.42	159.75
12.01	1377.96	653689.73	12.04	60.81	6.24	9537.50	53.50	24.40	5.47	184.61
12.17	1286.46	624978.96	10.10	71.72	9.44	9277.95	93.30	35.05	7.01	198.88
12.33	1355.82	640853.88	9.33	87.38	7.19	8787.08	96.76	34.12	4.72	196.21
12.48	1240.51	575878.28	9.07	83.27	6.55	9020.32	71.55	29.13	5.09	169.22
12.64	2143.90	507863.36	8.55	65.32	6.87	9392.07	70.14	24.91	5.79	172.48
12.80	1165.84	721377.39	7.65	64.86	3.65	10651.45	206.59	25.58	5.61	179.79
12.96	1123.74	650389.68	7.39	91.23	10.07	10294.05	156.50	30.05	9.26	201.34
13.12	1251.94	572988.45	6.62	79.10	5.90	10527.26	112.14	30.46	7.11	182.55
13.27	1228.26	585594.71	5.07	91.34	12.96	11515.20	111.68	32.98	6.12	181.86
13.43	1196.69	615062.82	6.36	101.03	6.85	11069.59	85.66	29.90	6.78	173.28
13.59	1329.47	589071.41	4.81	86.23	4.60	11139.79	82.96	28.35	5.61	182.58
13.75	1009.98	606208.15	5.45	79.46	8.13	11783.25	110.62	32.01	5.93	195.18

PYR-6-L1-FM-4 Tpr

t (sec)	Ti (ppm)	Fe (ppm)	Ni (ppm)	Cu (ppm)	Zn (ppm)	As (ppm)	Ag (ppm)	Sb (ppm)	Au (ppm)	Pb (ppm)
13.91	1267.37	557154.89	3.90	75.82	5.24	11023.52	135.61	37.57	5.65	203.91
14.06	1522.81	516752.63	4.55	84.66	8.45	11119.12	71.78	34.94	5.79	186.74
14.22	1617.07	648700.21	3.52	86.80	7.80	11084.81	75.84	41.38	8.04	180.77
14.38	1584.30	595372.98	5.71	96.44	10.69	11134.29	75.64	36.28	7.76	220.47
14.54	1753.48	583437.44	4.42	95.81	6.51	12395.30	89.52	35.40	6.40	193.24
14.70	1724.42	594533.78	4.94	92.27	6.19	14393.13	59.53	32.05	6.59	209.43
14.85	1561.94	656455.60	5.97	113.66	4.90	16035.24	69.78	39.00	9.16	204.63
15.01	2443.01	586710.44	7.00	120.98	5.86	18196.36	67.38	56.18	7.90	222.79
15.17	1574.76	558410.82	6.49	162.57	6.82	17679.15	56.68	62.32	7.81	272.12
15.33	1964.02	596165.21	6.23	175.03	9.71	19512.08	101.20	86.49	6.45	345.01
15.49	1634.14	573585.65	7.52	189.00	5.53	18134.08	138.37	100.81	8.60	396.38
15.64	1413.86	698238.98	5.97	186.10	5.21	17872.07	130.64	86.80	8.74	362.25
15.80	1540.83	678399.82	9.33	179.72	4.89	18458.77	135.03	75.40	8.09	325.86
15.96	1467.96	711151.58	8.68	148.01	5.53	18319.37	189.27	83.89	10.24	302.88
16.12	1178.21	567115.23	5.84	168.55	9.37	20942.63	170.53	92.44	10.71	325.41
16.28	1008.14	622104.05	4.81	199.97	8.09	23024.69	162.98	104.64	11.22	326.75
16.43	802.60	526859.76	4.68	231.25	14.18	20068.31	221.41	95.81	11.83	320.98
16.59	845.48	700700.93	5.71	159.76	7.44	23198.29	135.27	81.30	11.13	340.25
16.75	990.18	618463.28	3.39	172.49	9.04	21187.26	117.63	77.72	7.24	352.43
16.91	494.32	607277.60	4.68	167.54	11.93	24969.55	109.18	112.49	10.24	390.08
17.07	292.78	585109.55	4.16	201.65	9.04	24817.01	100.78	97.83	8.23	329.62
17.22	273.84	514297.24	5.58	203.23	9.35	21313.47	116.92	109.83	8.93	380.16
17.38	266.28	512125.73	3.13	173.22	11.60	20034.61	129.36	106.14	9.86	312.27
17.54	247.73	525913.60	4.55	156.02	13.84	20481.21	229.71	62.26	7.80	254.99
17.70	227.78	499844.85	5.84	119.44	9.67	20714.57	119.28	50.75	8.46	223.09
17.86	91.23	479122.21	5.97	104.35	17.04	19198.57	77.61	44.71	10.71	196.17
18.01	63.50	488013.43	5.58	97.93	18.32	20042.99	81.92	46.72	9.35	172.99
18.17	58.84	482093.26	4.68	73.77	16.07	17637.29	89.18	48.06	9.82	186.29
18.33	60.36	452015.86	4.16	87.98	20.24	17258.73	122.25	58.17	12.81	212.93
18.49	37.93	410616.84	3.39	133.93	21.84	17364.03	121.49	41.98	8.37	131.02
18.65	13.70	198364.72	1.58	44.77	5.48	3631.64	37.77	10.16	3.92	34.55
18.80	9.70	71451.92	0.67	17.11	8.04	1171.93	12.23	2.93	0.60	15.71

PYR-9-L1-FM-25b Tbr

t (sec)	Ti (ppm)	Fe (ppm)	Ni (ppm)	Cu (ppm)	Zn (ppm)	As (ppm)	Ag (ppm)	Sb (ppm)	Au (ppm)	Pb (ppm)
0.00	66.51	457067.14	5.49	46.98	67.36	876.45	547.17	8.12	0.24	56.36
0.16	107.92	515857.65	5.09	116.04	16.99	838.89	58.25	7.06	0.09	45.74
0.32	109.48	501652.57	5.89	63.43	10.78	927.31	39.11	5.68	0.19	51.02
0.47	140.87	471841.72	6.16	40.34	9.40	941.16	26.58	6.58	0.14	50.32
0.63	128.19	457955.32	5.89	68.76	6.64	900.71	42.08	6.00	0.09	46.17
0.79	79.24	483448.25	4.03	44.80	10.43	779.62	37.08	6.05	0.43	52.67
0.95	59.24	437580.59	4.16	30.72	9.74	814.85	29.39	6.58	0.28	46.99
1.11	63.41	457857.71	7.90	27.86	8.02	847.01	29.96	6.00	0.33	46.28
1.26	89.78	476497.18	6.70	50.49	9.74	760.43	18.12	6.00	0.33	50.23
1.42	129.96	429288.25	4.96	40.07	11.47	788.88	20.19	6.64	0.28	51.88
1.58	224.90	424779.33	4.69	46.98	7.33	794.51	17.75	7.54	0.19	57.33
1.74	217.81	453335.45	6.96	56.50	16.64	788.58	20.56	7.11	0.19	75.23
1.90	184.03	437638.83	8.30	28.65	9.05	802.10	15.06	8.28	0.04	70.04
2.05	248.70	373281.91	4.16	23.83	6.64	791.38	12.67	9.66	0.28	77.24
2.21	232.31	367118.51	6.96	31.20	9.74	788.83	33.39	10.40	0.28	77.87
2.37	357.14	456643.02	1.76	31.62	15.60	780.37	15.47	9.87	0.09	73.69
2.53	246.25	437174.91	3.23	35.76	2.85	768.24	25.07	9.92	0.09	74.09
2.69	251.92	404030.17	5.36	29.82	5.95	770.77	12.62	11.30	0.33	89.76
2.84	352.12	392323.98	4.16	22.60	9.40	846.33	12.41	12.84	0.09	103.15
3.00	359.47	356470.63	1.89	19.53	10.43	953.15	13.08	11.89	0.24	94.93
3.16	379.54	452793.77	1.09	19.26	12.84	965.87	12.51	13.11	0.14	103.58
3.32	409.65	377018.35	0.42	22.92	6.98	984.83	9.30	13.53	0.04	95.59
3.48	276.08	405012.29	0.96	18.79	6.98	853.07	9.87	11.36	0.28	95.63
3.63	289.90	380373.51	4.56	23.45	6.64	898.24	12.82	10.14	0.09	93.26
3.79	282.90	458251.47	0.56	20.43	9.05	955.35	10.28	10.19	0.19	89.08
3.95	268.23	423588.10	1.22	16.19	6.64	1013.67	9.09	11.57	0.28	91.68
4.11	240.13	513089.24	1.62	17.41	3.88	993.55	9.71	9.02	0.24	77.22
4.27	186.71	487284.90	2.69	16.56	11.46	1064.68	11.32	9.87	0.04	72.93
4.42	167.05	491224.13	2.02	14.70	4.23	1032.91	8.99	7.06	0.14	58.25
4.58	96.38	389811.11	1.22	11.42	4.91	1023.54	8.37	6.21	0.19	56.80
4.74	88.02	480076.29	1.36	12.64	8.01	1037.99	9.19	5.73	0.00	59.78
4.90	122.00	568889.03	2.29	10.31	4.57	1085.06	7.54	6.90	0.04	58.56
5.06	102.71	459723.25	1.09	10.41	8.70	1029.74	9.25	7.32	0.09	56.05
5.21	76.34	437641.60	1.49	9.51	5.60	1057.51	6.76	6.85	0.04	49.31
5.37	149.05	412305.75	1.22	7.77	10.77	1086.44	10.70	8.49	0.09	101.50
5.53	89.96	431102.32	2.02	15.76	13.87	1175.07	15.83	10.56	0.04	158.35
5.69	107.37	546701.75	5.76	17.35	11.80	1086.98	15.93	14.86	0.09	236.13
5.85	40.34	437278.02	5.49	26.41	8.36	1041.87	19.35	16.93	0.14	246.34
6.00	78.69	509573.86	5.89	24.13	6.98	1102.85	27.71	18.46	0.19	261.30
6.16	81.47	501499.81	4.96	22.17	6.29	1082.69	24.49	13.69	0.09	206.31
6.32	47.66	471809.12	2.96	19.52	4.57	1136.06	16.97	13.21	0.04	184.67
6.48	33.56	415588.84	4.43	19.10	8.70	1141.44	13.29	9.82	0.24	140.19
6.64	41.36	461273.56	4.43	12.85	3.19	1083.78	15.67	9.92	0.14	108.33
6.79	71.36	464235.84	3.09	12.42	2.85	1035.56	15.26	8.44	0.24	130.88

PYR-9-L1-FM-25b Tbr

t (sec)	Ti (ppm)	Fe (ppm)	Ni (ppm)	Cu (ppm)	Zn (ppm)	As (ppm)	Ag (ppm)	Sb (ppm)	Au (ppm)	Pb (ppm)
6.95	108.29	455021.50	4.16	17.40	3.88	1081.21	14.43	6.21	0.24	105.48
7.11	79.24	532678.08	4.69	12.58	5.94	1097.37	12.82	7.54	0.19	104.41
7.27	64.87	484741.21	6.43	22.59	4.22	1116.09	26.46	7.11	0.19	104.64
7.43	91.45	510346.53	8.83	69.63	11.45	1143.07	16.96	6.85	0.19	112.59
7.58	83.13	421705.18	13.76	50.94	8.70	1013.96	13.39	8.86	0.04	112.08
7.74	140.11	464645.39	12.83	122.80	12.14	933.86	17.85	8.91	0.04	121.86
7.90	59.57	413798.00	13.90	139.94	10.08	939.79	22.62	7.96	0.24	127.02
8.06	67.06	502228.73	11.36	174.21	10.42	1006.85	16.86	7.75	0.24	201.03
8.22	91.28	442386.87	16.56	95.47	4.22	962.11	14.53	8.22	0.19	431.89
8.37	96.01	453860.21	12.69	72.14	11.80	683.22	14.89	4.25	0.24	200.99
8.53	23.83	142098.35	4.96	15.86	2.84	161.50	3.03	1.44	0.00	46.40

Spot Analyses

Label	Ti (ppm)	Fe (ppm)	Ni (ppm)	Cu (ppm)	Zn (ppm)
PYR-3-S1-FTpl-12	1.79 ± 0.25	175000 ± 41000	2.40 ± 0.71	12.6 ± 3.4	900 ± 520
PYR-8-S1-FTbr-25b	376 ± 53	375000 ± 38000	96 ± 11	2520 ± 810	620 ± 210
PYR-9-S1-FTbr-25b	94 ± 35	269000 ± 40000	1.88 ± 0.42	36000 ± 10000	86 ± 43
UG-1-S1-FTpr-4	0.723 ± 0.062	11300 ± 1000	0.045 ± 0.052	720 ± 160	560000 ± 49000
PYR-7-S1-FTpr-4	143 ± 42	273000 ± 59000	18.1 ± 4.3	33.2 ± 6.4	15.1 ± 1.7
PYR-7-S2-FTpr-4	131 ± 42	402000 ± 49000	19.8 ± 3.1	106 ± 15	10.0 ± 1.9

Spot Analyses

Label	As (ppm)	Ag (ppm)	Sb (ppm)	Au (ppm)	Pb (ppm)
PYR-3-S1-FTpl-12	1770 ± 520	43 ± 16	32 ± 11	1.13 ± 0.49	2000 ± 2000
PYR-8-S1-FTbr-25b	1860 ± 280	91 ± 14	39.0 ± 5.4	0.48 ± 0.10	659 ± 87
PYR-9-S1-FTbr-25b	211 ± 45	205 ± 55	3.99 ± 0.51	0.042 ± 0.015	103 ± 43
UG-1-S1-FTpr-4	-2.01 ± 0.13	20.1 ± 4.1	1.08 ± 0.15	0.0072 ± 0.0055	0.61 ± 0.16
PYR-7-S1-FTpr-4	11800 ± 2800	17.0 ± 3.6	44.0 ± 9.7	1.27 ± 0.39	97 ± 23
PYR-7-S2-FTpr-4	10900 ± 1800	66.3 ± 8.7	61.8 ± 7.0	1.94 ± 0.41	164 ± 30

Appendix C: ArcPro 3D Model Methods

ArcPro was employed to visualize the features of the deposit in three dimensions in a cost effective and accessible way. Ore grades were first extracted from an Integra Resources technical report and organized in Excel (Fig. C1). The first layer of the ArcPro project was a map of the open mine pits of Florida Mountain that was created using the latitude and longitude locations of the drill holes (Fig. 8). Geometry (angle and hole direction) and longitude/latitude values were used to place the end point of the drill core and determine the vertical depth of the hole from that point (Fig. 45). That new location and depth was input into a new excel file and then added as layer. An extrusion tool was used so that the end point of the drill core could be visualized and then the start point of the drill core was connected to the end point with the tool “link”. This created a spatial model of each drill core (Fig. 45). Although the figure here is two-dimensional, this model can be physically manipulated in ArcPro in the x- y- and z-directions and incorporate additional petrographic and geochemical data to easily view the spatial relationships between changes in properties and compositions. For the samples studied here, a correlation of higher-grade zones can be seen vertically and horizontally.

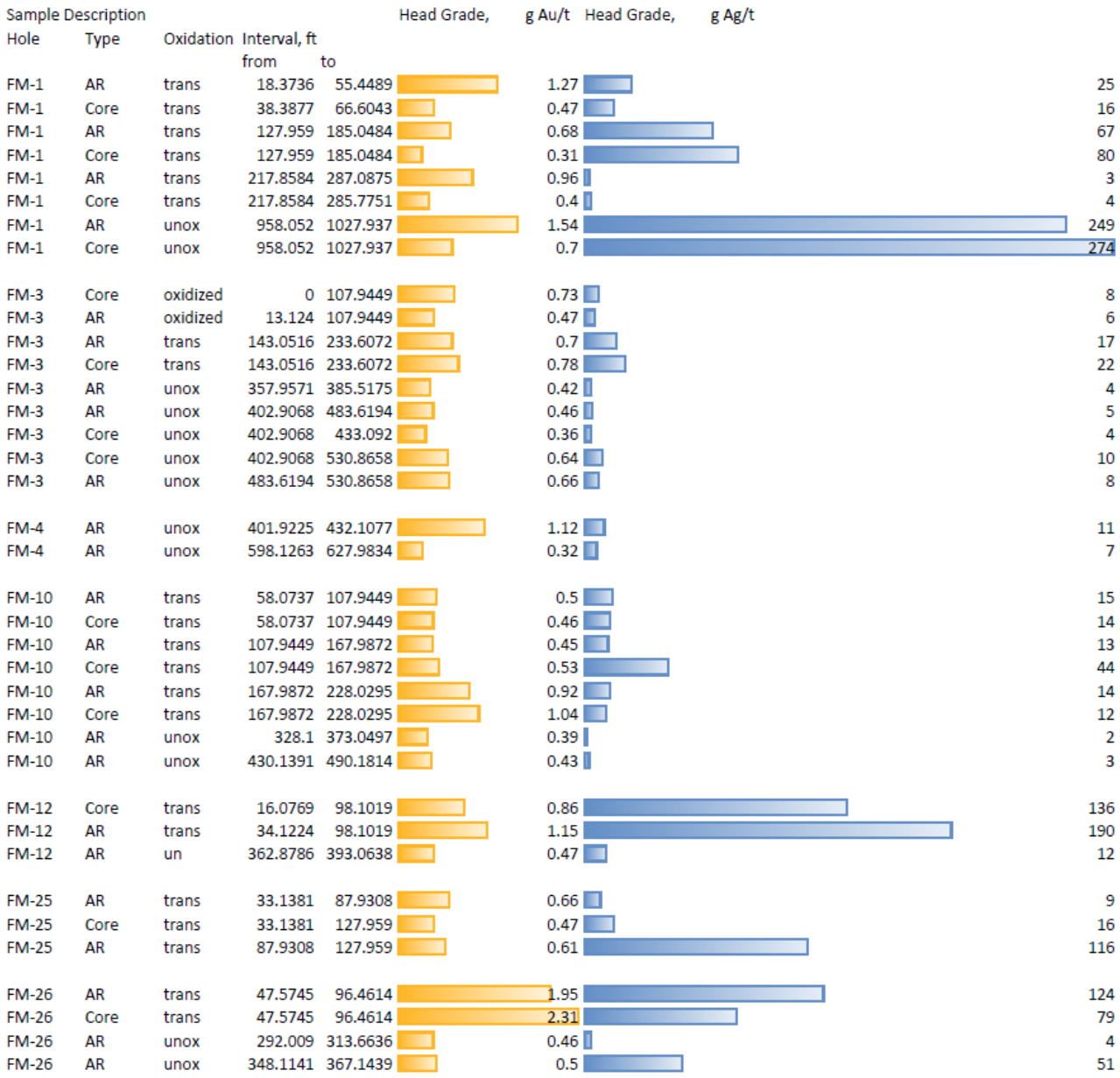

Sample Description			Interval, ft		Head Grade, g Au/t	Head Grade, g Ag/t
Hole	Type	Oxidation	from	to		
FM-1	AR	trans	18.3736	55.4489	1.27	25
FM-1	Core	trans	38.3877	66.6043	0.47	16
FM-1	AR	trans	127.959	185.0484	0.68	67
FM-1	Core	trans	127.959	185.0484	0.31	80
FM-1	AR	trans	217.8584	287.0875	0.96	3
FM-1	Core	trans	217.8584	285.7751	0.4	4
FM-1	AR	unox	958.052	1027.937	1.54	249
FM-1	Core	unox	958.052	1027.937	0.7	274
FM-3	Core	oxidized	0	107.9449	0.73	8
FM-3	AR	oxidized	13.124	107.9449	0.47	6
FM-3	AR	trans	143.0516	233.6072	0.7	17
FM-3	Core	trans	143.0516	233.6072	0.78	22
FM-3	AR	unox	357.9571	385.5175	0.42	4
FM-3	AR	unox	402.9068	483.6194	0.46	5
FM-3	Core	unox	402.9068	433.092	0.36	4
FM-3	Core	unox	402.9068	530.8658	0.64	10
FM-3	AR	unox	483.6194	530.8658	0.66	8
FM-4	AR	unox	401.9225	432.1077	1.12	11
FM-4	AR	unox	598.1263	627.9834	0.32	7
FM-10	AR	trans	58.0737	107.9449	0.5	15
FM-10	Core	trans	58.0737	107.9449	0.46	14
FM-10	AR	trans	107.9449	167.9872	0.45	13
FM-10	Core	trans	107.9449	167.9872	0.53	44
FM-10	AR	trans	167.9872	228.0295	0.92	14
FM-10	Core	trans	167.9872	228.0295	1.04	12
FM-10	AR	unox	328.1	373.0497	0.39	2
FM-10	AR	unox	430.1391	490.1814	0.43	3
FM-12	Core	trans	16.0769	98.1019	0.86	136
FM-12	AR	trans	34.1224	98.1019	1.15	190
FM-12	AR	un	362.8786	393.0638	0.47	12
FM-25	AR	trans	33.1381	87.9308	0.66	9
FM-25	Core	trans	33.1381	127.959	0.47	16
FM-25	AR	trans	87.9308	127.959	0.61	116
FM-26	AR	trans	47.5745	96.4614	1.95	124
FM-26	Core	trans	47.5745	96.4614	2.31	79
FM-26	AR	unox	292.009	313.6636	0.46	4
FM-26	AR	unox	348.1141	367.1439	0.5	51

Figure C1. Ore grades and oxidation extent reported by Integra Resources, as organized in Excel. Yellow bars represent relative gold grade; blue bars illustrate relative silver grade.